ANALYSIS OF POSTULATED POOL DRAINING ACCIDENTS IN THE MNR

ANALYSIS OF POSTULATED POOL DRAINING ACCIDENTS IN THE MNR

By A. SHLOMO SCHNEIDER, B. SC.

A Thesis Submitted to the School of Graduate Studies in Partial Fulfilment of the Requirements for the Degree Master of Applied Science

MASTER OF APPLIED SCIENCE (2015) McMaster University
(Engineering Physics) Hamilton, Ontario

TITLE:	Analysis of Postulated Pool Draining Accidents in the MNR
AUTHOR:	Alexander Shlomo Schneider B.Sc. (Physics) Tel-Aviv University, Israel
SUPERVISOR:	Dr. John C. Luxat, Professor NSERC/UNENE IRC in Nuclear Safety Analysis Department of Engineering Physics McMaster University
NUMBER OF PAGES:	ix, 127

Abstract

A safety analysis for the McMaster Nuclear Reactor has been carried out for postulated scenarios of loss or termination of forced flow in the reactor core in a state of shutdown, with loss of pool inventory of different magnitudes including core uncovery. Models were developed to evaluate the natural convection flow through the core assemblies for the different conditions within the aforementioned envelope. The flow rate was used to get the temperature or enthalpy rise along the heated channel in order to estimate the corresponding clad temperatures in the given scenarios.

The models were constructed from first principles using the one-dimensional momentum conservation law, incorporating the Boussinesq approximation for the single-phase case and the Homogeneous Equilibrium Model assumptions when a two-phase mixture was present. In order to obtain the flow rate and enthalpy rise along the channel, knowledge of the assembly power and inlet temperature is required. The power was calculated using a well known decay power correlation. The pool temperature which was used as the assembly inlet temperature was calculated via a lumped parameter model using a simple energy balance between the core output (again by using the decay-heat profile) and the pool heatup. Heat losses from the pool were neglected and the model allowed for reaching saturation temperature in the pool. In this case, water vaporization was calculated using the latent heat to assess pool inventory loss rate.

For all scenarios before core uncovery, the models predict that clad and fuel temperatures remained well below limits associated with clad blistering or melting. Consequently, it is asserted natural convection and acceptable temperatures will be sustained in the McMaster Nuclear Reactor while the core remains covered. In the most severe draining before uncovery, in which the pool drains to just before exposing the core, it takes approximately a week (180 hours) after shutdown for boiling to start in the core's hottest channel. For core uncovery, the models predict that the clad remains below the blistering temperature for pool height at 9.4% of the heated channel's height (corresponding to exposing about 61.7 cm of the assembly), and below melting temperature for pool height at 8.1% of the heated channel's height (corresponding to exposing about 62.5 cm of the assembly). Both heights are below the height of the bottom of the lowest beam tube, at which the worst draining case will end.

Acknowledgements

First and foremost I wish to thank my supervisor Dr. John Luxat for his guidance throughout this process. Had I been smarter, I could have spent my time more wisely by simply following his instructions instead of the months of searching for related literature, that eventually led me back to his exact original suggestions. I would also like to thank Dr. David Novog, whose advice I occasionally sought as well, for taking interest and offering assistance and an additional perspective.

This work wouldn't have been completed without the help of the people at the McMaster Reactor, mainly the Director of Nuclear Operations & Facilities, Chris Heysel, who introduced me to the staff and helped me obtain valuable documents and reports required for this work, and Dr. Simon Day, who greatly helped me in dissecting through the data and technical drawings to filter out the additional information I needed and couldn't find elsewhere.

I would like to acknowledge the knowledgeable and seasoned PhD students and postdocs in our branch and department in past and present, some of which are already doctors and all of whom deserve that title. Ken, Hummel, Kurt, Jay and Fred, James, Remon, Abhi, Matt and Brad. It has been a pleasure getting to know all of you.

Thank you to my peers, friends and Master's students in past and present; Izaak, Eddy, Salma, Shaun, Andrew, Changrui, Travis, Zachary, MengMeng, Curtis and everyone else who I might have forgotten. Darryl, Joseph and Mehtaab, thank you for being who you are, stay classic. Ivan and Emilia, keep philosophizing. Thank you to the incredible Jewish community in Hamilton, McMaster's Hillel, Rabbi B. and especially Michal and Amnon.

Last but not least, thank you to all the people back home to whom I disappeared during these past two years. Most importantly, thank you dear mom and dad. All of which I have accomplished and who I am today is only thanks to you.

Дорогие мама и папа, я вас очень люблю.

Contents

List of Figures

List of Tables

List of Abbreviations and Symbols

A_1 - A_5 Cross sectional flow areas through the MNR assembly sections, [m^2]

$A_{\mathbf{pool}}$ Reactor pool surface area, [m^2]

$\bar{C}_p$ Average specific heat capacity of the pool between two temperatures, [$J\,kg^{-1}\,K^{-1}$]

$D_{\mathbf{e}}$ Hydraulic diameter, [m]

E Total heat emitted in a time interval, [J]. Used for the heat generated by the decay heat profile

G Mass flux, [$kg\,m^{-2}\,s^{-1}$]

H Depth of the core below the pool surface / height of the pool surface above the core, [m]

$H_{\mathbf{core}}$ Height of the core bottom above the pool floor, [m]

$H_{\mathbf{full}}$ Height of the water in the MNR pool at nominal full inventory, [m]

$H_{\mathbf{pool}}$ Pool height in cases where draining uncovers the assemblies. Measured from the bottom of the heated section (section 4 as in Figures 4.1 to 4.3)

$H_{\mathbf{swell}}$ Height of the swell i.e. the two-phase mixture inside the channels under steady steaming

$H_{\mathbf{tot}}$ Height of pool water for various draining heights above the core H, [m]

K Minor loss coefficient used in estimating the pressure loss due to geometrical changes along the flow path

L_1 - L_5 Vertical lengths of the different sections in a MNR assembly, [m]

$L_{\mathbf{AD}}$ Vertical dimensions of a MNR assembly (from point A to D in Figure 4.1), [m]

$L_{\mathbf{BC}}$ Active length of the fuel in the heated channel, [m]

$L_{1\phi}$ Length of heated channel occupied by single-phase liquid in two phase flow, [m]

$\dot{M}$ Coolant flow rate through a MNR assembly, [$\mathrm{kg\,s^{-1}}$]

M_{∞} Mass of the water in the reactor pool, [kg]

P Power, [W]. Specifically used here to indicate decay heat power profile

$\dot{Q}$ Power output/heat rate of a MNR assembly, [W]

S Slip ratio. The ratio between the velocity of vapour and liquid in two-phase flow

T Temperature, [°C]

$\bar{T}$ Average temperature in the core (along the assembly) for obtaining water properties, [°C]

T_{∞} Temperature of the pool water, [°C]

$T_{\mathbf{c}}$ Temperature of the MNR fuel plate clad, [°C]

$T_{\mathbf{exit}}$ Temperature of the coolant exiting the assembly, [°C]

$T_{\mathbf{fm}}$ Temperature of the MNR fuel plate centerline (fuel centerline), [°C]

$V_{\mathbf{core}}$ Assumed volume of geometrical changes, core and instrumentation in the MNR pool, [$\mathrm{m^3}$]

$V_{\mathbf{fm}}$ Fuel meat volume inside a MNR fuel plate, [$\mathrm{m^{-3}}$]

$V_{\mathbf{nom}}$ Nominal volume of water in the MNR pool, [$\mathrm{m^3}$]

$V_{\mathbf{tot}}$ Volume of the MNR pool structure (surface area times height of water), [$\mathrm{m^3}$]

$\bar{c}_p$ Average specific heat capacity between core inlet and outlet, [$\mathrm{J\,kg^{-1}\,K^{-1}}$]

f The Darcy friction factor used in estimating the pressure loss due to friction in fluid flow

$f_{\mathbf{lam}}$ The friction factor at laminar flow conditions

$f_{\mathbf{tur}}$ The friction factor for turbulent flow conditions

g Gravitational acceleration constant, $[\mathrm{m\,s^{-2}}]$

h Heat transfer coefficient, $[\mathrm{W\,m^{-2}\,K^{-1}}]$

Δh Enthalpy rise required to bring the liquid from subcooled pool enthalpy to saturated steam enthalpy

$h_{\mathbf{fg}}$ Latent heat of vaporization, $[\mathrm{J\,kg^{-1}}]$. Dependent on pressure

$h_{\mathbf{f}}$ Enthalpy of saturated liquid, $[\mathrm{J\,kg^{-1}}]$. Dependent on pressure

$h_{\mathbf{g}}$ Enthalpy of saturated steam, $[\mathrm{J\,kg^{-1}}]$. Dependent on pressure

$h_{2\phi}$ Heat transfer coefficient of a two-phase mixture, $[\mathrm{W\,m^{-2}\,K^{-1}}]$

$k_{\mathbf{c}}$ Heat conductivity of the clad of a MNR fuel plate, $[\mathrm{W\,m^{-1}\,K^{-1}}]$

$k_{\mathbf{fm}}$ Heat conductivity of the fuel meat inside a MNR fuel plate, $[\mathrm{W\,m^{-1}\,K^{-1}}]$

$k_{\mathbf{w}}$ Heat conductivity of water, $[\mathrm{W\,m^{-1}\,K^{-1}}]$

l Effective length of a MNR flow channel (between two fuel plates), [m]

$\dot{m}$ Flow rate through a single channel (between two fuel plates), $[\mathrm{kg\,s^{-1}}]$

p Thermodynamic or hydrostatic pressure, [Pa]

$\Delta p_{\mathbf{b}}$ Pressure difference due to hydrostatic and buoyancy driving forces, [Pa]

$\Delta p_{\mathbf{f}}$ Pressure difference due to friction losses, [Pa]

$\Delta p_{\mathbf{maj}}$ Pressure loss from friction, [Pa]

$\Delta p_{\mathbf{min}}$ Pressure loss from geometry changes along the flow path, [Pa]

$\bar{p}$ Average pressure in the core (along the assembly) for obtaining water properties, [Pa]

$\dot{q}'''$ Volumetric power/heat output density inside a MNR plate (inside the fuel meat), $[\mathrm{W\,m^{-3}}]$

$\dot{q}$ Power output/heat rate of a MNR plate, [W]

t Time, [s]

w Effective width (thickness) of a MNR flow channel (between two fuel plates), [m]

$w_{\mathbf{c}}$ Thickness of the clad adjacent to the fuel meat in a MNR fuel plate, [m]

$w_{\mathbf{fm}}$ Width of the fuel meat inside a MNR fuel plate, [m]

x Flow quality. The fraction of vapour mass flow or flux out of the total mass flow or flux. In the HEM model this also equals the thermodynamic quality, which is the fraction of the two phase mixture enthalpy out of vapour saturation enthalpy

x_∞ Thermodynamic quality of the pool water

$x_{\mathbf{exit}}$ Flow quality of the two-phase mixture flowing out of the assembly

$L_{2\phi}$ Length of heated channel occupied by two-phase mixture in two phase flow, [m]

α Void fraction. The ratio of volume occupied by vapour flow to the total volume of flow in two-phase flows.

β Thermal expansion coefficient or thermal expansivity of liquid water, [K^{-1}]

δ Fraction or percentage of pool water covering the heated section from outside the assembly (not to be confused with ϵ)

ϵ Ratio of the swell height to the length of the heated section

γ Unitless grouping of the variables saturated liquid density, saturated steam density and exit quality into $x_{\mathrm{exit}}\rho_{\mathrm{f}}/\rho_{\mathrm{g}}$

μ Water viscosity, [Pa s] or [$\mathrm{kg\,s^{-1}\,m^{-1}}$]

$\bar{\phi}^2$ Average two-phase multiplier along a certain flow path

ϕ^2 Two phase multiplier. Portraying the enhancement to friction losses occuring two-phase flow conditions

$\bar{\rho}_{\mathbf{l}}$ Average density of liquid water in the heated channel, [$\mathrm{kg\,m^{-3}}$]

$\bar{\rho}_{\mathbf{m}}$ Average density of a two-phase mixture along a certain flow path

ρ_{∞} Density of the pool water, [$\mathrm{kg\,m^{-3}}$]

$\rho_{\mathbf{exit}}$ Density of coolant exiting the assembly, [$\mathrm{kg\,m^{-3}}$]

$\rho_{\mathbf{f}}$ Density of saturated liquid, [$\mathrm{kg\,m^{-3}}$]

$\rho_{\mathbf{g}}$ Density of saturated steam, [$\mathrm{kg\,m^{-3}}$]

$\rho_{\mathbf{m}}$ Density of a two-phase mixture, [$\mathrm{kg\,m^{-3}}$]

θ Grouping of the inlet and exit quality variables into $-x_{\infty}/(x_{\mathrm{exit}} - x_{\infty})$

$\xi_{\mathbf{lam}}$ Friction loss coefficient correction factor for rectangular channels for laminar flow

$\xi_{\mathbf{tur}}$ Friction loss coefficient correction factor for rectangular channels for turbulent flow

°C Temperature units Celsius

J Energy units Joule

K Temperature units Kelvin

W Power units Watt

Nu The Nusselt number. Ratio of convective to conductive heat transfer

Pr The Prandtl number. Ratio between viscous and conduction forces

Re The Reynolds number. Ratio between inertial to viscous forces

HEM Homogeneous Equilibrium Model

MNR McMaster Nuclear Reactor

MTR Material Testing Reactor

Chapter 1

Introduction

The McMaster Nuclear Reactor (MNR) is a pool type, light water research reactor of the Material Testing Reactor (MTR) type. It is licenced to operate at up to 5 MW powers and currently operates at 3 MW. Its construction began in 1957 and first criticality was achieved in 1959. The MNR uses Low Enriched Uranium (LEU) fuel fabricated to MTR type fuel assemblies, widely used in research reactors in the United Stated and elsewhere.

The reactor pool structure contains a number of tubes exiting from its walls through the biological shield called beam tubes, used for various experiments such as neutron diffraction, neutron radiography, photo-neutron spectroscopy and others. A holdup tank is located beneath the reactor pool level and under normal operation the water from the pool drains to the tank by gravity through a grid plate. A pump restores the water from the tank to the reactor pool, thus sustaining forced flow through the reactor channels under normal operation. Under conditions of low flow and other initiating events, a device called "flapper" automatically opens, allowing for a path for natural convection in the reactor pool.

As described in the MNR safety report [1], several initiating events including loss of power will lead to reactor shutdown. The reactor automatic shutdown system initiates at either low pool level, low flow or at indication that the flapper has opened. This results in the combined shutdown of the reactor with termination of forced flow conditions. A draining event will also lead to flapper opening, resulting again in reactor shutdown and termination of forced flow. Additional action will also be taken to isolate the pool from the holdup tank to maintain the water inventory in the pool.

The isolation however, is not essential to achieving a fail safe state, since even after the holdup tank is completely filled the core remains under several meters of water. An extreme case of draining and loss of pool inventory could eventually lead to core uncovery and loss of cooling by liquid, at which point a release of fission products becomes a serious concern.

Following termination of forced flow events, a natural convection flow, or 'thermosiphoning', will develop in the pool through the reactor channels. Natural convection and circulation flows occur when a fluid that is heated up by a heat source, is subsequently reduced in density and is then driven up by natural buoyancy. Provided sufficient driving head, the liquid cools down at the heat sink, is increased in density and is pulled back down by gravity. A natural convection[1] flow thus develops and can be sustained as long as the effective heat sink is above the heat source and an adequate flow path for the liquid back to heat source inlet exists.

To cause a loss of inventory rapid enough to uncover the core would take a substantial break. The most plausible initiator of a considerable leak is a break in one of the beam tubes. It is assessed in the MNR safety analysis report that it would take about 3.5 hours to uncover the top of the core in an event as such. A partially uncovered core will also allow for a sustained natural convection flow upwards as long as there is sufficient head provided by colder liquid column outside the core. When the pool level drops further, the liquid (or two-phase mixture) level inside the core, although higher in volume, will eventually also drop and expose fractions of the fuel plates to cooling by steam production from the covered portion. The MNR safety report predicts some fuel melting in this case.

To further investigate such events and in support of the MNR safety analysis, a study on reactor behaviour under the above accident scenarios has been conducted. The scenarios chosen were those of loss of forced flow accompanied by reactor shutdown, added by various degrees of loss of pool inventory. Although detailed qualitative discussion on the matter is presented in the MNR safety report, quantitative assessments for the natural convection scenarios have not yet been conducted for the MNR, at least to the knowledge of the author. Quantitative treatment of these scenarios is therefore, in addition to academic interest, beneficial in support of the MNR safety analysis. The heat source for the conditions in all scenarios covered in this study is

[1] In closed loops this process is referred to as 'natural circulation' and for an open pool setting a more appropriate term would be 'natural convection'.

the reactor decay heat after shutdown. The studied physical phenomena in this work are therefore those of natural convection and core uncovering under decay heat powers. It is essentially a study on decay heat removal capability.

It is customary to conduct best estimate and conservative calculations for the purpose of safety assessments and accident scenario modelling for nuclear reactors. These assessments are often required when experimental data is lacking [2]. Following this guiding philosophy, this work was performed using known and conventional methods and models.

The natural convection related calculations were performed using the one-dimensional (1-D) momentum conservation law, from which a pressure balance between the buoyancy force and friction losses is obtained. As will be shown in the literature review, this method is in standard use for natural circulation in reactor applications. Calculations of the pool heatup by decay heat powers and possible vaporization were performed using simple energy balance considerations. Calculations for the uncovered core were performed by use of similar pressure balance considerations as for the natural convection in the covered cases. Use of correlations is often required for estimating variables and coefficients such as friction factors and heat transfer coefficients. These also have been taken from the literature for identical or similar uses to those used in this work.

The assessment consists of three main distinguishable stages, in their presumed physical order of occurrence in an accident of the sort discussed. First, a single-phase natural convection treatment of a submerged core was conducted in order to establish the conditions for the initiation of boiling in the core channels. It was sought to find under which conditions and at what time after shutdown boiling will occur. For this purpose a simple model was fabricated to calculate pool heatup and vaporization and the matching flow and temperatures in the core that correspond to the evolution of the pool temperature and water level. As long as there is no boiling in the channels, only single phase considerations, correlations and treatment, are required in order to assess the temperatures of the coolant, clad and fuel.

The onset of boiling serves as a passage to the second stage. It is presumed (and supported by the results herein) that no significant rise in clad and fuel temperature will occur under two-phase boiling flow, since the two-phase heat transfer tends to be significantly higher than convection to single-phase liquid. The limit sought at this stage was for the conditions for the first appearance of superheated steam in the channel. The steam may be superheated to temperatures well beyond saturation,

causing subsequent temperature rise in the clad and fuel up to blistering and melting. Here, a two-phase natural-convection model was used to treat the steam quality rise in the channels.

The third stage deals with core uncovery. This uncovery may happen as a result of ongoing loss of pool inventory following either the first or first-and-second stages, but is more likely to happen as a result of a large break as above-mentioned. It may theoretically also happen for a submerged core, but as will be shown, only happens for powers much higher than those expected in the MNR. The physical model used in this case is that of steady state steaming, where it is sought to find at which pool level the clad temperatures start approaching safety limits (temperature for clad blistering or melting).

This work consists of seven chapters. The second chapter presents a literature review on similar earlier treatments, methods and general literature concerning modelling of the above mentioned scenarios. The third chapter briefly illustrates the MNR facility and design features relevant to this safety assessment. The fourth chapter shows the theoretical background behind the construction of the models. The fifth chapter discusses the approach and decisions taken in order to numerically solve the theoretical equations and run the models. Chapter six presents the results obtained from modelling the accident scenarios and discusses the subsequent implication to safety and the maintaining of core integrity. The last chapter will present conclusions, overall insights and suggestions for continued work.

Chapter 2

Literature Review

The MNR safety report [1] states that the core can be safely operated in powers up to 110 kW under a natural convection regime. There is discussion about loss of forced circulation along with an unlikely unavailable shutdown. The report considers this natural circulation flow under shutdown state to be a safe state from stating that the large pool is a sufficient heat sink for the decay heat. It doesn't continue to demonstrate this with natural convection flow assessment. A review of additional MNR related documents shows little discussion regarding natural convection (or thermosiphoning) related phenomena. Garland [3] modelled the MNR core with the CATHENA code and has briefly mentioned that a correct qualitative behaviour, of upflow through the core, was observed for natural convection modelling. No quantitative results were discussed. He added that no direct experimental data has been obtained for this type of flow in the MNR. This is in accordance with the general scarcity of experimental data for research reactors [4].

A famous set of experiments by the name 'BORAX' were conducted on a dedicated series of research reactors in the US in the 1950s. The mode of heat removal from the core in the experiments was that of natural circulation as in the cases treated in this work, but the focus of the experiments was on steady state operation and power excursions and not on decay heat and loss of pool inventory. Another set of experiments with very similar conditions to those in the MNR was conducted by Gambill and Bundy [5]. They performed studies on natural circulation flow in thin rectangular channels at near atmospheric pressures (both in an open pool setting and with restrictions along the return path) in order to measure and correlate the

onset of Critical Heat Flux (CHF) under these conditions. Some of the dimensions and aspect ratios of their test sections were quite close to those of an MNR channel[1]. They correlated their results by comparing the heat flux that produces a natural circulation flow rate to the maximum heat flux that can be removed by the same flow rate before burnout occurs. To calculate the natural circulation induced flow rate resulting from a given heat flux they solved the pressure balance between the density gradient driving pressure and the pressure losses along the flow path. They concluded that for two-phase flow in thin channels, using no-slip condition (i.e. the Homogeneous Equilibrium Model - HEM) is appropriate, for "phase slip appears to be strongly inhibited by small flow passages, and the homogeneous-flow method outlines allows reasonably accurate prediction of burnout heat fluxes for low pressure water in natural circulation through channels with equivalent diameter less than ¼ inch". They also showed agreement with earlier studies on the observation that CHF doesn't occur in long vertical channels (channel with height-to-diameter greater than 40) cooled by water unless relatively high values of heat flux and vapour quality are reached; $3 \times 10^5\,\mathrm{Btu\,h^{-1}\,ft^{-2}}$ (about $950\,\mathrm{kW\,m^{-2}}$) and a 70% quality.

Zvirin [6] and Grief [7] both did comprehensive surveys on natural circulation and thermosiphoning. Grief mentions earlier LWR related studies have used the momentum conservation as well; "The flow rate is obtained from momentum balance considerations and the integral of the momentum equation around the loop is utilized". Zvirin showed similar usage of methods for calculation of the steady state flow in natural circulation, taking the fluid properties at an average temperature. Zvirin mentions earlier studies which pointed that using this method leads to uncertainty on the order of 30%. This is mostly due to issues of compatibility of forced flow friction factor and heat transfer coefficient correlations with natural circulation. He sums, "... these forced flow correlations are not generally valid in natural circulation flows. Since the driving flow mechanism is different in the free convection loops, the velocity distributions are also different", "... comparison of data for temperature differences with analytical results based on forced flow calculations ... shows an uncertainty of order 30%". He adds that the transition from laminar to turbulent flow is around Re=1500 as opposed to higher Reynolds numbers for forced flow. The above literature on natural circulation and thermosiphoning shows a recurring theme for estimating

[1]The channels came essentially in 3 aspect ratios. One of those had roughly the dimensions $3 \times 52.5 \times 595$ mm, whereas an equivalent rectangular channel having the same hydraulic diameter as an MNR channel has roughly the dimensions $3.1 \times 66.9 \times 600$ mm, as will be shown later.

the flow rate by integrating the 1-D momentum equation around the flow loop.

For scenarios of core uncovering, the sequence of events, as described in the MNR safety report, is as follows. The covered fuel plus some portion of the uncovered part are assumed to conduct heat to the water still covering the fuel. The uncovered part is transferring heat by convection to superheated steam created from the heat transferred by the covered part to the liquid underneath. The analysis predicts reaching steady state after some melting and relocation of fuel down to the liquid covered part. The calculations used to perform the assessment are not presented. Chatzidakis and Ikonomopoulos performed parametric analysis for a loss of inventory accident progression in a research reactor, providing a useful outlining for the associated scope of event progressions leading to core uncovering as well [8]. Using the RELAP code, they examined the different trends for different breaks sizes in various pipes. They also observed that an outlet pipe break may cause a power increase in the reactor due to increase in forced flow rate which serves to add positive reactivity.

Authors Bousbia-Salah, Hamidouche and Si-Ahmed have been dealing extensively with research reactor accident analysis [9–11]. Amongst discussions on the applicability of different safety analysis methods and use of best estimate codes[2] they performed an assessment on the IAEA benchmark MTR reactor for uncovered core scenarios [9] using a discretized 3-D numerical heat conduction scheme, taking into consideration full core conduction including the grid plate and assuming heat is removed to air in the uncovered part. They showed that under certain circumstances, partial core uncovery leads to a more severe outcome than full inventory loss in which cooling can be sustained by natural circulation of air.

Drier and Winkler studied partial core uncovery in the swiss SAPHIR MTR both theoretically and experimentally [13, 14]. In their theoretical study, they modelled the transient plate temperature excursion in a single channel. The model included conduction within the plate and heat transfer to the liquid and steam in the covered and uncovered portions respectively while neglecting radiation heat transfer and conduction to other core components. For the heat transfer coefficient of the covered part they used Rosenhow's correlation for pool boiling heat transfer. For the heat transfer in the uncovered part they assumed that heat is transferred in some fashion to coolant rising along the channel due to vaporization albeit stating that exact knowledge is lacking

[2]Extensive thermalhydraulic system codes that have been validated experimentally and have reached a high degree of maturity. Examples for these would be RELAP, ATHLET and CATHARE, among others [12].

on the flow pattern with which this happens. Therefore, they performed a parametric study of the temperature rise along the channel as dependent on the flow regime and corresponding heat transfer coefficient. They showed that the plate temperatures are indeed strongly dependent on the flow regime and that the overall transient behaviour, even for this case of core uncovering, is relatively slow, especially with respect to the fast temperature transient within the relatively high conducting plate. To validate their theoretical work they performed experimental work on a test section mocking a number of channels within the SAPHIR reactor. They found that in low powers (below 250 W for a plate) the uncovered part sees a flow of only vapour[3], whereas in higher powers slugs of liquid may be geysered out of the channel due to strong boiling. The latter, involving convection to liquid water, produces much better heat transfer and cooling of the plates than the former where only steam is present.

Aharon and Hochbaum performed experimental work on an electrically heated test section mocking an MTR channel with dimensions close to that of the MNR assembly channels[4] [15]. They studied the temperature rise along the channels for various powers at 50% uncovery. Adding to observations similar to Drier and Winkler's, they also showed that for intermediate powers (around 225 W for their uncovery level) the liquid slug didn't persist throughout the entire channel, leaving high temperatures at the channel top edge as happens with low powers.

It was also recognized by the author that literature on similar conditions for pool heatup and core uncovery may appear in treatments of spent fuel pools. It appears that literature analysing fuel uncovery other than the above-mentioned, both in reactor cores and spent fuel pools, mostly uses best estimate codes[5] to assess the temperatures and potential fuel damage [8, 10, 16–20]. Spent fuel pool literature also suggests different methods for pool heatup calculations. Whereas some sources suffice with a simple energy balance [21, 22] others use either system codes or more sophisticated heat and mass transfer calculations that require knowledge of the containment air temperature and humidity [23].

In general, IAEA Tec-Doc 1474 [2] which deals with natural circulation in power reactors, suggests that for lack of experimental knowledge in the field, evaluations should rely on numerical modelling. IAEA safety report 55 adds that for lack of experimental databases for research reactors it is becoming popular to use best estimate codes with

[3] Probably due to the quiescent nature of boiling in low heat rates.
[4] $2 \times 60 \times 600$ mm.
[5] Mostly RELAP.

conservative data input [4]. In addition, in the MNR safety analysis methodology overview [24], Garland and Heysel suggest that because of both the simplicity of single-phase thermalhydraulics and uncertainties associated with fission product release, it is preferable to perform augmented hand calculations for the MNR. This again is in agreement with the general trend of performing research reactor safety analysis using conservative computational tools and is only now begining to change towards best estimate assessments [11].

Garland and Heysel also mention that water properties are relatively unchanged in the liquid water domain for near atmospheric pressures, particularly in the range from MNR pool operational temperatures to saturation. This seems to get along with Zvirin's use of average fluid properties in this range for thermalhydraulic calculations to justify such use in the model in this work. The tools for obtaining water properties used by the MNR safety analysis are in accordance with 1997 IAPWS Industrial Formulation for the thermodynamic properties of water and steam.

Additional MNR documents provide useful reference and correlations for modeling components of the core and fuel assemblies. Blahnik [25, 26] and Garland [27] deal amongst other issues with a proper representation for the MNR assembly hydraulic resistances. Blahnik justifies using the classical literature correlations for friction and form losses. Garland suggests a complete set of friction factors for the MNR assembly which were used for example by Ha [28]. Justification for approximation of the MNR plate assembly as flat rectangular parallel plates, has been shown by Osamusali et al. [29] and used by Yu [30] and Ha [28]. These methods are used to model friction and form losses in other MNR related documents such as the aforementioned by Blahnik or by Ha and Garland [31].

Chapter 3

MNR Overview

The MNR design is covered extensively in the MNR safety report [1] and other MNR related technical and research documents, for example Ha's master's thesis [28]. This section will focus on the design features concerning the scenarios covered, being mainly the reactor pool, core and fuel assemblies.

The MNR uses MTR type fuel fabricated to MTR plate-type assemblies containing 18 fuel plates, the outer two being 'dummy' plates containing no fuel. The fuel is made from Low Enriched Uranium (LEU) in a form of sintered powder mixture of uranium silicide and aluminium, containing about 73% uranium by weight. The plates are rectangular with a small curvature radius to insure that each two plates don't bend towards each other should they start deforming. The cladding over the fuel meat is made of aluminium. Drawings of the assembly are shown in Figure 3.1.

The MNR fuel assemblies can be conceptually considered as the 'channels' in the core. A sub-channel is subsequently viewed as the flow region between every two plates. For the 18 plates there are thus 17 sub-channels. Since most of the discussion in the following chapters is going to be focused on an individual assembly, the aforementioned sub-channels are henceforth simply referred to as 'channels' for simplicity.

The assembly can also be divided conceptually into 5 vertically ascending sections distinguished by their different cross-section flow areas as shown from bottom up in Figure 3.2(b). The bottom end fitting, also called the 'snout', fits into a grid plate to hold the assembly in its required position in the core. A gradual expansion in the snout called the reducer, connects the bottom part to a wider circular duct, which itself is connected to a rectangular shaped duct constructed from two side-plates and the two

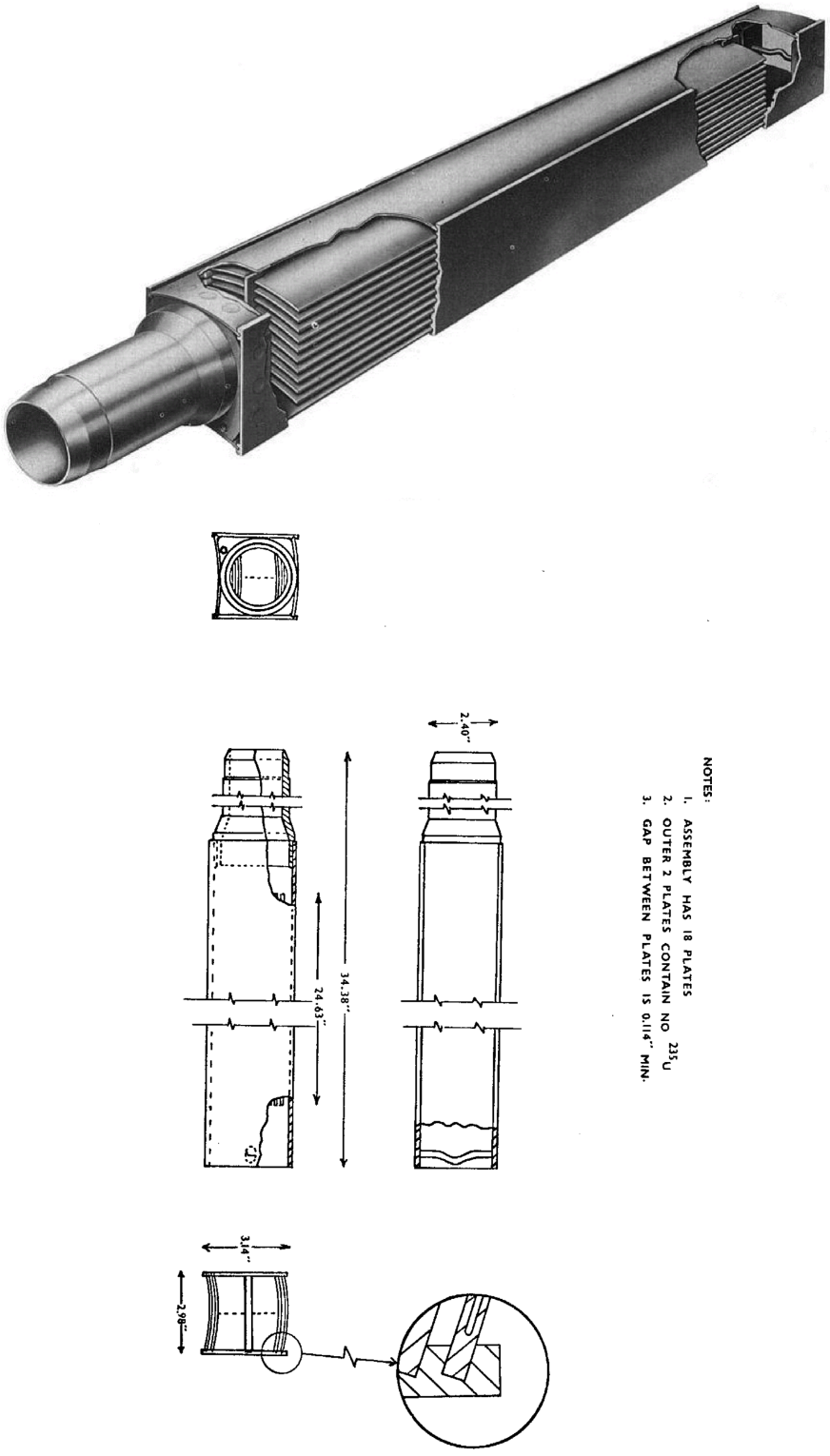

Figure 3.1: Standard MNR fuel assembly drawing. Taken from p. 5-8 in the MNR safety report [1].

dummy plates forming the main part of the assembly. The fuel plates are smaller in length than the main part, and are located 2.54 cm above the main rectangular part's bottom edge, thus dividing it into 3 distinguishable geometries; the bottom rectangular duct, the parallel plates section and the upper rectangular duct. The bottom and upper rectangular ducts both naturally have the same flow area cross section.

Apart from the standard assembly described above, other types of assemblies used in the MNR core are Control Fuel Assemblies, Capsule Irradiation Assemblies and a Beryllium Assembly. The MNR also incorporated the use of 10-plate fuel assemblies in the past but these are no longer in use. The control fuel assemblies are externally similar to the standard fuel assemblies, differing mostly in internal composition. They contain 9 fuel plates, with no dummy plates (outer plates containing fuel as well). An absorber channel is located in the 'middle' of the assembly, north of 4 plates and south from the other 5. The fuel plates are identical in dimensions to the fuel plates in a standard assembly, but contain a little less fuel. The powers produced by the control assemblies will thus be somewhat lower than those of a standard assembly. The Capsule Irradiation assemblies and Beryllium assembly contain no fuel.

A schematic of the reactor cooling system is presented in Figure 3.4. It should be kept in mind that the schematic is not drawn with reference to elevation and the holdup tank is indeed located at a lower height than the reactor pool level, resulting in gravitation driven flow under normal operation. The holdup tank's main function is to create a delay in the re-pumping of water to the pool to allow for the decay of short-lived isotopes from activation of the water flowing through the core (mostly ^{16}N). The gravitationally driven flow enters the core assemblies from the top, flowing downward and exiting through the bottom fitting.

The reactor pool which hosts the core is a reinforced concrete structure providing biological shielding during normal operation. It is divided into two sections, north and south. The north end is meant to host the core, and has the entrances in its wall for the beam tubes. The south section is larger and used primarily to store spent fuel. An aluminium gate can be installed to divide the two sections. Additionally, the core, which is hung from a bridge structure, can be moved to different parts of the pool. The beam tubes are located at an elevation leveled with the centerline of the core as can be seen in Figure 3.3. There are six of them, two 20 cm diameter tubes and four which are 15 cm in diameter.

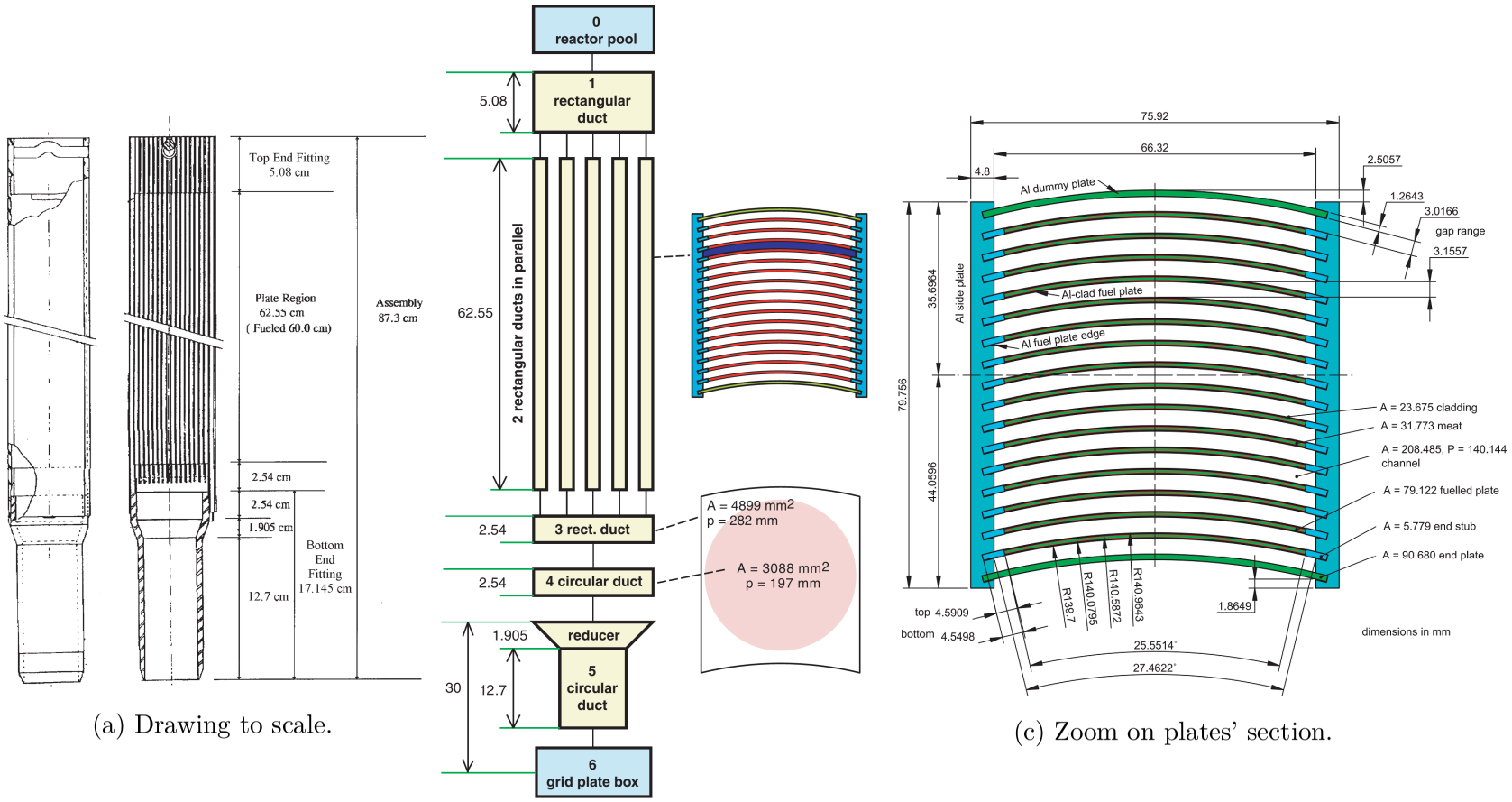

(a) Drawing to scale.

(b) Schematic drawing.

(c) Zoom on plates' section.

Figure 3.2: Standard MNR fuel assembly drawings. (a) taken from p. 13 in [28]. (b) taken from p. 5-8 in the MNR safety report [1] (The snout's bottom part length caption corrected to 12.7 cm from original). (c) is also from the MNR safety report, p. 16.3-23 in the MNR safety report.

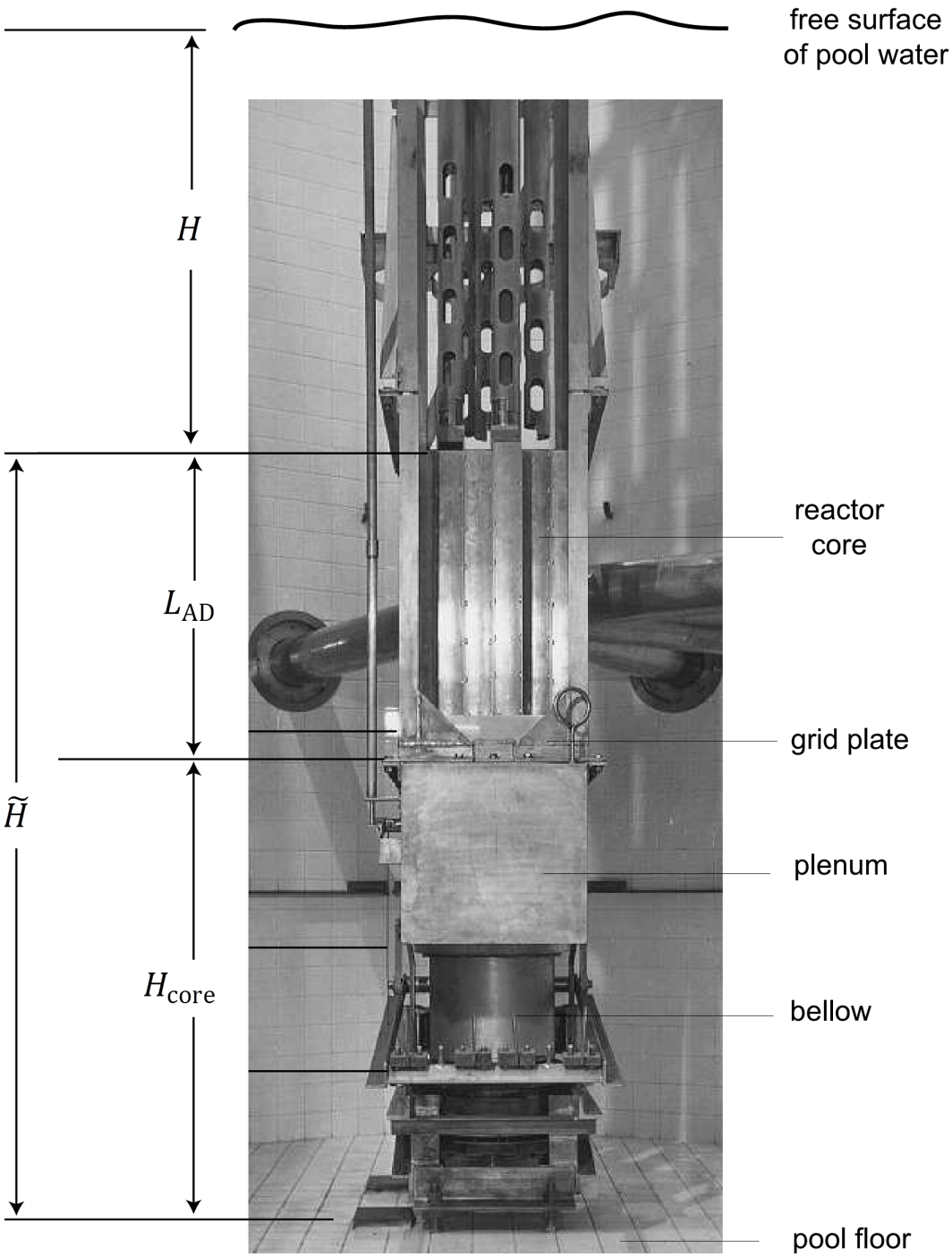

Figure 3.3: A sketch of the pool and core, depicting height of the core above the pool floor and height of the pool surface above the core top. The parameters H, L_{AD} and $\tilde{H}$ are as they appear in calculations throughout the document. Using drawing from p. 30 in Ha's Thesis [28].

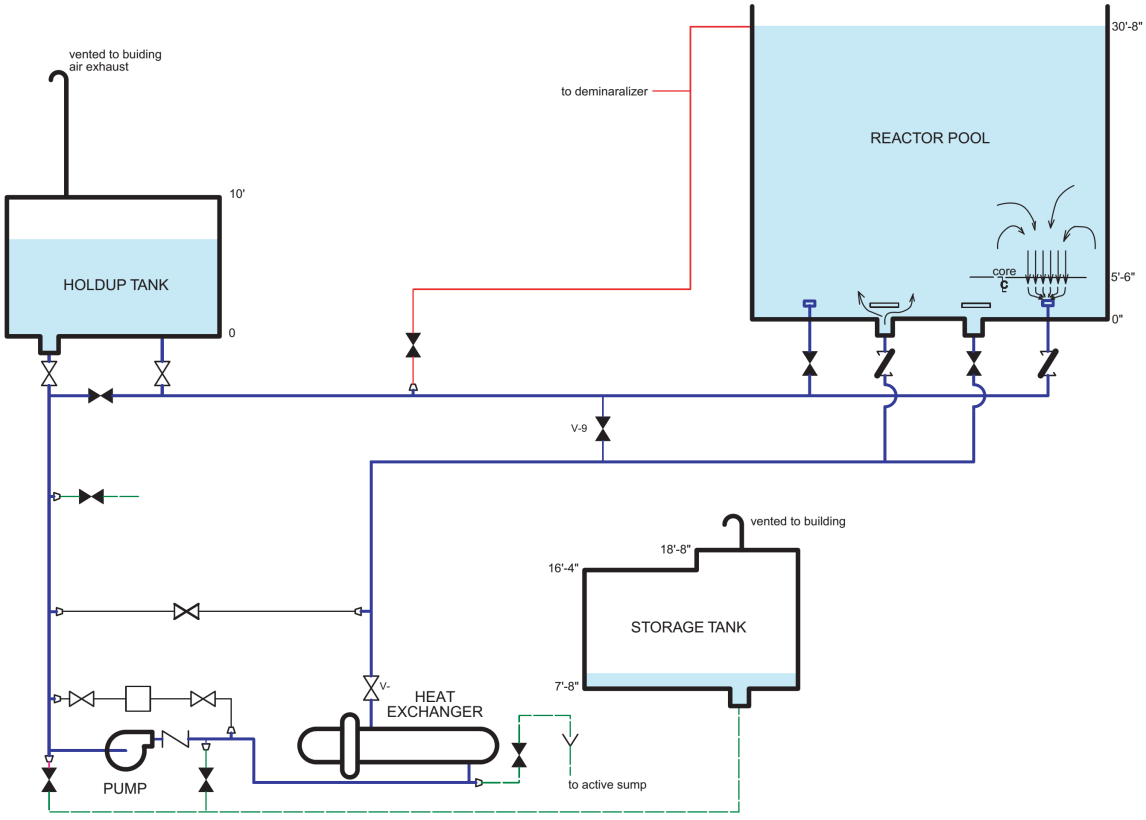

Figure 3.4: Reactor cooling system. Taken from p. 16.3-33 in the MNR safety report [1].

Chapter 4

Theory

4.1 Single Phase Natural Convection

Natural buoyancy flow arises when a fluid is locally heated under gravitation. The changes in density that develop from the temperature rise of the fluid induce buoyancy flow of the lighter less dense fluid upwards. Under steady heating a steady state natural convection flow develops in the system. The following treatment estimates this steady state flow rate. The treatment is of a steady state, since changes in all parameters occur very slowly in accident conditions under decay heat. As mentioned earlier and shown in the MNR safety report [1], the fastest design basis draining scenario entails that draining to the core level would take at least 3.5 hours. Similarly, since the pool is very large, decay heat powers change its temperature very slowly even when it is isolated from the external heat sink as mentioned earlier. It can be thus seen that the accident progression in the treated scenarios, at least before core uncovery takes place, is a slow process. For these reasons, it's appropriate to treat the accident with a quasi steady-state model, taking steady-state 'snapshots' of the core and pool at different points on the timeline of accident progression.

In chapter 3 of the book Nuclear Systems II [32], Todreas and Kazimi present a one dimensional (1-D) natural circulation treatment for a Pressurized Water Reactor (PWR) loop, modelling the full primary circuit which requires among other input, the full core's hydraulic resistance. Since the MNR core resides in an open pool as opposed to a closed pressurised loop as in PWRs, the model requires a few adjustments in order to be used for the MNR. The forced flow regime in the MNR is driven by pressure

difference across the entire core, originating from the connection to the hold-up tank, and is a full-core phenomenon. However, the driving force in the natural convection mode will originate in each MNR assembly individually, governed by the assembly's own heat generation and hydraulic resistance, making the flow under this regime mainly an individual assembly phenomenon. This has been argued by Zvirin [6], who expressed that the flow mechanisms of natural and forced flow differ in nature and is reinforced by Garland [3]: "For thermosiphoning, the flow in a channel will be governed by the channel density (i.e. local power) and the overall channel resistance (again dominated by the exit and entrance losses of the assembly)"[1]. Additionally, the parameters sought for, primarily the individual channel flow and clad temperatures, are also individual assembly parameters, and would otherwise need to be obtained from the full core flow averaged out over all of the assemblies. Thus, assessing the core's effective hydraulic resistance under natural convection for the purpose of obtaining core flow, which would prove a formidable task, is not necessary for this work's purpose. For these reasons, and from not expecting any mixing between different assemblies, the same logic applying to the entire core in the PWR treatment, is tailored to an individual assembly in this work.

The treatment is based on a standard assembly since it is the highest power fuel configuration in the core. The control assemblies hold almost twice as little fuel plates which themselves contain smaller amounts of fuel. It is expected therefore that boiling, dryout, or melting would occur in a standard fuel assembly before it occurs in a control assembly in the given scenarios. Therefore, calculations proving standard assembly integrity, and in particular the integrity of the hottest channel in the core, will suffice to prove a safe state in the core.

Based on the treatment by Todreas and Kazimi, a loop treatment is tailored to a MNR assembly as shown in Figure 4.1 where the z axis is pointing upward (from the circular parts towards the fuel-plates section). The assembly is separated to sections according to the different geometric regions in it. For convenience, in agreement with the natural-convection flow direction, the sections are numbered in an opposite order to the section numbering in the MNR safety report (see Figure 3.2(b)). The fuel meat within the plates is found vertically between points B and C in Figure 4.1 and does not fill section 4 entirely, being slightly shorter in length than the plate itself (see length BC in contrast to the length of section 4). The exit and inlet distances are

[1] Brackets appear as originally in the source.

infinitesimal such that points A and F are on the same height, and so are D and E.

The 1-D momentum conservation equation for single-phase flow in a channel parallel to the z axis is:

$$\frac{\partial G}{\partial t} + \frac{\partial}{\partial l}\left(\frac{G^2}{\rho}\right) = -\frac{\partial p}{\partial l} - f\frac{G\,|G|}{2D_{\mathrm{e}}\rho} - \rho g \ , \tag{4.1}$$

where G is the mass flux in $\mathrm{kg\,m^{-2}\,s^{-1}}$, ρ the density in $\mathrm{kg\,m^{-3}}$, p the thermodynamic pressure in Pa, f the friction factor (unitless) and g the gravitational acceleration constant in $\mathrm{m\,s^{-2}}$. D_{e} is the effective (hydraulic) diameter which is a broadened definition of the diameter to include non circular ducts. The differentiation with respect to l indicates a path derivative. Equation (4.1) is integrated along the loop shown in Figure 4.1. For steady state, the first term on the left hand side vanishes. Also, without a pump, the second term on the left hand side - the spatial acceleration, and first term on the right - the thermodynamic static pressure, vanish (after integration) such that the left hand side is equal to zero. The terms remaining are:

$$\oint f\frac{G\,|G|}{2D_{\mathrm{e}}\rho}\,dl = -\oint \rho g\,dl \ . \tag{4.2}$$

The left hand side of the equation symbolizes the pressure losses and for simplicity can be represented by Δp_{f}. The right-hand side represents the driving pressure difference and is similarly represented by Δp_{b}, making Equation (4.3) into:

$$\Delta p_{\mathrm{f}} = \Delta p_{\mathrm{b}} \ . \tag{4.3}$$

The above is the notation used by Todreas and Kazimi which depicts the main physical mechanisms behind natural convection and circulation.

4.1.1 Hydrostatic-Buoyancy Term

The term on the right-hand side of Equation (4.3) is the hydrostatic term. Due to the density changes along the loop this term incorporates within it the representation of the buoyancy effects. It is integrated along the loop in the following fashion (where dl

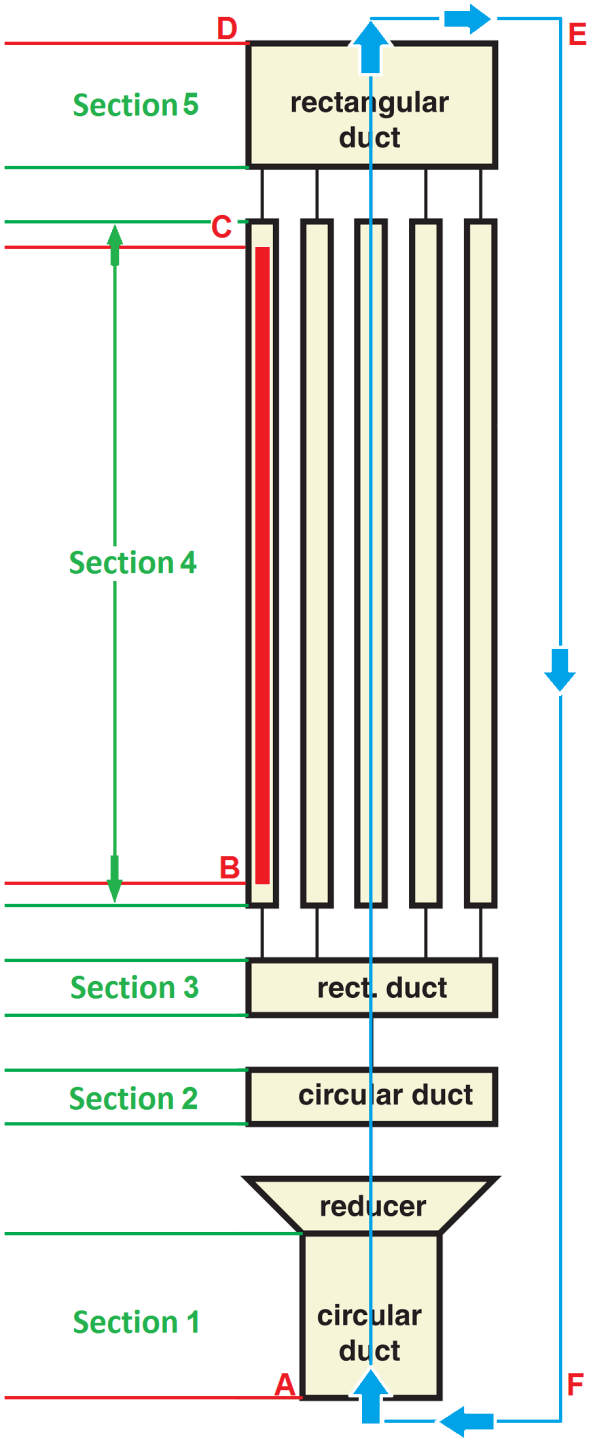

Figure 4.1: Representation of the single-phase flow loop through the MNR standard fuel assembly. Size of length BC in comparison to the length of section 4 is not to scale. Using fuel technical drawing on p. 16.3-24 from the MNR safety report [1].

turns to dz for 1-D):

$$\Delta p_{\mathrm{b}} = -\oint \rho\,(z)\,g\,dz = -\int_{H_{\mathrm{A}}}^{H_{\mathrm{B}}} \rho g\,dz - \int_{H_{\mathrm{B}}}^{H_{\mathrm{C}}} \rho g\,dz - \int_{H_{\mathrm{C}}}^{H_{\mathrm{D}}} \rho g\,dz - \int_{H_{\mathrm{D}}}^{H_{\mathrm{E}}} \rho g\,dz - \int_{H_{\mathrm{E}}}^{H_{\mathrm{F}}} \rho g\,dz - \int_{H_{\mathrm{F}}}^{H_{\mathrm{A}}} \rho g\,dz\ , \quad (4.4)$$

where H_{A} is the corresponding height to position A as shown in the Figure 4.1, with the same logic applying to B through F. The integrals of the horizontal sections, from D to E and from F to A are equal to zero since there is no elevation change in them. The density from A to B is constant and equal to the ambient liquid density of the bulk pool water, since heating begins only at point B. The density change takes place from B to C. From C to D there is no density change but this new density is now lower, after having been heatup between B and C. It is assumed that due to the large body of water, the warm liquid dissipates to the bulk immediately after leaving the assembly at point D. The density from E to F is therefore equal to the ambient liquid density. Equation (4.4) becomes:

$$\Delta p_{\mathrm{b}} = -\rho_{\infty} g L_{\mathrm{AB}} - \int_{H_{\mathrm{B}}}^{H_{\mathrm{C}}} \rho g\,dz - \rho_{\mathrm{exit}} g L_{\mathrm{CD}} + \rho_{\infty} g L_{\mathrm{EF}}\ , \quad (4.5)$$

where ρ_{∞} is the density of the bulk pool water, ρ_{exit} the density of water just after point C in the rest of section CD, and L_{AB}, L_{CD} and L_{EF} the lengths of sections AB, CD and EF respectively (henceforth denote the length between any two indicators I and J as L_{IJ}). Observing that $L_{\mathrm{EF}} = L_{\mathrm{AD}}$ and that $L_{\mathrm{AD}} - L_{\mathrm{AB}} = L_{\mathrm{BC}} + L_{\mathrm{CD}}$ Equation (4.5) can be written as:

$$\Delta p_{\mathrm{b}} = \rho_{\infty} g\,(L_{\mathrm{BC}} + L_{\mathrm{CD}}) - \int_{H_{\mathrm{B}}}^{H_{\mathrm{C}}} \rho g\,dz - \rho_{\mathrm{exit}} g L_{\mathrm{CD}}\ . \quad (4.6)$$

The remaining integral from B to C is evaluated under the assumption that the change in density is linear with temperature T i.e., $d\rho/dT = const.$ Another approximation in the model is for the heat flux along the heated section to be constant, thus giving a linear rise in temperature along the section i.e. $dT/dz = const.$ The heat-flux profile (or axial power distribution) is known to be closer to a cosine shape along the z axis in a typical reactor. However, it has been shown that the difference between the uniform approximation and the exact solution is on the order of 5% [33][2].

[2]Todreas [32] referencing to Zvirin [33].

By using these assumptions the resulting density rise is also linear in the heated section;

$$\frac{d\rho}{dz} = \frac{d\rho}{dT}\frac{dT}{dz} = const \ , \tag{4.7}$$

producing:

$$\int_{H_\mathrm{B}}^{H_\mathrm{C}} \rho g \, dz = \bar{\rho}_\mathrm{l} g L_\mathrm{BC} = \frac{\rho_\infty + \rho_\mathrm{exit}}{2} g L_\mathrm{BC} \ , \tag{4.8}$$

where $\bar{\rho}_l$ represents the liquid average density with the subscript 'l' standing for liquid. This is a standard result to an integral for a linear function along a section, which equals its average times the section length[3].

Inputting Equation (4.8) into Equation (4.6) and rearranging results in:

$$\Delta p_\mathrm{b} = (\rho_\infty - \rho_\mathrm{exit}) \left(\frac{L_\mathrm{BC}}{2} + L_\mathrm{CD} \right) \ . \tag{4.9}$$

The assumption that the density dependence on temperature is linear is embodied in the Bousinnesq approximation for buoyancy driven flows, which describes the density profile along the heated section as:

$$\rho\,(T) = \rho_\infty \left(1 - \beta \left(T - T_\infty\right)\right) \ , \tag{4.10}$$

where T_∞ is the pool bulk temperature and β is the thermal expansion coefficient or thermal expansivity in units K^{-1}. The thermal expansivity is defined as:

$$\beta = \frac{1}{\nu}\left(\frac{\partial \nu}{\partial T}\right)_p \ , \tag{4.11}$$

where ν is the specific volume in units $\mathrm{m}^3\,\mathrm{kg}^{-1}$ and p is the pressure. The subscript p serves to notify that the partial derivative is taken under constant pressure, demonstrating also that β is pressure dependent. The values for the thermal expansion coefficient for water are taken from the literature. The Boussinesq approximation assumes small differences in density such that the only explicit dependency on the density is expressed in the buoyancy head term. Inputting Equation (4.10) into Equation (4.9) produces:

$$\Delta p_\mathrm{b} = \rho_\infty g \beta \left(T_\mathrm{exit} - T_\infty\right) \left(\frac{L_\mathrm{BC}}{2} + L_\mathrm{CD} \right) \ . \tag{4.12}$$

[3]The linear function $\rho(z)$ is tailored such that $\rho\,(z = H_\mathrm{B}) = \rho_\infty$ and $\rho(z = H_\mathrm{C}) = \rho_\mathrm{exit}$.

where T_{exit} is the exit temperature from the assembly.

In steady state, the equation for the exit temperature from a MNR assembly generating a heat output $\dot{Q}$ is:

$$T_{\text{exit}} = T_{\infty} + \frac{\dot{Q}}{\dot{M}\bar{c}_p} \,, \tag{4.13}$$

where $\dot{Q}$ is in W, $\dot{M}$ is the flow rate through the assembly in $\mathrm{kg\,s^{-1}}$ and $\bar{c}_p$ is the liquid average specific heat capacity along the heated section. Equation (4.13) is derived from first principles of thermodynamics [34] and is true for any pipe or channel heated by time-constant heat flux, regardless of flow direction. It is originally derived for the temperature profile and in order to specify a temperature at a point along the channel a knowledge of the axial heat flux shape is required. It is however not necessary for the knowledge of the exit temperature since only the total heat and not the heat flux profile is required for the calculation of the total temperature rise at the channel's exit. It should nonetheless be remembered that the flux shape was approximated to be uniform in an earlier assumption as embodied in Equation (4.7). For additional discussion on the axial power profile see Appendix A.

Using Equation (4.13), the temperature difference can be replaced with the assembly power to give the flow-rate dependent expression for the hydrostatic term:

$$\Delta p_{\text{b}} = \rho_{\infty} g \beta \frac{\dot{Q}}{\dot{M}\bar{c}_p} \left(\frac{L_{\text{BC}}}{2} + L_{\text{CD}} \right) \,. \tag{4.14}$$

Equivalent treatments can be performed to achieve the above result. All of these refer to Equation (4.3) which, given the assumptions in its development, is the main governing equation for all scenarios in this work. The difference is with the definitions of the driving term Δp_{b}, which are all equivalent. It is useful to present these parallel definitions at this point since they will be useful for the the two-phase and uncovered core treatments later on. The first alternative starts with the following identity shown by Todreas and Kazimi and adjusted to the MNR assembly:

$$\Delta p_{\text{b}} \equiv -\oint \rho\left(z\right) g \, dz = \left(\bar{\rho}_{\text{cold}} - \bar{\rho}_{\text{hot}}\right) g \left(H_{\text{D}} - H_{\text{B}}\right) \,, \tag{4.15}$$

where $\left(H_{\text{D}} - H_{\text{B}}\right)$ is the length between points D and B, and $\bar{\rho}_{\text{cold}}$ and $\bar{\rho}_{\text{hot}}$ are the heat

sink (pool) and heat source (plates section BC) mean densities respectively, defined as:

$$\bar{\rho}_{\text{cold}} = -\frac{1}{H_{\text{D}} - H_{\text{B}}} \int_{H_{\text{D}}}^{H_{\text{E}'}} \rho \, dz \qquad ; \qquad \bar{\rho}_{\text{hot}} = \frac{1}{H_{\text{D}} - H_{\text{B}}} \int_{H_{\text{B}}}^{H_{\text{D}}} \rho \, dz \; , \tag{4.16}$$

where E′ would be a point along the path EF parallel in height to B (parallel to DB, see Figure 4.1). The densities are averaged out over the hot and cold sections respectively. The hot section driving the flow includes the entire length BD since the liquid in CD, although not heating up anymore, is still hotter than the liquid outside the assembly. As shown in Equation (4.5) the colder section integrals from E′ to E and from A to B cancel out due to opposite signs (the density ρ_∞ remains constant in all of the cold section). The integrals in the horizontal sections naturally cancel out as mentioned earlier. Hence the mean cold density is integrated only from D to E′ in Equation (4.16). Inputting Equation (4.16) into Equation (4.15), the length terms $(H_{\text{D}} - H_{\text{B}})$ cancel out leaving:

$$\Delta p_{\text{b}} = g \left(- \int_{H_{\text{D}}}^{H_{\text{E}'}} \rho \, dz - \int_{H_{\text{B}}}^{H_{\text{D}}} \rho \, dz \right) \; . \tag{4.17}$$

The first integral on the right hand side of Equation (4.17), following the path from D through E to E′ is easily calculated since the density along its path is constant:

$$- \int_{H_{\text{D}}}^{H_{\text{E}'}} \rho \, dz = 0 - \rho_\infty \left(H_{\text{E}'} - H_{\text{D}} \right) = \rho_\infty L_{\text{BD}} = \rho_\infty (L_{\text{BC}} + L_{\text{CD}}) \; , \tag{4.18}$$

noticing that horizontal path integral between D and E is equal to zero and that the distance between E and E′ is equal to the distance between B and D. The second integral is solved similarly by separating it into the path from B to C and from C to D:

$$- \int_{H_{\text{B}}}^{H_{\text{D}}} \rho \, dz = - \int_{H_{\text{B}}}^{H_{\text{C}}} \rho \, dz - \int_{H_{\text{C}}}^{H_{\text{D}}} \rho \, dz \; . \tag{4.19}$$

The first integral on the right hand side of Equation (4.19) was solved in Equation (4.8). The second integral from C to D is also performed under constant density:

$$- \int_{H_{\text{C}}}^{H_{\text{D}}} \rho \, dz = -\rho_{\text{exit}} \left(H_{\text{D}} - H_{\text{C}} \right) = -\rho_{\text{exit}} L_{\text{CD}} \; . \tag{4.20}$$

Inputting Equations (4.8) and (4.20) into Equation (4.19) and then Equations (4.18)

and (4.19) back into Equation (4.17) results in:

$$\Delta p_{\mathrm{b}} = g\left[\rho_{\infty}(L_{\mathrm{BC}} + L_{\mathrm{CD}}) - \frac{\rho_{\infty} + \rho_{\mathrm{exit}}}{2} L_{\mathrm{BC}} - \rho_{\mathrm{exit}} L_{\mathrm{CD}}\right] = \ldots$$
$$= (\rho_{\infty} - \rho_{\mathrm{exit}})\left(\frac{L_{\mathrm{BC}}}{2} + L_{\mathrm{CD}}\right) \ , \quad (4.21)$$

which is identical to the result achieved with the first method in Equation (4.9), which was then manipulated with the Bousinnesq approximation.

The second alternative definition for the driving term is derived from another starting point. Fundamentally, any flow is driven by a pressure difference and the natural convection upwards flow emerges from the pressure difference between the column of cold water outside the assembly and the column of hotter water within it. The driving term is therefore:

$$\Delta p_{\mathrm{b}} = p_{\mathrm{cold}} - p_{\mathrm{hot}} = \rho_{\infty} g\,(L_{\mathrm{AB}} + L_{\mathrm{BC}} + L_{\mathrm{CD}} + H)$$
$$- (\rho_{\infty} g L_{\mathrm{AB}} + \bar{\rho}_{\mathrm{l}} g L_{\mathrm{BC}} + \rho_{\mathrm{exit}} g L_{\mathrm{CD}} + \rho_{\infty} g H) \ , \quad (4.22)$$

where H is the height of the pool above the assembly (see Figure 3.3). The term on the left in the first transition is the pressure of the cold water column outside the assembly and the term on its right is the pressure of the warmer (at least in some parts) column of water passing through the assembly. This takes into account the assumption of immediate dissipation of hot water at the assembly exit to the cold pool water, where the column of water remaining above the assembly resumes the cold water density ρ_{∞}. After cancelling out the remaining terms are:

$$\Delta p_{\mathrm{b}} = \rho_{\infty} g\,(L_{\mathrm{BC}} + L_{\mathrm{CD}}) - (\bar{\rho}_{\mathrm{l}} g L_{\mathrm{BC}} + \rho_{\mathrm{exit}} g L_{\mathrm{CD}}) \ . \quad (4.23)$$

Using the definition of the average density from Equation (4.8) and rearranging yields again Equations (4.9) and (4.21) proving that the alternative definition for the driving term in Equation (4.22) is also equivalent.

Define the lengths of section 4 and section 5 as L_4 and L_5 respectively (and length of any section i as L_i). The MNR safety report specifies the active fuel length L_{BC} which is slightly smaller than the total length of the plates ($L_{\mathrm{BC}} < L_4$, $L_{\mathrm{CD}} > L_5$, see Figure 4.1). The length L_{CD} is conservatively taken as the slightly smaller length of

section 5, which results in a slightly smaller driving term than in reality[4]:

$$L_{\mathrm{CD}} \cong L_5 \ . \tag{4.24}$$

Equation (4.14) is then modified to:

$$\Delta p_{\mathrm{b}} \cong \rho_\infty g \beta \frac{\dot{Q}}{\dot{M} \bar{c}_p} \left(\frac{L_{\mathrm{BC}}}{2} + L_5 \right) \ . \tag{4.25}$$

4.1.2 Pressure Loss Term

The term on the left-hand side of Equation (4.3) represents the pressure losses along the loop. In Equation (4.2) only the friction term f is shown but if the form losses are significant it's appropriate to add them as well to the total pressure loss as Todreas and Kazimi suggest in their two-phase treatment [32]:

$$\Delta p_{\mathrm{f}} = \Delta p_{\mathrm{maj}} + \Delta p_{\mathrm{min}} \ , \tag{4.26}$$

where 'maj' and 'min' depict major and minor respectively. The loop integral results only in losses in the assembly since there is no associated loss for the flow through the rest of the open pool. The equivalent diameters of sections 3-5 are denoted as D_{e3} - D_{e5} respectively.

The major loss is by definition:

$$\Delta p_{\mathrm{maj}} = \sum_{i=1}^{5} \frac{f_i L_i}{D_{\mathrm{e}}^i} \frac{\rho_\infty v_i^2}{2} \ , \tag{4.27}$$

where i is summed over the 5 sections of the assembly with their associated friction factors f_i, lengths L_i, diameters D_{e}^i and fluid velocities v_i. The density remains unchanged in the calculation in accordance with the usage of the Bousinnesq assumption in the model, which ignores the density change in the heated section in all but the hydrostatic term. Discussion regarding the choice of values for the density and other water properties will follow in the modelling chapter.

The flow rate through the assembly is constant and common among all compart-

[4]No more than 2.5 cm difference for a combined length of about 67 cm.

ments, as follows from non-compressible steady state flow mass conservation:

$$\dot{M} = \rho_\infty A_i v_i \ , \tag{4.28}$$

where A_i is the cross sectional area of flow of section i and Equation (4.28) is true for all sections. Inputting Equation (4.28) into Equation (4.27) yields:

$$\Delta p_{\text{maj}} = \sum_{i=1}^{5} \frac{f_i L_i}{D_{\text{e}}^i} \frac{\dot{M}^2}{2\rho_\infty A_i^2} \ . \tag{4.29}$$

The friction loss coefficient for laminar flow can be analytically found from basic principles and is written as [35]:

$$f_{\text{lam}} = \frac{64}{\text{Re}} \ , \tag{4.30}$$

where Re is the Reynolds number, defined for flow in a duct as:

$$\text{Re} \equiv \frac{\rho\, v D_{\text{e}}}{\mu} = \frac{\dot{M} D_{\text{e}}}{\mu A} \ , \tag{4.31}$$

in which Equation (4.28) is used in the representing of v in terms of $\dot{M}$, μ is the viscosity in units Pa s and A is as earlier the cross-sectional flow area.

As justified in Chapter 2, when applicable, the assembly's curvature is neglected. A correction to Equation (4.30) is suggested by Garland for rectangular channels [27]:

$$f_{\text{lam}}^{\text{rect}} = \xi_{\text{lam}} f_{\text{lam}}$$

$$\xi_{\text{lam}} = 1.503 - 1.894r + 2.034r^2 - 0.755r^3 \ , \tag{4.32}$$

where r is the ratio of channel width (thickness) to channel length, equalling 1 for a perfect square and 0 for infinite parallel plates (the smaller side always divided by the bigger).

In turbulent flow, the friction factor is calculated using the Colebrook equation [35]:

$$\frac{1}{\sqrt{f_{\text{tur}}}} = -2\log_{10}\left(\frac{\epsilon/D_{\text{e}}}{3.7} + \frac{2.51}{\text{Re}\sqrt{f_{\text{tur}}}}\right) \ , \tag{4.33}$$

where ϵ is called the surface roughness and given in mm. The roughness value taken is

for the roughness of aluminium [36] which is the clad's build material. Similarly to the correction for the laminar friction factor, a correction for the turbulent friction factor is given by Garland in the same document:

$$f_{\text{tur}}^{\text{rect}} = \xi_{\text{tur}} f_{\text{tur}}$$

$$\xi_{\text{tur}} = 1.097 - 0.177r + 0.083r^2 \ . \tag{4.34}$$

From similar considerations stemming from Equation (4.28) the minor losses can be represented as follows:

$$\Delta p_{\min} = \sum_j K_j \frac{\rho_\infty v_j^2}{2} = \sum_j K_j \frac{\dot{M}^2}{2\rho_\infty A_j^2} = \left(\frac{K_{\infty 1}}{A_1^2} + \frac{K_{1-2}}{A_1^2} + \frac{K_{2-3}}{A_2^2} + \frac{K_{3-4}}{A_4^2} + \frac{K_{4-5}}{A_4^2} + \frac{K_{5\infty}}{A_5^2} \right) \frac{\dot{M}^2}{2\rho_\infty} \ , \tag{4.35}$$

where K_j are the minor loss coefficients $K_{\infty 1}$ to $K_{5\infty}$ representing the geometry-change related pressure losses between every two sections; e.g. $K_{\infty 1}$ is the loss coefficient due to liquid entering from the outside into section 1, K_{1-2} is the loss coefficient due to the geometry change when crossing from section 1 into section 2 etc. The minor pressure loss between two geometries is defined conservatively by the higher flow velocity among them. Alternatively, by using Equation (4.28) with the density being constant as discussed before, using the smaller cross-section area will produce the same result. Therefore, as can be seen in Equation (4.35), the A_j values vary with their corresponding K_j coefficients.

4.1.3 Steady State Natural Convection Flow

Inputting Equations (4.29) and (4.35) into Equation (4.26), and Equations (4.25) and (4.26) into Equation (4.3), and rearranging provides the expression for the flow rate:

$$\dot{M} = \sqrt[3]{\frac{2\rho_\infty^2 g\beta\dot{Q}}{\bar{c}_p} \frac{L_{\text{BC}}/2 + L_5}{\sum_i {}^{f_i L_i}/_{D_{\text{e}}^i A_i^2} + \sum_j {}^{K_j}/_{A_j^2}}} \ , \tag{4.36}$$

where the full sums are as in Equations (4.29) and (4.35).

Although seemingly analytical, Equation (4.36) requires iterations in order to be

solved. This comes from the fact that the friction factors f_i, as shown in Equations (4.30) and (4.33), are themselves dependent on the Reynolds number and therefore on the flow rate. Iterations of this sort and general modelling considerations will be addressed later in Chapter 5. The given flow rate allows to calculate the temperature rise along the channels for a given assembly power using Equation (4.13). The flow rate is also used to assess the heat transfer coefficient, as will be addressed next, and through that the clad and fuel temperatures as will be addressed in Section 4.4.

4.1.4 Heat Transfer Correlation

In order to evaluate the clad and fuel temperatures, knowledge of the heat transfer coefficient between the coolant and clad is required. Heat transfer correlations are usually of the form $\mathrm{Nu} = f(\mathrm{Re}, \mathrm{Pr})$ where Re is again the Reynolds number earlier defined in Equation (4.31). Nu is the Nusselt number defined as:

$$\mathrm{Nu} \equiv \frac{hD_\mathrm{e}}{k_\mathrm{w}} \,, \tag{4.37}$$

where h is the convective heat transfer coefficient in units $\mathrm{W\,m^{-2}\,K^{-1}}$ and k_w is the heat conductivity of water in units $\mathrm{W\,m^{-1}\,K^{-1}}$. Pr is the Prandtl number defined as:

$$\mathrm{Pr} \equiv \frac{c_p \mu}{k_\mathrm{w}} \,, \tag{4.38}$$

where μ is the viscosity in $\mathrm{Pa\,s}$.

As noted in the literature review, there is an uncertainty assigned with the heat transfer coefficient in natural convection flows. Garland [3] refers to the book "Introduction to Heat Transfer" by Incropera and Dewitt [37] for a suitable correlation for laminar flow in thin rectangular channels. The book gives figures for a selected number of channel width-to-thickness ratios, closest of which are for the ratio of 8 and infinity (parallel plates)[5]. The same ratio for a MNR channel is somewhere between the two, being close to 20. The Nusselt number was discovered to be independent of the flow rate and Reynolds number in laminar flow, and for the two relevant ratios is

[5]The information in the book is borrowed from Kay and Crawford's "Convection Heat and Mass Transfer" [38] where also no additional information or general formula are present.

as given in "Introduction to Heat Transfer":

$$\mathrm{Nu}_{\mathrm{lam}} = \begin{cases} 6.49 & \text{if } \dfrac{1}{r} = 8 \\ 8.23 & \text{if } \dfrac{1}{r} = \infty \end{cases} , \tag{4.39}$$

where r is the inverse ratio to the one mentioned here, as used in Equations (4.32) and (4.34).

The classic Dittus-Boelter correlation is used to evaluate the heat transfer coefficient between the clad and the coolant in turbulent flow. It is valid for single-phase flows of both liquid water and superheated[6] steam. The correlation is [34]:

$$\mathrm{Nu}_{\mathrm{tur}} = 0.023\mathrm{Re}^{0.8}\mathrm{Pr}^{0.4} . \tag{4.40}$$

The Nusselt and Reynolds numbers are usually written as Nu_D and Re_D to denote that the correlation is based on the diameter D (or equivalent diameter D_{e}). Different correlations for the Nusselt and Reynolds numbers exist for different geometries denoted by other subscripts. From the above, the convective heat transfer coefficient for single-phase flow within a channel is found to be:

$$h = \begin{cases} \dfrac{\mathrm{Nu}_{\mathrm{lam}} k_{\mathrm{w}}}{D_{\mathrm{e4}}} & \text{for laminar} \\ 0.023 \left(\dfrac{D_{\mathrm{e4}} \dot{m}}{\mu A_4 / 17} \right)^{0.8} \left(\dfrac{c_p \mu}{k_{\mathrm{w}}} \right)^{0.4} \dfrac{k_{\mathrm{w}}}{D_{\mathrm{e4}}} & \text{for turbulent} \end{cases} . \tag{4.41}$$

4.2 Two Phase Natural Convection

Similarly to the single-phase treatment in the last section, an expression for the steady-state natural-convection flow rate is developed for 1-D two-phase conditions. The model for this segment deals with vapour qualities up to 100% such that there is no occurrence of superheated steam along the heated section. Cases in which superheated steam above the two-phase region does appear will be modelled in the uncovered core treatment. Relying back on Todreas and Kazimi, the treatment starts again with the

[6]Superheating is the state of gas being above the energy of saturation. For water it is the gaseous phase otherwise known as steam.

1-D momentum conservation in Equation (4.1). The same assumptions leading to Equation (4.3) hold such that the driving phenomena is as earlier the balance of the hydrostatic term with the pressure loss term. This time, the density in the governing Equation (4.3) is handled differently, and thus the hydrostatic and pressure loss terms need to be redeveloped.

In order to begin the treatment an additional glance at the assembly is required. A zoom onto section 4 from Figure 4.1 is presented in Figure 4.2. The 'cold' pool liquid passes through sections 1-3 and enters section 4 subcooled[7]. It starts picking up heat at point B and remains single phase until it reaches saturation. The fraction in height of the heated section (BC) occupied by the single-phase liquid is denoted as $L_{1\phi}$ as shown in Figure 4.2. At this point the liquid becomes a two-phase mixture growing in vapour quality[8] as it moves up the channel. Finally after reaching the end of the heated section at point C the quality remains constant at its exit value until the mixture can come in contact with the cold liquid at the exit from the assembly, being the exit from section 5. The fraction in height of the heated section occupied by the two-phase mixture is denoted as $L_{2\phi}$ as shown in Figure 4.2.

4.2.1 Hydrostatic Term

As shown in Equation (4.15) the hydrostatic term can be represented as the difference between the mean cold and mean hot densities multiplied by the length which they occupy and the gravity constant. Rewriting Equation (4.15) by replacing $(H_{\mathrm{D}} - H_{\mathrm{B}})$ in terms of the lengths shown in Figure 4.2 results in:

$$\Delta p_{\mathrm{b}} = (\bar{\rho}_{\mathrm{cold}} - \bar{\rho}_{\mathrm{hot}})\, g\, (L_{\mathrm{BC}} + L_{\mathrm{C-5}} + L_5) \ , \tag{4.42}$$

where the mean densities $\bar{\rho}_{\mathrm{cold}}$ and $\bar{\rho}_{\mathrm{hot}}$ will be recalculated here for the two-phase case.

Refer to the simplification given in Equation (4.24). It was introduced as a conservative simplification to ignore the small gap between the point where the fuel ends and the point where the clad ends, denoted as $L_{\mathrm{C-5}}$ in Figure 4.2. Taking into account both $L_{\mathrm{C-5}}$ and $L_{3-\mathrm{B}}$ considerably complicates, not only the hydrostatic term

[7]Subcooling is the state of liquid being below the energy of saturation.

[8]The flow quality is defined as the flow fraction of vapour out of the total flow. The term will be properly presented later.

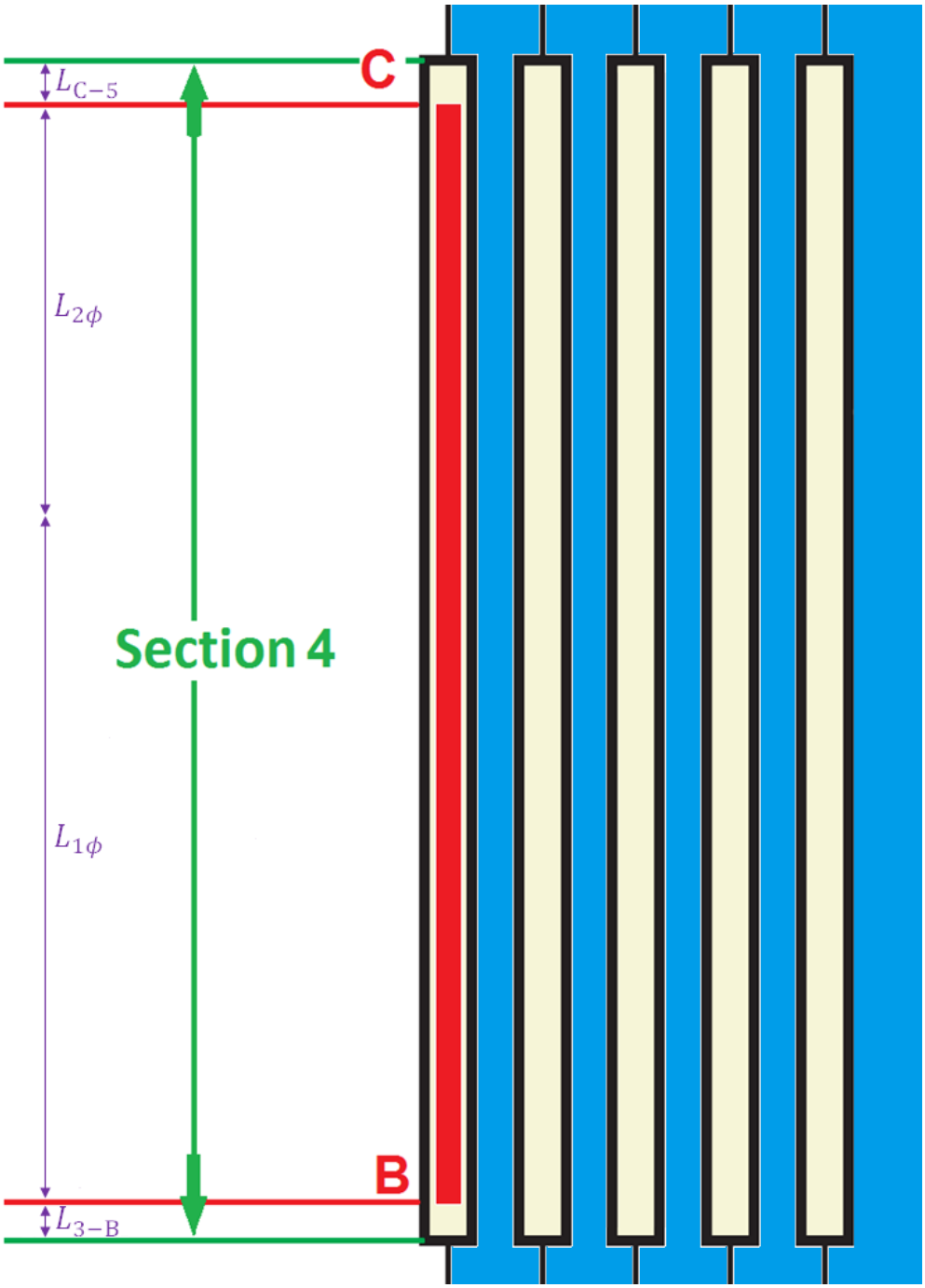

Figure 4.2: A two-phase representation of section 4 in the MNR assembly. New length figures are presented, where $L_{1\phi}$ is the (arbitrary and changing with different assembly powers and parameters) length of the single-phase region, $L_{2\phi}$ the corresponding length of the two-phase region, and L_{3-B} and L_{C-5} are the gaps between the edges of the fuel and the edges of the plate. Using fuel technical drawing on p. 16.3-24 from the MNR safety report [1].

as in the single-phase case, but also the pressure loss term in the two-phase case as will be addressed shortly. Since these gaps are small compared to the plate's height, and since the clad is the relatively high conducting aluminium, the simplification in Equation (4.24) is used again. It is implemented in a broader sense such that in addition to Equation (4.24) section 4 is now the heated section, being slightly larger than BC in reality:

$$L_{\mathrm{BC}} \cong L_4 \ , \tag{4.43}$$

meaning also that

$$L_4 \cong L_{1\phi} + L_{2\phi} \ . \tag{4.44}$$

It is not necessarily conservative anymore since although the exit section where there is no more change in density is smaller in accordance with Equation (4.24) ($L_5 < L_{\mathrm{CD}}$), the heated section is slightly larger than in reality ($L_4 > L_{\mathrm{BC}}$). This effect is assumed to be small since L_4 is larger than L_{BC} by less than 5%.

Applying assumptions from Equation (4.24) and Equations (4.43) and (4.44) in Equation (4.42) changes it to:

$$\Delta p_{\mathrm{b}} = (\bar{\rho}_{\mathrm{cold}} - \bar{\rho}_{\mathrm{hot}})\, g\, (L_4 + L_5) \ . \tag{4.45}$$

An important parameter in two-phase flow is the void fraction, defined as the volume of vapour divided by the volume of the total mixture in the channel:

$$\alpha \equiv \frac{V_{\mathrm{g}}}{V_{\mathrm{g}} + V_{\mathrm{f}}} \ , \tag{4.46}$$

where V_{g} and V_{f} are the volumes of the vapour and liquid phases respectively.

Another important parameter in two-phase flow is the flow quality, defined as the flow fraction of vapour out of the total flow:

$$x \equiv \frac{\dot{M}_{\mathrm{g}}}{\dot{M}_{\mathrm{g}} + \dot{M}_{\mathrm{f}}} \ , \tag{4.47}$$

where as earlier the subscripts g and f stand for the vapour (gas) and liquid (fluid) respectively.

Adding to the void fraction and quality, a third important parameter in two-phase

flows is the slip ratio S, which is defined as the ratio of the vapour and liquid velocities:

$$S \equiv \frac{v_{\mathrm{g}}}{v_{\mathrm{f}}} \,, \tag{4.48}$$

where the subscripts g and f mean the same as earlier.

Finally, a useful relation between the void fraction, quality and slip ratio for 1-D two-phase flow is given by manipulating the parameters above [39]:

$$\alpha = \frac{1}{1 + \dfrac{1-x}{x}\dfrac{\rho_{\mathrm{g}}}{\rho_{\mathrm{f}}}S} \,, \tag{4.49}$$

where ρ_{g} is the density of single-phase saturated vapour and ρ_{f} is the density of the single-phase saturated liquid. This is a fundamental relation in two-phase flow and different correlations are used for mostly the slip ratio in order to obtain a definitive relation between α and x.

As discussed in Chapter 2, the HEM model is appropriate for the given treatment due to the narrow channels of the MNR assemblies which impede slip. In the HEM model, the two phases are considered to be in thermodynamic equilibrium as well as flowing at the same rate, such that the slip ratio in Equation (4.48) becomes a unity. This turns Equation (4.49) into:

$$\alpha = \frac{1}{1 + \dfrac{1-x}{x}\dfrac{\rho_{\mathrm{g}}}{\rho_{\mathrm{f}}}} \,. \tag{4.50}$$

The mixture density in two-phase flow can now be presented. It is defined as:

$$\rho_{\mathrm{m}} = \alpha\rho_{\mathrm{g}} + (1-\alpha)\rho_{\mathrm{f}} \,. \tag{4.51}$$

Following again the treatment by Todreas and Kazimi, inputting the HEM expression for α from Equation (4.50) into Equation (4.51) and manipulating the expression algebraically the mixture density becomes:

$$\rho_{\mathrm{m}} = \frac{\rho_{\mathrm{f}}}{1 + x\left(\dfrac{\rho_{\mathrm{f}}}{\rho_{\mathrm{g}}} - 1\right)} \cong \frac{\rho_{\mathrm{f}}}{1 + x\dfrac{\rho_{\mathrm{f}}}{\rho_{\mathrm{g}}}} \,, \tag{4.52}$$

where the last approximation is valid since, both for high pressures in a PWR such as in the treatment in Todreas and Kazimi and more so at close to atmospheric pressures such as in the MNR, the saturated liquid density is orders of magnitude larger than that of the saturated vapour, $\rho_{\mathrm{f}}/\rho_{\mathrm{g}} \gg 1$.

Next, define the exit quality from the assembly by x_{exit}. The HEM model retains linearity in all axially dependent parameters in the heated section, similarly to the single-phase treatment, provided the axial power distribution remains constant as before. Therefore, the quality rise along the two-phase portion of the heated section is also linear as can be expressed by:

$$\frac{dx}{dz} = \frac{x_{\mathrm{exit}}}{L_{2\phi}} \, . \tag{4.53}$$

Last, it is useful to group the liquid and vapour densities, and the exit quality to a single variable as follows:

$$\gamma \equiv x_{\mathrm{exit}} \frac{\rho_{\mathrm{f}}}{\rho_{\mathrm{g}}} \, . \tag{4.54}$$

At this point, returning to Equation (4.45), the mean densities can be calculated again using Equation (4.16) by incorporating the traits of the two phase mixture. Approaching to calculate the mean cold leg density, the same assumption as in the single-phase case holds. The hot substance dissipates immediately into the cold pool as soon as it exits from the assembly. Therefore the mean cold density is simply:

$$\bar{\rho}_{\mathrm{cold}} = \rho_{\infty} \, . \tag{4.55}$$

The average hot leg density, using Equation (4.16) along with the assumptions in Equation (4.24) and Equations (4.43) and (4.44), can be written as:

$$\bar{\rho}_{\mathrm{hot}} = \frac{1}{L_4 + L_5} \int_{Z_4}^{Z_{\mathrm{D}}} \rho \, dz = \frac{1}{L_4 + L_5} \left(\int_{Z_4}^{Z_{\mathrm{f}}} \rho \, dz + \int_{Z_{\mathrm{f}}}^{Z_5} \rho_{\mathrm{m}} \, dz + \int_{Z_5}^{Z_{\mathrm{D}}} \rho_{\mathrm{m}} \, dz \right) \, , \tag{4.56}$$

where Z_4 denotes the height of entrance into section 4, Z_5 denotes the height of entrance into section 5 and Z_{f} denotes the saturation point of the liquid along section 4, pointing to where the two-phase region starts. The first term on the right accounts for the liquid density in the single-phase region, the second for the mixture density in the two-phase region and the third for section 5 which is unheated but still holds the

two-phase mixture which dissipates only outside of it.

The first integral on the right is similar to the one in Equation (4.8). Assuming that the density rise along the single-phase part is linear as before its result is the average density in that part:

$$\int_{Z_4}^{Z_\mathrm{f}} \rho \, dz = \frac{\rho_\infty + \rho_\mathrm{f}}{2}(Z_\mathrm{f} - Z_4) = \frac{\rho_\infty + \rho_\mathrm{f}}{2} L_{1\phi} = \bar{\rho}_\mathrm{l} L_{1\phi} \ , \tag{4.57}$$

where the density average was denoted again as $\bar{\rho}_\mathrm{l}$, only this time the exit density is fixed to the liquid saturation density.

The second integral on the right is solved by inputting the expression for the mixture density obtained in Equation (4.52) into Equation (4.56) resulting in:

$$\int_{Z_\mathrm{f}}^{Z_5} \rho_\mathrm{m} \, dz = \int_{Z_\mathrm{f}}^{Z_5} \frac{\rho_\mathrm{f}}{1 + x\frac{\rho_\mathrm{f}}{\rho_\mathrm{g}}} \, dz \ . \tag{4.58}$$

Next, the relation in Equation (4.53) is used to change the variable of integration from the height z to the quality x:

$$\int_{Z_\mathrm{f}}^{Z_5} \rho_\mathrm{m} \, dz = \int_{x_{(z=Z_\mathrm{f})}}^{x_{(z=Z_5)}} \frac{\rho_\mathrm{f}}{1 + x\frac{\rho_\mathrm{f}}{\rho_\mathrm{g}}} \frac{dz}{dx} \, dx = \rho_\mathrm{f} \frac{L_{2\phi}}{x_\mathrm{exit}} \int_0^{x_\mathrm{exit}} \frac{dx}{1 + x\frac{\rho_\mathrm{f}}{\rho_\mathrm{g}}} = \rho_\mathrm{f} \frac{L_{2\phi}}{x_\mathrm{exit}} \frac{\rho_\mathrm{g}}{\rho_\mathrm{f}} \ln\left(1 + x\frac{\rho_\mathrm{f}}{\rho_\mathrm{g}}\right) . \tag{4.59}$$

Using Equation (4.54), Equation (4.58) becomes:

$$\int_{Z_\mathrm{f}}^{Z_5} \rho_\mathrm{m} \, dz = \frac{\ln(1+\gamma)}{\gamma} \rho_\mathrm{f} L_{2\phi} \ . \tag{4.60}$$

The third integral on the right is solved by noticing that the quality doesn't change in section 5 since there is no more heating, remaining x_exit after the exit from section 4:

$$\begin{aligned} \int_{Z_5}^{Z_\mathrm{D}} \rho_\mathrm{m} \, dz = \int_{Z_5}^{Z_\mathrm{D}} \frac{\rho_\mathrm{f}}{1 + x\frac{\rho_\mathrm{f}}{\rho_\mathrm{g}}} \, dz = \frac{\rho_\mathrm{f}}{1 + x_\mathrm{exit}\frac{\rho_\mathrm{f}}{\rho_\mathrm{g}}} \int_{Z_5}^{Z_\mathrm{D}} dz = \frac{\rho_\mathrm{f}}{1+\gamma}(Z_\mathrm{D} - Z_5) \\ = \frac{1}{1+\gamma} \rho_\mathrm{f} L_5 \ . \end{aligned} \tag{4.61}$$

Inputting Equations (4.57), (4.60) and (4.61) into Equation (4.56), the average hot

leg density is found to be:

$$\bar{\rho}_{\text{hot}} = \frac{1}{L_4 + L_5}\left(\bar{\rho}_{\text{l}} L_{1\phi} + \frac{\ln(1+\gamma)}{\gamma}\rho_{\text{f}} L_{2\phi} + \frac{1}{1+\gamma}\rho_{\text{f}} L_5\right) . \tag{4.62}$$

Inserting the expressions for the cold and hot leg mean densities in Equations (4.55) and (4.62) into the expression for the hydrostatic driving term in Equation (4.45) gives:

$$\Delta p_{\text{b}} = \left(\rho_\infty (L_4 + L_5) - \bar{\rho}_{\text{l}} L_{1\phi} - \frac{\ln(1+\gamma)}{\gamma}\rho_{\text{f}} L_{2\phi} - \frac{1}{1+\gamma}\rho_{\text{f}} L_5\right) g . \tag{4.63}$$

4.2.2 Pressure Loss Term

In two-phase flow, the friction and form losses are multiplied by a factor called the 'two-phase multiplier'. This multiplier represents the sharp increase in losses due to the change in density from vaporization. In the HEM model it is given by the ratio of the saturated liquid density to the mixture density [32]:

$$\phi^2 \cong \frac{\rho_{\text{f}}}{\rho_{\text{m}}} . \tag{4.64}$$

Both friction factors and two-phase multipliers are calculated by various methods in different two-phase models. In the HEM model, both quantities are calculated and used as for the liquid phase, denoted by the 'liquid only' subscripts, f_{lo} and ϕ^2_{lo}. This means that in the calculation of the friction loss, Equations (4.33) and (4.34) remain valid by use of the liquid-only Reynolds number and liquid properties in Equation (4.31). Since only the the HEM model is used in this work, the subscript 'lo' is dropped with the consent that all properties are liquid properties.

As with the hydrostatic term, the losses term is taken from the balance in Equation (4.3) and modified for the two-phase case. The major loss is as in Equations (4.26) and (4.29) and is given by:

$$\begin{aligned}\Delta p_{\text{maj}} = \Bigg(&\frac{f_1 L_1}{2\rho_\infty D_1 A_1^2} + \frac{f_2 L_2}{2\rho_\infty D_2 A_2^2} + \frac{f_3 L_3}{2\rho_\infty D_{\text{e}3} A_3^2} + \frac{f_4 L_{3-\text{B}}}{2\rho_\infty D_{\text{e}4} A_4^2} + \frac{f_4 L_{1\phi}}{2\bar{\rho}_{\text{l}} D_{\text{e}4} A_4^2} \\ &+ \bar{\phi}^2_{\text{fC}} \frac{f_4 L_{2\phi}}{2\rho_{\text{f}} D_{\text{e}4} A_4^2} + \bar{\phi}^2_{\text{CD}} \frac{f_4 L_{\text{C}-5}}{2\rho_{\text{f}} D_{\text{e}4} A_4^2} + \bar{\phi}^2_{\text{CD}} \frac{f_5 L_5}{2\rho_{\text{f}} D_{\text{e}5} A_5^2}\Bigg) \dot{M}^2 ,\end{aligned} \tag{4.65}$$

where $\bar{\phi}_{\mathrm{fC}}$ and $\bar{\phi}^2_{\mathrm{CD}}$ are averaged two-phase multipliers over the boiling length $L_{2\phi}$ and non heated two-phase length L_{CD} respectively. The two-phase multipliers mathematically appear from the density in the heated and adiabatic two-phase sections, which changes to ρ_{m} instead of ρ_∞ and $\bar{\rho}_{\mathrm{l}}$ in the earlier terms. By multiplying these terms by $\rho_{\mathrm{f}}/\rho_{\mathrm{f}}$, the expression for the mixture density is replaced by the expression for the saturation density divided by the two-phase multiplier as given in Equation (4.64).

As mentioned earlier, in agreement with the approximation done in the hydrostatic term in Equations (4.43) and (4.44), ignoring the small edges $L_{3-\mathrm{B}}$ and $L_{\mathrm{C}-5}$ and taking the heated section BC as the entire section 4, section CD is taken as section 5, as in Equation (4.24). This simplification helps prevent complications associated with mixing the terms relating to the heated sections (BC and CD) which are mostly hydrostatic-term dependent and terms relating to geometry which are mostly friction and minor loss related (4 and 5), as can be seen by the cumbersome expression in Equation (4.65).

Subsequently, the expression in Equation (4.65) becomes:

$$\Delta p_{\mathrm{maj}} = \left(\frac{f_1 L_1}{2\rho_\infty D_1 A_1^2} + \frac{f_2 L_2}{2\rho_\infty D_2 A_2^2} + \frac{f_3 L_3}{2\rho_\infty D_{\mathrm{e}3} A_3^2} + \frac{f_4 L_{1\phi}}{2\bar{\rho}_{\mathrm{l}} D_{\mathrm{e}4} A_4^2} + \bar{\phi}_4^2 \frac{f_4 L_{2\phi}}{2\rho_{\mathrm{f}} D_{\mathrm{e}4} A_4^2} + \bar{\phi}_5^2 \frac{f_5 L_5}{2\rho_{\mathrm{f}} D_{\mathrm{e}5} A_5^2} \right) \dot{M}^2 \,, \quad (4.66)$$

where $\bar{\phi}_4^2$ and $\bar{\phi}_5^2$ are replacing $\bar{\phi}_{\mathrm{fC}}$ and $\bar{\phi}^2_{\mathrm{CD}}$ respectively, now that interval BC is approximated as section 4 and interval CD as section 5.

The aforementioned section averaged two-phase multipliers are calculated from the HEM two-phase multiplier definition in Equation (4.64) as follows. For section 4:

$$\bar{\phi}_4^2 = \frac{1}{L_{2\phi}} \int_{Z_{\mathrm{f}}}^{Z_5} \frac{\rho_{\mathrm{f}}}{\rho_{\mathrm{m}}} \, dz = \frac{1}{L_{2\phi}} \int_{x=0}^{x=x_{\mathrm{exit}}} \frac{\rho_{\mathrm{f}}}{\rho_{\mathrm{f}} / \left(1 + x \frac{\rho_{\mathrm{f}}}{\rho_{\mathrm{g}}}\right)} \frac{dx}{dx} \, dz = \ldots = 1 + \frac{\gamma}{2} \,, \quad (4.67)$$

in resemblance to Equations (4.58) to (4.60). For section 5, in a similar way, the following expression is obtained:

$$\bar{\phi}_5^2 = 1 + \gamma \,, \quad (4.68)$$

In accordance with Equation (4.35), the minor loss is given by:

$$\Delta p_{\min} = \left(\frac{K_{\infty 1}}{2\rho_\infty A_1^2} + \frac{K_{1-2}}{2\rho_\infty A_1^2} + \frac{K_{2-3}}{2\rho_\infty A_2^2} + \frac{K_{3-4}}{2\rho_\infty A_4^2} + \phi_5^2 \frac{K_{4-5}}{\rho_\mathrm{f} A_4^2} + \phi_5^2 \frac{K_{5\infty}}{2\rho_\mathrm{f} A_5^2} \right) \dot{M}^2 \ , \quad (4.69)$$

where the two-phase multiplier ϕ_5 is not an average but the local multiplier since the minor loss is local. It is however, for both terms concerned with it, identical to $\bar{\phi}_5^2$ since the quality in both is already the, no longer changing, exit quality x_{exit}.

$$\phi_5^2 = 1 + \gamma \ . \quad (4.70)$$

4.2.3 Steady State Natural Convection Flow

By inserting Equations (4.66) and (4.69) along with the definitions for the two-phase multipliers (Equations (4.67), (4.68) and (4.70)) into Equation (4.26), and Equations (4.26) and (4.63) into Equation (4.3) the expression for the two-phase natural-convection flow rate is obtained:

$$\left(\rho_\infty (L_4 + L_5) - \bar{\rho}_\mathrm{l} L_{1\phi} - \rho_\mathrm{f} \frac{\ln(1+\gamma)}{\gamma} L_{2\phi} - \rho_\mathrm{f} \frac{1}{1+\gamma} L_5 \right) g = \left(\sum_i \frac{f_i L_i}{2\rho_i D_\mathrm{e}^i A_i^2} + \sum_j \frac{K_j}{2\rho_j A_j^2} \right) \dot{M}^2 \ , \quad (4.71)$$

where similarly to Equation (4.36), the full expressions for the major and minor losses, fully described in Equations (4.66) and (4.69), have been spared from the viewer's eyes. The friction and form loss factors are calculated as in the single-phase case (Equations (4.33) and (4.34)) from the use of liquid-only parameters. The values for $L_{1\phi}$ and $L_{2\phi}$ and obviously γ are directly related to the flow rate through the quality, making, on top of the dependence of the friction factors on the flow rate, Equation (4.71) analytically unsolvable.

In order to present the dependence of $L_{1\phi}$, $L_{2\phi}$ and γ on the flow rate and quality, a short discussion on 'Thermodynamic Quality' is required. For that purpose first define the latent heat of vaporization:

$$h_\mathrm{fg} = h_\mathrm{g} - h_\mathrm{f} \ , \quad (4.72)$$

where h_g is the specific enthalpy[9] of saturated gaseous water (vapour) and h_f the specific enthalpy of saturated fluid water (liquid), both in units $\mathrm{J\,kg^{-1}}$. The flow thermodynamic quality, or 'Equilibrium Quality' (in short TD quality), is defined as [39]:

$$x_e = \frac{h(x_e) - h_f}{h_{fg}} \,, \tag{4.73}$$

where $h(x_e)$ is the specific enthalpy of the fluid (either subcooled, two phase or superheated) at the given point (corresponding to the TD quality). It denotes how 'close' the mixture is to being either saturated liquid or saturated vapour (from 0 for fully saturated liquid to 1 for fully saturated vapour) but is also valid beyond that range for subcooled or superheated conditions ($-\infty < x_e < \infty$). Under HEM conditions, the flow quality and TD quality are one, since the phases are at equilibrium. Care should be taken when using the TD quality, since Equation (4.71) and particularly γ are both valid and defined only for the range $0 < x < 1$ in the model.

With the agreement that the flow quality can be represented by means of the TD quality, define the inlet quality as:

$$x_\infty = \frac{h_\infty - h_f}{h_{fg}} \,, \tag{4.74}$$

where h_∞ is the specific enthalpy of the bulk cold pool liquid. The exit quality in a MNR assembly is therefore:

$$x_{exit}(\dot{M}) = x_\infty + \frac{\dot{Q}}{\dot{M} h_{fg}} \,. \tag{4.75}$$

Equation (4.75) is input into Equation (4.54) in order to obtain the dependence of γ on the flow rate to be used in Equation (4.71). Lastly, due to the linearity of the model and subsequent linear quality rise along the heated section, the single and two-phase lengths' dependence on the flow rate can be obtained by using Equation (4.75). This allows to calculate the thermodynamic quality rise to the point of liquid saturation enthalpy and the total quality rise in the channel. Dividing one by the other the following is obtained [32]:

$$\frac{L_{1\phi}}{L_4} = \frac{0 - x_\infty}{x_{exit} - x_\infty}$$

[9]Notice the difference between h, which is the convective heat transfer coefficient, and various water enthalpy notations such as h_f.

$$L_{1\phi} = -\frac{x_\infty}{x_{\text{exit}} - x_\infty} L_4 \qquad ; \qquad L_{2\phi} = L_4 - L_{1\phi} \,. \tag{4.76}$$

The solution to the pressure-drop balance in Equation (4.71) specifies the flow rate for a given assembly power $\dot{Q}$ as in the single-phase case. The suggested approach by Todreas and Kazimi to numerically solve Equation (4.71) is by separating the constants to one side of the equation and plotting the two sides of the equation against each other. The constant term remaining consists of the hydrostatic column of cold liquid along the height of the heated section, being $\rho_\infty(L_4 + L_5)g$. The intersections of the curve on the variable side of the equation with the driving term are the solutions for the possible flow rates at the given power.

Since the fluid coming out of the assembly is a two-phase mixture, its temperature will be bound by the saturation temperature at core depth. The flow rate and exit quality are used to calculate the two-phase heat transfer coefficient as shown in the next section. The exit temperature (saturation) and the heat transfer coefficient are used as earlier to asses the temperature of the clad and fuel at the upper edge of the channel. The derivation of the clad and fuel temperatures, again, will be described in Section 4.4.

4.2.4 Heat Transfer Correlation

Onset of boiling has a positive increasing effect on the heat transfer so long as heat flux values are below those that create big stable patches of vapour on the solid surface, corresponding with the CHF phenomena. As noted in the literature review, this does not occur for conditions similar to those in the MNR for heat fluxes below $950\,\text{kW}\,\text{m}^{-2}$ [5]. Calculating the MNR plate heat flux for reference core and plate power shows it to be around $415\,\text{kW}\,\text{m}^{-2}$. Therefore, even in higher powers corresponding to two-phase flow and heat transfer, the conditions in the MNR case do not raise a concern for burnout by reaching of CHF and there is no need to check for it.

The increase in heat transfer compared to the single-phase case is usually by several orders of magnitude, thus bringing clad tempeartures much closer to coolant temperature. A wide applicability correlation developed by Kandlikar [40] is suggested in the book "Fundamentals of Heat and Mass Transfer" [34] and translates to an MNR

channel as:

$$h_{2\phi} = h(1-x)^{0.8} \times \max \left\{ \begin{array}{l} 1.136x^{0.72}(1-x)^{-0.72} \left(\frac{\rho_{\mathrm{f}}}{\rho_{\mathrm{g}}}\right)^{0.45} + 667.2 \left(\frac{\dot{q}'' A_4/17}{\dot{m} h_{\mathrm{fg}}}\right)^{0.7} \\ 0.6683x^{0.16}(1-x)^{-0.16} \left(\frac{\rho_{\mathrm{f}}}{\rho_{\mathrm{g}}}\right)^{0.1} + 1058 \left(\frac{\dot{q}'' A_4/17}{\dot{m} h_{\mathrm{fg}}}\right)^{0.7} \end{array} \right\}, \tag{4.77}$$

where h is the previously defined single-phase-liquid heat transfer coefficient (Equation (4.41)) and $\dot{q}''$ is the heat flux from the clad to the coolant, which will be addressed later. Equation (4.77) is calculated for any flow quality x, particularly recommended for use in the range $0 < x < 0.8$ [34]. It is calculated at the edge of the heated channel (with x_{exit}) since the expected behaviour for the heat transfer coefficient is to diminish with rising quality, thus being a conservative estimate. Also, similarly to the single-phase case, the power of a channel used for the calculation is taken as the power of the hottest one.

In his paper, Kandlikar proposes to use the Dittus-Boelter correlation for the liquid heat transfer coefficient (with the exception of using a Reynolds number modified by factor $(1-x)$) [40]. He also suggests that the fluid properties for the calculation should be those at saturation. In a following paper he proposes instead the use of a correlation by Gnielinski and a correlation by Petukhov and Popov, which better account for Prandtl number behaviour in different fluids [41]. These are also the proposed correlations in "Fundamentals of Heat and Mass Transfer". Since the latter are strictly for use in turbulent flows (in single phase) which isn't necessarily the case in the MNR channels under decay heat, and since apparently the switch was made to accommodate for different liquids than water, this work keeps the use of the classic Dittus-Boelter equation. As will be shown later, the two-phase heat transfer coefficient is mainly addressed in order to establish that even with correlation error, it's order of magnitude is expected to be so large such that clad temperature is going to be very close to that of the coolant.

4.3 Uncovered Core Overflow and Steaming

At the stage right before core uncovery the liquid was naturally convected upwards, with or without boiling. As will be shown in the results, none of the covered core

scenarios for conditions in the MNR produce superheated steam at the assembly exit but rather a two-phase mixture at most. When the water in the pool starts uncovering the fuel assemblies, two distinct stages can be recognized depending on the pool water height.

At the first stage, although the pool water around the assembly starts uncovering it, the water within the assembly and particularly in the channels keeps the entire assembly covered. If the coolant was leaving the assembly as a two-phase mixture at the point of uncovering, it had already increased its specific volume compared to the cold water outside such that it will keep covering the assembly and spilling out of it until achieving conditions for which it reaches vapour saturation enthalpy at the end of the heated channel. Alternatively, if the water in the channels was subcooled at the onset of uncovering, the increase in volume will be much more modest and as the pool level decreasing continues the level inside may drop below the top of the assembly. However, this will not remain at a steady state as the stagnant water in the channels will shortly after start boiling as well, leading either to the two-phase steady state just described or intermittent geysering. For these conditions Figure 4.2 can be referred to for visualizing the flow and associated parameters in the assembly.

The second stage is after the coolant has reached saturated vapour quality in the heated channel. At this point the two phase mixture itself starts uncovering the heated section, leaving the uncovered part exposed to heat removal by superheated steam. This point, from which clad melting begins being an issue of concern, occurs for pool levels substantially lower than those at the onset of uncovering, being closer to the bottom of the heated section (section BC as in Figure 4.1). The height of the two-phase mixture is henceforth referred to as 'swell height'. For convenience both the pool height and the swell height for these scenarios are measured from the bottom of the heated section and not from the bottom of the assembly[10]. The height for which the swell height drops below the top of the heated section and uncovering of the fuel plates starts is henceforth referred to as 'critical height'. These new parameters can be seen in the conceptual drawing in Figure 4.3.

The treatment as before is that of steady state due to the slow nature of the transient. The approximations and simplifications that were used in the single and two-phase natural convection cases as given in Equations (4.24) and (4.43) are also

[10]The swell height, being dependent on heating from the plates, cannot be lower than the bottom of the plate's section or exist for pool heights below that level either. For pool heights lower than the bottom of the heated section heat is removed from the plates to air.

used for the same reasons, and therefore since the swell height is still covering the entire section 4 at this point, Equation (4.44) remains also true (refer back to Figures 4.1 and 4.2). This also includes the simplification in taking the heat flux in the heated channel as constant and not as a cosine shape. Discussion on the applicability of using the latter simplification for the uncovered case is found in Appendix A.

4.3.1 Hydrostatic Term

For pool heights above the critical height, the two-phase mixture covers the entire assembly, and the driving term, as defined in Equation (4.22), is given by:

$$\Delta p_{\mathrm{b}} = p_{\mathrm{cold}} - p_{\mathrm{hot}} = \rho_{\infty} g \left(L_{\mathrm{AB}} + H_{\mathrm{pool}} \right) - \left(\rho_{\infty} g L_{\mathrm{AB}} + \bar{\rho}_{\mathrm{l}} g L_{1\phi} + \bar{\rho}_{\mathrm{m}} g L_{2\phi} + \rho_{\mathrm{m}}^{\mathrm{exit}} g L_5 \right) , \tag{4.78}$$

where H_{pool} is the pool height, $\bar{\rho}_{\mathrm{l}}$ is the single-phase average density as defined in Equation (4.57) and $\bar{\rho}_{\mathrm{m}}$ is the average density of the two-phase mixture covering the two-phase length, defined by:

$$\bar{\rho}_{\mathrm{m}} = \frac{1}{L_{2\phi}} \int_{Z_{\mathrm{f}}}^{Z_5} \rho_{\mathrm{m}} \, dz \ . \tag{4.79}$$

An almost identical formula was solved in Equations (4.58) to (4.60) giving:

$$\bar{\rho}_{\mathrm{m}} = \frac{\ln(1+\gamma)}{\gamma} \rho_{\mathrm{f}} \ , \tag{4.80}$$

The exit mixture density $\rho_{\mathrm{m}}^{\mathrm{exit}}$ is the density at the exit from the heated section corresponding to the quality x_{exit}, which can be obtained by inserting x_{exit} into the definition of the mixture density in Equation (4.52):

$$\rho_{\mathrm{m}}^{\mathrm{exit}} = \frac{1}{1+\gamma} \rho_{\mathrm{f}} \ . \tag{4.81}$$

Rearranging and canceling terms in Equation (4.78) produces:

$$\Delta p_{\mathrm{b}} = \left(\rho_{\infty} H_{\mathrm{pool}} - \bar{\rho}_{\mathrm{l}} L_{1\phi} - \frac{\ln(1+\gamma)}{\gamma} \rho_{\mathrm{f}} L_{2\phi} - \frac{1}{1+\gamma} \rho_{\mathrm{f}} L_5 \right) g \ . \tag{4.82}$$

The last equation is very similar to the driving term in the two-phase convection case as in Equation (4.63), the difference being in the first term representing the cold water

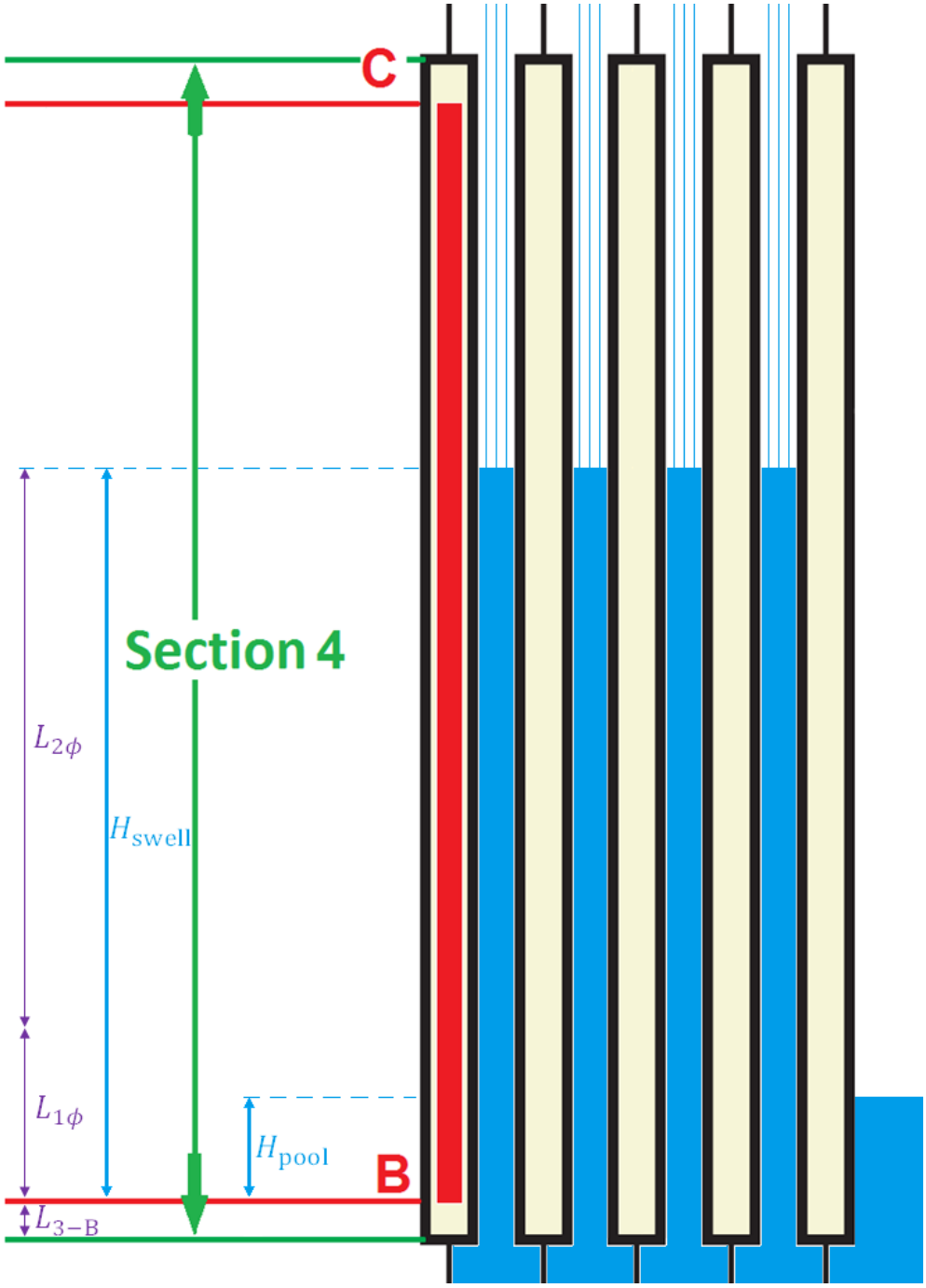

Figure 4.3: Representation of an uncovered MNR assembly. New length figures are presented, where $L_{1\phi}$ and $L_{2\phi}$ are bounded by the swell height H_{swell}. Pool height is H_{pool}. Using fuel technical drawing on p. 16.3-24 from the MNR safety report [1].

column pressure. This term here starts to diminish as the draining progresses since $H_{\text{pool}} < L_4 + L_5$.

For pool heights below the critical height, the swell height is at most as tall as section 4 and for steady state treatment cannot exist at an intermediate height anywhere within section 5. This is due to the fact that in that case there will be no flow out from the assembly (neither superheated steaming nor two-phase mixture). Therefore, at the point where pool height reaches the critical height, the last term vanishes in Equation (4.78) as no more two-phase mixture exists in section 5. The driving term becomes:

$$\Delta p_{\text{b}} = \left(\rho_\infty H_{\text{pool}} - \bar{\rho}_{\text{l}} L_{1\phi} - \frac{\ln(1+\gamma)}{\gamma} \rho_{\text{f}} L_{2\phi} \right) g \ . \tag{4.83}$$

Also, notice that Equation (4.76) is no longer valid since now:

$$L_{1\phi} + L_{2\phi} = H_{\text{swell}} \ , \tag{4.84}$$

where H_{swell} is the swell height. This will be elaborated on later in determining the flow rate and swell height.

4.3.2 Pressure Loss Term

For pool heights above the critical height, the two-phase mixture flows through the entire assembly and therefore both the major and the minor losses remain as in Equations (4.66) and (4.69) respectively, including their respective two-phase multipliers.

For pool heights below the critical height, as earlier, the two-phase mixture doesn't flow through section 5 anymore. Therefore, for the major losses, the last term in Equation (4.66) vanishes:

$$\Delta p_{\text{maj}} = \left(\frac{f_1 L_1}{2\rho_\infty D_1 A_1^2} + \frac{f_2 L_2}{2\rho_\infty D_2 A_2^2} + \frac{f_3 L_3}{2\rho_\infty D_{\text{e}3} A_3^2} + \frac{f_4 L_{1\phi}}{2\bar{\rho}_{\text{l}} D_{\text{e}4} A_4^2} + \bar{\phi}_4^2 \frac{f_4 L_{2\phi}}{2\rho_{\text{f}} D_{\text{e}4} A_4^2} \right) \dot{M}^2 \ , \tag{4.85}$$

Similarly, for the minor losses, the last two terms in Equation (4.69) vanish as well:

$$\Delta p_{\text{min}} = \left(\frac{K_{\infty 1}}{2\rho_\infty A_1^2} + \frac{K_{1-2}}{2\rho_\infty A_1^2} + \frac{K_{2-3}}{2\rho_\infty A_2^2} + \frac{K_{3-4}}{2\rho_\infty A_4^2} \right) \dot{M}^2 \ . \tag{4.86}$$

4.3.3 Steady State Two Phase and Steaming Flows

For pool height above the critical height the definitions for the single and two-phase lengths remain the same as in Equation (4.76). Therefore similarly to Equation (4.71) the pressure balance from which the flow rate can be deducted is:

$$\left(\rho_\infty H_{\text{pool}} - \bar{\rho}_\text{l} L_{1\phi} - \rho_\text{f} \frac{\ln(1+\gamma)}{\gamma} L_{2\phi} - \rho_\text{f} \frac{1}{1+\gamma} L_5\right) g = \left(\sum_i \frac{f_i L_i}{2\rho_i D_\text{e}^i A_i^2} + \sum_j \frac{K_j}{2\rho_j A_j^2}\right) \dot{M}^2 \ , \quad (4.87)$$

where the only difference from Equation (4.71) lies in the first term representing the cold water column pressure, being now $\rho_\infty H_{\text{pool}} g$ instead of $\rho_\infty (L_4 + L_5) g$. The dependence on $L_{1\phi}$, $L_{2\phi}$ and γ remains as in the two-phase covered case governed by Equations (4.75) and (4.76), where the exit quality x_{exit} remains a variable and the above figures are direct functions of the flow rate. The dependence of the flow rate on power is through the quality rise described in Equation (4.75). Equation (4.87) is therefore solved graphically in the same way Equation (4.71) is solved, to obtain the flow rate through the assembly.

For pool heights below the critical height the quality rise in the channel, similarly to the treatment in Equation (4.76), is now:

$$x_\text{f} = 0 = x_\infty + \frac{\dot{Q} L_{1\phi}/L_4}{\dot{M}} \ , \quad (4.88)$$

for the rise to saturated liquid quality x_f, and:

$$x_\text{g} = 1 = x_\infty + \frac{\dot{Q} H_{\text{swell}}/L_4}{\dot{M}} \ , \quad (4.89)$$

for the rise to saturated steam quality. Note that x_{exit} is no longer associated with the exit from section 4 but occurs somewhere below that point. Also directly related to the former, is the fact that the quality reaches 100% at the edge of the swell height, turning x_{exit} and subsequently γ into constants in a similar way the single-phase parameters and especially the density, was bound by liquid saturation values, turning it into a constant in the earlier two-phase convection case.

Dividing Equation (4.88) by Equation (4.89) yields this scenario's parallel to

Equation (4.76) in:

$$\frac{L_{1\phi}}{H_{\text{swell}}} = \frac{-x_\infty}{x_\text{g} - x_\infty} \equiv \theta \,, \tag{4.90}$$

where θ is used to group the expression for qualities in the last transition for convenience and is a constant since $x_{\text{exit}} = 1$. The single and two-phase lengths are now:

$$L_{1\phi} = \theta H_{\text{swell}} \qquad ; \qquad L_{2\phi} = (1-\theta)\, H_{\text{swell}} \,. \tag{4.91}$$

The mass flow rate out of the assembly at this point is by the steady steaming above the froth level of H_{swell} and is given by:

$$\dot{M}_\text{s} = \frac{\dot{Q} H_{\text{swell}}/L_4}{\Delta h} \,, \tag{4.92}$$

where Δh is the enthalpy rise required to bring the liquid from subcooled pool enthalpy to saturated steam enthalpy:

$$\Delta h = h_\text{f} - h_\infty + h_\text{fg} = h_\text{g} - h_\infty \,. \tag{4.93}$$

Since the heat flux is assumed constant, the power generating the steam in the covered fraction is just the full power times the covered fraction.

The pressure balance below the critical height can now be written as:

$$\left(\rho_\infty H_{\text{pool}} - \bar{\rho}_\text{l} L_{1\phi} - \rho_\text{f} \frac{\ln(1+\gamma)}{\gamma} L_{2\phi}\right) g = \left(\sum_i \frac{f_i L_i}{2\rho_i D_\text{e}^i A_i^2} + \sum_j \frac{K_j}{2\rho_j A_j^2}\right) \dot{M}_\text{s}^2 \,, \tag{4.94}$$

where the friction term is summed up to section 4 and the form losses term is summed for the area changes up to section 4 as in Equations (4.85) and (4.86). Note again that γ, $\bar{\phi}_4^2$ and θ are now constants wherease $L_{1\phi}$, $L_{2\phi}$ and $\dot{M}_\text{s}$ are directly dependent on H_{swell}. Also, note that the dependence of the governing equation on power comes now from Equation (4.92) in contrast to the earlier case where the dependence on power was portrayed through x_{exit} as in Equation (4.75).

The governing Equation (4.94) has therefore become an equation for the swell height rather than the flow rate, and can be rewritten and solved numerically in terms

of H_{swell} by inserting Equations (4.91) and (4.92):

$$\left(\rho_\infty H_{\text{pool}} - \bar{\rho}_\text{l}\theta H_{\text{swell}} - \rho_\text{f}\frac{\ln(1+\gamma)}{\gamma}(1-\theta)H_{\text{swell}}\right) g = \left(\frac{f_1 L_1}{2\rho_\infty D_1 A_1^2} + \frac{f_2 L_2}{2\rho_\infty D_2 A_2^2} + \frac{f_3 L_3}{2\rho_\infty D_{\text{e}3} A_3^2} + \frac{f_4 \theta H_{\text{swell}}}{2\bar{\rho}_\text{l} D_{\text{e}4} A_4^2} + \bar{\phi}_4^2 \frac{f_4(1-\theta)H_{\text{swell}}}{2\rho_\text{f} D_{\text{e}4} A_4^2} + \sum_j \frac{K_j}{2\rho_j A_j^2}\right)\left(\frac{\dot{Q} H_{\text{swell}}/L_4}{\Delta h}\right)^2 . \tag{4.95}$$

Equation (4.95) is solved graphically as well, similarly to the earlier Equations (4.71) and (4.87) with the exception that the independent variable is the swell height and not the flow rate. The critical pool height for a given power as earlier defined is the height for which $H_{\text{swell}} = L_4$ from which fuel uncovery begins. Inserting the above condition into Equation (4.95) produces an algebraic equation for the solution of the critical height H_{crit} (the corresponding friction factors are the ones calculated from the flow rate in Equation (4.92) which satisfies the condition on the swell height). It can be seen that the critical height is dependent on the assembly power directly but also on the inlet temperature through the term Δh. For cases of quick draining, the pool temperature will nearly remain unchanged and in this context it can be said that the critical height is dependent mainly on the assembly power.

Whereas in the two-phase and above-critical-height cases the temperatures at the edge of the heated section could be calculated from the exit quality and flow rate, the below-critical-height case requires an additional equation for the enthalpy rise above the swell height to find the coolant parameters at the channel exit. This enthalpy rise starts from saturated steam enthalpy at the swell height and is heated up by the remaining fraction of the heated channel:

$$h_{\text{exit}} = h_\text{g} + \frac{\dot{Q}(L_4 - H_{\text{swell}})/L_4}{\dot{M}_\text{s}} , \tag{4.96}$$

where h_g is the saturated steam enthalpy, and since the heat flux profile was assumed constant, the fraction of power in the uncovered section heating the vapor is just the fraction of its length along the heated channel times the full power. For convenience, denote the ratio of the swell height to the length of the heated section:

$$\epsilon \equiv \frac{H_{\text{swell}}}{L_4} . \tag{4.97}$$

Equation (4.96) becomes:

$$h_{\text{exit}} = h_{\text{g}} + \frac{\dot{Q}(1-\epsilon)}{\dot{M}_{\text{s}}} \ , \tag{4.98}$$

and Equation (4.92) becomes:

$$\dot{M}_{\text{s}} = \frac{\epsilon \dot{Q}}{\Delta h} \ . \tag{4.99}$$

Inputting Equation (4.99) into Equation (4.98) and cancelling out terms, the expression for the exit enthalpy becomes:

$$h_{\text{exit}} = h_{\text{g}} + \frac{1-\epsilon}{\epsilon} \Delta h \ . \tag{4.100}$$

From the exit enthalpy, the steam temperature can be obtained directly (from the literature), and from the flow rate the heat transfer coefficient is obtained. From these the clad and fuel temperatures are calculated, as will be addressed in the next section.

4.3.4 Heat Transfer Coefficients

The heat transfer coefficient for pool heights above the critical height is the Kandlikar coefficient as in Equation (4.77) since the flow is still of a two-phase mixture. For pool heights below the critical height, the steam at the exit is superheated, and the single-phase Dittus-Boelter heat transfer coefficient as in Equation (4.41) is appropriate.

4.4 Clad and Fuel Temperatures

In order to establish the temperatures of the fuel and clad let us zoom on a single plate. A sketch of the rectangular representation of two neighbouring plates is drawn in Figure 4.4. The z axis is representing the upward direction. In neglecting the plate's curvature[11], it can be seen from symmetry that half of the plate's power is transferred through its right face and half through its left (neglecting heat flow through the narrow up and bottom edges, since the plates are very thin compared to their length). Denote the power density within the fuel meat within a plate as:

$$\dot{q}''' \equiv \frac{\dot{q}}{V_{\text{fm}}} \ , \tag{4.101}$$

[11] As was deemed appropriate earlier, see in Chapter 2.

where V_{fm} is the fuel meat volume. The heat flux from the meat to the clad on either the left or right side is:

$$\dot{q}'' = \dot{q}'''w_{\text{fm}}/2 \ , \tag{4.102}$$

where w_{fm} is the width of the fuel meat (see Figure 4.4). The power density $\dot{q}'''$ and heat flux $\dot{q}''$ are in units W m^{-3} and W m^{-2} respectively.

In order to obtain the temperatures within the clad and fuel, a steady state heat conduction treatment is required. The steady state temperature distribution within a medium with internal volumetric heat generation is given by:

$$\nabla^2 T + \dot{q}'''/k = 0 \ , \tag{4.103}$$

where k is the heat conductivity of the material. In the MNR fuel plates, conduction in axis $\hat{z}$ and $\hat{y}$ can be neglected since these dimensions are approximately infinite with regards to the $\hat{x}$ dimension (see Figure 4.4). Alternatively, the heat transfer through the face of the plate is going to be considerably larger than from the sides connecting to the side plates or the top and bottom edges. Therefore, only the derivative d^2/dx survives in Equation (4.103). It is usually derived by use of the Fourier Law tying the temperature gradient to the corresponding heat flux. For the 1-D case of conduction in the x dimension it is given as [34]:

$$\dot{q}'' = -k\frac{dT}{dx} \tag{4.104}$$

With the assumption that the heat conductivity of the mediums is constant and that the volumetric heat generation in the fuel is also constant, Equation (4.103) can be integrated twice to give the expression for the temperature distribution inside the fuel meat. Using lecture notes by Luxat [42] this temperature profile is found and used to calculate the temperature difference between the centerline and clad interface, which is:

$$T_{\text{fm}} - T_{\text{s}} = \frac{\dot{q}'''}{2k_{\text{fm}}}\left(\frac{w_{\text{fm}}}{2}\right)^2 \ , \tag{4.105}$$

where T_{fm} is the fuel centerline temperature and T_{s} is the fuel-clad interface temperature.

There is no gas filled gap between the fuel and clad in the plates as opposed to other types of fuel and therefore the temperature of the fuel and clad at their interface can be considered the same. The clad's temperature at the interface with the fuel is not the same as the clad's surface temperature in contact with the liquid, albeit

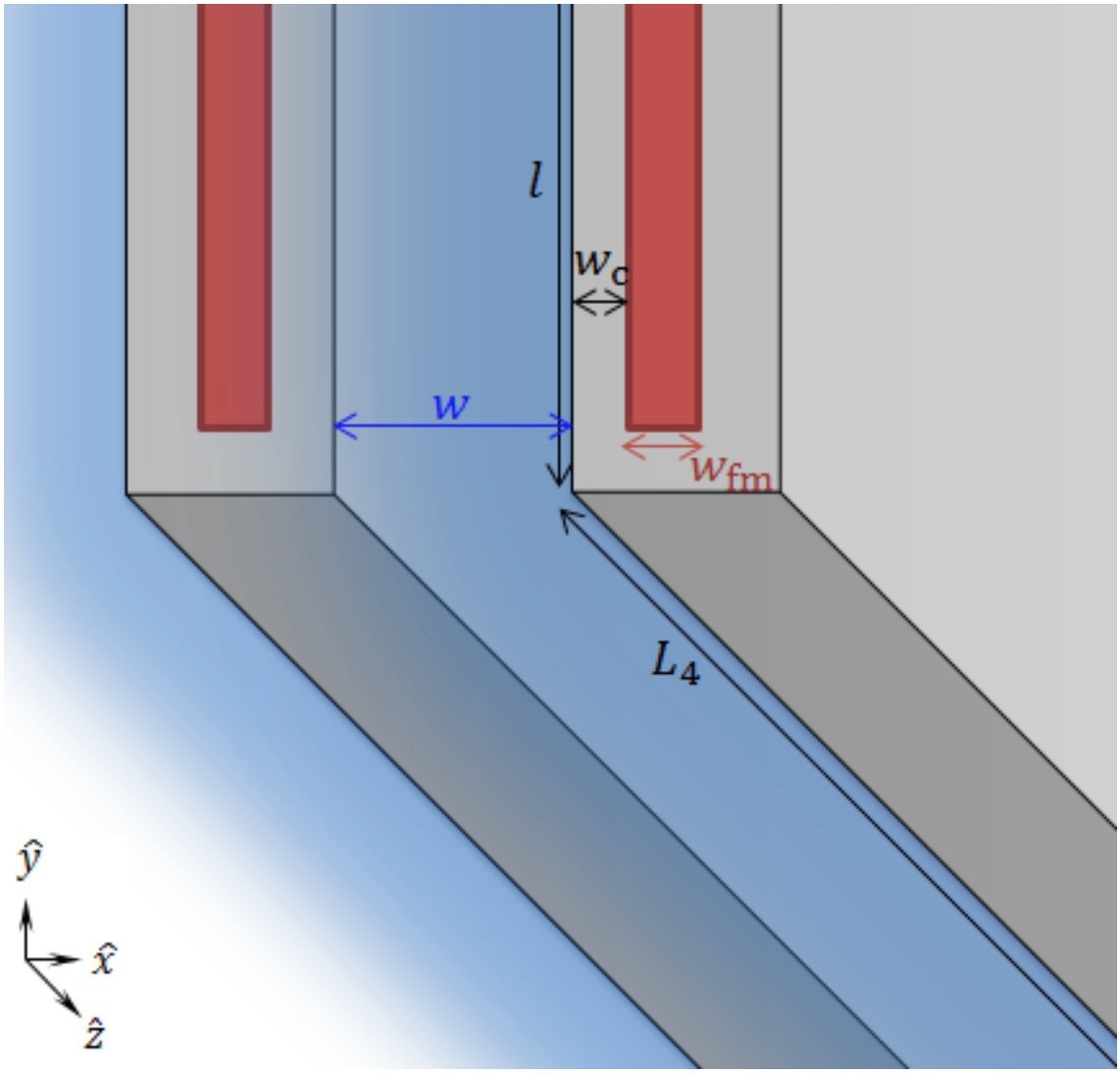

Figure 4.4: Fuel plates and channel sketch, ignoring plate curviness and not to scale. The blue halo symbolizes the water flowing in the channels between the plates. The direction $\hat{z}$ is the upward direction. The inner region in red having the width w_{fm} is the fuel meat, w_{c} is the thickness of the clad (ignoring the small region on the edges where the clad has the full plate's thickness). l and w are the length and width of a flow channel between two plates and L_4 is the height of the plates (length of section 4 from Figure 4.1). Notice l and L_4 extend beyond the borders of the drawing.

the difference is small due to the relatively high conductivity of the aluminium and the thinness of the clad. This difference is nonetheless relatively easy to calculate analytically assuming again that the heat conductivity within the clad is constant. Since the clad isn't generating any heat, the term $\dot{q}'''/k$ in Equation (4.103) disappears and the temperature profile in the clad is linear. Since the temperature gradient in the clad is linear, its derivative with respect to x is constant. Using Equation (4.104) the temperature gradient along the clad is therefore [34, 42]:

$$\dot{q}'' = k_{\mathrm{c}} \frac{T_{\mathrm{s}} - T_{\mathrm{c}}}{w_{\mathrm{c}}} \ , \tag{4.106}$$

where k_{c} is the clad's heat conductivity and w_{c} is the clad's width or thickness. Equation (4.106) is appropriate since the heat flux $\dot{q}''$ is constant throughout the clad into the coolant, meaning that the heat flux through the fuel-clad surface and the clad-liquid surface are equal. Equation (4.106) can be rearranged to give:

$$T_{\mathrm{s}} - T_{\mathrm{c}} = \frac{\dot{q}'' w_{\mathrm{c}}}{k_{\mathrm{c}}} = \frac{\dot{q}''' w_{\mathrm{fm}} w_{\mathrm{c}}}{2k_{\mathrm{c}}} \ , \tag{4.107}$$

where Equation (4.102) was used in the last identity.

Adding Equation (4.105) and Equation (4.107) gives the temperature difference between the fuel centerline and the clad-liquid surface:

$$T_{\mathrm{fm}} - T_{\mathrm{c}} = \frac{\dot{q}'''}{2k_{\mathrm{fm}}} \left(\frac{w_{\mathrm{fm}}}{2} \right)^2 + \frac{\dot{q}''' w_{\mathrm{fm}} w_{\mathrm{c}}}{2k_{\mathrm{c}}}$$

$$T_{\mathrm{fm}} = T_{\mathrm{c}} + \dot{q}''' \left(\frac{w_{\mathrm{fm}}^2}{8k_{\mathrm{fm}}} + \frac{w_{\mathrm{fm}} w_{\mathrm{c}}}{2k_{\mathrm{c}}} \right) \ . \tag{4.108}$$

The clad-liquid interface temperature is given by Newton's cooling law [42]:

$$\dot{q}'' = h \left(T_{\mathrm{c}} - T_{\mathrm{w}} \right)$$

$$T_{\mathrm{c}} = T_{\mathrm{w}} + \frac{\dot{q}''' w_{\mathrm{fm}}/2}{h} \ , \tag{4.109}$$

where T_{w} is the temperature of the coolant (either liquid or steam) and Equation (4.102) was used again to interchange between $\dot{q}''$ and $\dot{q}'''$. Equation (4.109) is true for any point z along the channel, by inputting the corresponding temperature and heat transfer coefficient at that point. Thus the temperature of the clad can be found through

Equation (4.109) by knowledge of the coolant temperature, and the temperature of the fuel can be subsequently found from Equation (4.108) by inserting the corresponding clad temperature.

4.5 Decay Heat Power Profile

The input parameters that go into the natural convection models are the assembly powers and the assembly inlet temperature, being the temperature of the pool. In order to asses the individual assembly, channel and the total core power with time, a decay heat correlation is used. The correlation is taken from El-Wakil [43]:

$$P(t) = 0.095 P_0 t^{-0.26} \,, \tag{4.110}$$

where P is the reactor power[12] in units W, P_0 is the initial power right before shutdown and t is the time after shutdown in seconds. The same equation holds true for the power of an assembly, henceforth denoted as $\dot{Q}$, and the power of a single plate, henceforth denoted as $\dot{q}$. Equation (4.110) is valid for times greater than 200 seconds and is conservative with regards to the ANS-5.1 standard[13] for times before that [45]. This correlation is for infinite operational time at power P_0 before shutdown. A correction to the correlation for finite reactor run times is given by multiplying Equation (4.110) by the function $f(t) = 1 - (1 + t_{\text{op}}/t)^{-0.2}$ where t_{op} is the reactor operation time before shutdown [43]. Since for finite times $f(t) < 1$, Equation (4.110) is conservative to any finite running time form of the correlation. It is therefore from conservative considerations that Equation (4.110) is used although the MNR usually shuts down overnight.

For obtaining the total energy or heat emitted by the core from shutdown to some later time t, Equation (4.110) can be integrated to produce [43]:

$$E(t) = \int_0^t P(t')\, dt' = 0.128 P_0 t^{0.74} \,, \tag{4.111}$$

where E is in units J. The same is true for the heat emitted by an assembly Q, and the heat emitted from a plate q. Alternatively, for the same conditions, the time it

[12] Notice the difference between pressure in lowercase p and the uppercase P denoting core power.
[13] The standard curve for ^{235}U in light water reactors. See the American National Standard [44].

would take to emit a given amount of heat E is:

$$t = \left(\frac{E}{0.128 P_0}\right)^{1.35} . \tag{4.112}$$

4.6 Pool Heatup and Vaporization

The pool temperature serves as an important input variable into the natural convection models. In the treated scenarios, the pool is isolated from the holdup tank while the flapper opens, allowing for natural convection flows to develop within the reactor pool. This entails a loss of the heat sink, removing from this point on the core produced heat only into the reactor pool. Since the pool is very large and the core is located beneath its surface (at least before uncovery), the heat is considered to be released to the pool water only. Also, as the pool contains a significant amount of water, heat losses from the pool to the containment and by evaporation are neglected. The temperature rise in the pool for any given time is calculated with the first law of thermodynamics:

$$E = M_\infty \bar{C}_p \Delta T_\infty$$

$$T_\infty(t) = T_\infty(0) + \frac{E(t)}{M_\infty \bar{C}_p} , \tag{4.113}$$

where M_∞ is the mass of water in the pool in kg and $T_\infty(t)$ is the ambient pool temperature at time t in either K or °C. $\bar{C}_p$ is the average specific heat capacity of the ambient pool[14] at atmospheric pressure over the temperature rise ΔT_∞ in units $\mathrm{J\,kg^{-1}\,K^{-1}}$:

$$\bar{C}_p = \frac{\Delta h}{\Delta T_\infty} , \tag{4.114}$$

where Δh is the specific enthalpy rise from initial to final temperatures[15]. The pool temperature at any time t can be found by inputting into Equation (4.113), the energy output up to time t given by Equation (4.111). By using Equation (4.113) a few hidden conservative assumptions are employed. One is that the pool is isolated from the

[14]Notice the difference between the average specific heat in the assembly $\bar{c}_p$ in lowercase as in Equation (4.13) and the average specific heat of the ambient pool water $\bar{C}_p$ in uppercase. The difference is not only in the temperature rise in each, but also in the pressure p since the core assemblies are locally at a somewhat higher pressure, being under a column of water at a certain depth.

[15]Note this is not the enthalpy rise Δh to saturated steam in the uncovered case as in Equation (4.93).

environment such that there is no heat loss to the containment, or otherwise so large that the heat from the core doesn't dissipate fast enough to the pool edges. Another is the assumption that the evaporation during the heating process is insignificant. Such evaporation slightly increases the containment pressure and suppresses further evaporation. This phenomena becomes more significant if the pool reaches near saturation temperature, where vaporization[16] becomes a main mechanism in vapour production which is removing pool inventory at higher rates.

Vaporization is assumed to start immediately and only after the entire pool mass has reached saturation. From that point on the mass of water that has been evaporated is given by:

$$\Delta M_\infty = \frac{\Delta E}{h_{\mathrm{fg}}} \,, \tag{4.115}$$

where $\Delta E = \int_{t_\mathrm{f}}^{t} P(t')\,dt' = E(t) - E(t_\mathrm{f})$ is the amount of heat supplied to the water between the time of first saturation t_f and time t and h_{fg} is the water's latent heat of vaporization.

Using the pool's geometry, a unit volume ΔV is equal to a unit height ΔH times the pool's surface area A_{pool}. The height lost by vaporizing a mass of water ΔM_∞ is therefore:

$$\begin{aligned} \Delta M_\infty &= \rho_\mathrm{f} \Delta V = \rho_\mathrm{f} A_{\mathrm{pool}} \Delta H \\ \Delta H &= \frac{\Delta M_\infty}{\rho_\mathrm{f} A_{\mathrm{pool}}} = \frac{\Delta E}{h_{\mathrm{fg}} \rho_\mathrm{f} A_{\mathrm{pool}}} \,, \end{aligned} \tag{4.116}$$

where ρ_f is the density of saturated liquid water[17] (at atmospheric pressure for bulk pool calculations) and it is assumed the pool surface area is constant for the different heights. As discussed above, by using Equation (4.113) and the subsequent Equation (4.116) there lies a conservative assumption that the vapour is being well ventilated outside the containment. In truth, as long as the containment is sealed, the accumulating vapour will increase the pressure which will have a suppressing effect on additional vaporization.

In a draining scenario, the pool keeps heating up as the water is being drained.

[16] Note the difference between evaporation, which occurs at all temperatures by means of diffusion of the surface layer with air, and vaporization, which only occurs when liquid reaches saturated conditions.

[17] Notice that since the core is at a certain depth, the water properties there are a little different than at atmospheric pressure. The saturated liquid density ρ_f here for atmospheric pressure has therefore a different value than it did in Section 4.2.

Taking into account the rate of draining would somewhat complicate solving Equation (4.113) since the mass in the latter will be time-dependent. A simplifying assumption is made by performing the calculation with the final water inventory after draining as the constant mass in Equation (4.113), effectively assuming instant draining for this calculation. This may be justified by the fact that any pool draining down to core level would happen in a much shorter time span than it takes to heat the pool by any significant amount from the decay heat . It takes more than 10 days to heat up the pool by 10 °C (MNR safety report chapter 16.5.4) as opposed to the 3.5 hours to drain down to core level. This is also a realistically conservative simplification since the amount of pool water used in the calculation is less than any amount during the draining process, which predicts shorter times for pool heatup than by considering the time dependent inventory (the same amount of energy $E(t)$ is deposited into an effectively smaller mass of water).

Also, while draining is in progresses, forced flow, which is a better heat transfer mechanism than natural convection, is being sustained through the core. This is an additional rationale for not modelling the transient until reaching final height after draining since the natural convection calculation with final smaller pool inventory is conservative as well.

Chapter 5

Modelling

5.1 Assembly Geometry

The hydraulic diameter used in the various calculations throughout the models is defined as:

$$D_{\mathrm{e}} = \frac{4A}{P_{\mathrm{w}}} \,, \tag{5.1}$$

where P_{w} is the wetted perimeter in units m which, as its name suggests, is the perimeter encircling the flow area A in contact with the liquid. The figures for the flow areas and wetted perimeters of the different assembly parts are as in Figure 3.2. The hydraulic diameter of section 4 is found to be $D_{\mathrm{e4}} = 5.95$ mm. The hydraulic diameter of sections 3 and 5 is $D_{\mathrm{e3}} = D_{\mathrm{e5}} = 69.49$ mm.

For calculations requiring the approximation of the non circular parts as rectangles, the 'equivalent' sides are taken such that the flow area and hydraulic diameters remain the same as in the original curved geometry, similar to the treatment by Ha [28]. For this purpose the equivalent rectangle needs to comply with the following restrictions:

$$2(l + w) = P_{\mathrm{w}}$$

$$w \times l = A \,, \tag{5.2}$$

where w is the width (thickness) and l is the length of a rectangle of area A and perimeter P_{w}. For the channels in section 4, the resulting equivalent rectangle is the one having $l = 66.958$ mm and $w = 3.113$ mm. For sections 3 and 5 the result is

$W = 62.059$ mm and $L = 78.941$ mm

The lengths of the assembly sections L_1 to L_5 are required in order to calculate the friction pressure losses. These are taken from Figure 3.2(a), where the snout's flow length is taken as the combined length of the fitting and the reducer, as done by Blahnik [26]. Note again, as mentioned in Chapter 4, that the sections are numbered in an opposite order to the section numbering in the MNR safety report [1].

5.1.1 Rectangular Correction Coefficients

Referring back to Section 4.1.2, Garland mentions that the rectangular corrections for friction factors ξ range from 0.89 to 1.5 for laminar flow and from 1 to 1.1 for turbulent flow, where the limits are for a perfect square and infinite parallel plates respectively [27]. The rectangular correction is only valid for assembly sections 3 to 5, since 1 and 2 are cylinders. When ignoring the curvature of the plates, cross sections of compartments 3 and 5 become close to squares and the channels in section 4 become thin rectangles (see sizes in Figure 3.1).

Applying Equation (4.32) to the plates' region, i.e. inputting the figures for width and length of a channel in section 4, produces the following rectangular correction factor:

$$\xi_{\text{lam}}^{(4)} = 1.418 \, , \tag{5.3}$$

For the turbulent flow in section 4, the rectangular correction as in Equation (4.34) is:

$$\xi_{\text{tur}}^{(4)} = 1.088 \, . \tag{5.4}$$

Section 4 is modelled as a single equivalent duct describing the combined characteristics of the 17 channels between the fuel plates. The correction factor ξ_{lam} is calculated for the width and length of a single channel, since the friction factor is calculated for the equivalent diameter of a single channel as well.

Using Equation (4.32) again, the laminar correction for sections 3 and 5 is:

$$\xi_{\text{lam}}^{(3,5)} = 0.9 \, . \tag{5.5}$$

The turbulent correction for sections 3 and 5 is calculated by Equation (4.34) to be:

$$\xi_{\text{tur}}^{(3,5)} = 1.009 \, . \tag{5.6}$$

The last one is less than 1% larger than unity, which was found to be insignificant throughout the calculations (no effect within the significant digits range as will be addressed later) and is therefore neglected.

5.1.2 Minor Loss Coefficients

Minor loss coefficients vary in the literature even for the same types of geometry changes. The coefficients chosen were the conservative among the different sources examined. The first minor loss appears at the snout's bottom. It is taken as a loss from entrance to a pipe from a wall as [46, 47]:

$$K_{\infty 1} = 0.5 \ , \tag{5.7}$$

from observing that the grid plate acts as a wall rather than the case of a free standing pipe (see **??**).

The next loss is from section 1 into 2 via the reducer, through which the fluid expands in the flow direction of natural convection[1]. It is calculated by polynomial extrapolation between the two closest values for diameter ratios given in King's Handbook of hydraulics [48]:

$$K_{1-2} = 0.340 \ . \tag{5.8}$$

Next up is the snout's connection to the rectangular assembly body, which is a sudden expansion from the larger diameter of the snout and the equivalent diameter of the rectangular assembly 'frame'. A loss coefficient for sudden expansion is given by Idelchik [46] and also Munson [35]:

$$K_{2-3} = \left(1 - \frac{A_2}{A_3}\right)^2 = 0.136 \ , \tag{5.9}$$

calculated by inserting the flow area values of sections 2 and 3, A_2 and A_3 respectively.

The entry to the fuel plate region entails a complicated geometrical form loss. It can be approximated as a sudden contraction from the rectangular part's equivalent diameter to the fuel section's equivalent diameter, which has been the preferred representation in MNR related calculations (Ha [28, 31] or Blahnik [26] for example). This equivalent channel represents the combined flow area of the 17 channels, along

[1] In normal operation under forced flow the flow direction is downwards and the fluid sees a reduction in flow area in accordance with the reducer's name.

with the total wetted perimeter. Using Equation (5.1), the total flow area and total wetted perimeter cancel out to the flow area and perimeter of a single channel, thus giving the combined equivalent diameter as that of a single channel, which is very small. Inputting the above into the sudden contraction formula given by Crane [47] gives:

$$K_{3-4} = 0.5 \left[1 - \left(\frac{D_{e4}}{D_{e3}}\right)^2\right]^2 \cong 0.5 \,, \tag{5.10}$$

since $D_{e4} \ll D_{e3}$. In the studies of the 10 plate MNR fuel assembly, Osamusali et al. proposed a value of 0.66 instead for laminar flows [29]. Since it is conservative to all other methods it will be the one used in this work.

$$K_{3-4} = 0.66 \,. \tag{5.11}$$

The coefficient for the plate region's exit back to the top rectangular section 5 is given by the formula for sudden expansion. Crane proposes a different sudden expansion formula than the one used above for K_{2-3}, which produces a more conservative coefficient for the MNR geometry [47]:

$$K_{4-5} = \left[1 - \left(\frac{D_{e4}}{D_{e5}}\right)^2\right]^2 \cong 1 \,, \tag{5.12}$$

since similarly to Equation (5.10), $D_{e4} \ll D_{e5}$.

Lastly, the minor loss coefficient for exiting the assembly is that of a free discharge [46]:

$$K_{5\infty} = 1 \,. \tag{5.13}$$

There is an additional loss associated with a handle at the top of each assembly which is used to move the assembly when refuelling or shuffling. Blahnik associates a minor loss coefficient of 0.1 to this obstruction [26]. It was chosen to neglect this loss since all other coefficients used here are quite conservative to the ones used by Blahnik. This choice may also be justified by Ha and Garland [31] who showed that the effect of the handle on the flow distribution is negligible enough to be omitted in their CFD[2] analysis, at least for downward flow.

[2]Computation Fluid Dynamics

5.2 Fuel and Clad Properties

Among the required parameters for the fuel and clad temperature calculations given in Equations (4.108) and (4.109) are their heat conductivities and their dimensions and volumes. These are available in the MNR safety report. The conductivity of the fuel meat is $k_{\mathrm{f}} = 73 \pm 6\%$ and that of the clad is $k_{\mathrm{c}} = 123 \pm 6\%$, both in units $\mathrm{W\,m^{-1}\,K^{-1}}$. The fuel and clad thicknesses (w_{fm} and w_{c}) are 0.51 mm and 0.381 mm respectively where, as discussed earlier, the clad thickness is considered in the region where it sandwiches the fuel contrary to the full fuel plate thickness right at the edges (see Figure 4.4). The fuel meat volume is $V_{\mathrm{fm}} = 19.064\,\mathrm{mm}^3$. The surface roughness of the aluminium clad is 2 mm [36].

5.3 Friction Factors Treatment

The variation in flow rate by changing the friction factors between the laminar and turbulent formulae is rather small such that the Reynolds numbers aren't affected much by it. Educated guesswork shows that for the single-phase-flow case section 4 is always at the laminar flow regime and sections 1-3 and 5 are always at the turbulent regime for the span of parameters in the single-phase scenario. The exceptions are for extremely low powers, below 100 W for an entire assembly, where sections 1-3 and 5 reduce to laminar flow, or assembly powers above about 10% full power, where section 4 reaches the turbulent region. However, the assembly drops to below 10% power immediately after the first second in the given decay heat profile, and also approaches an asymptote at very long times that doesn't drop below 100 W. The above makes it simple to calculate the friction factors for the single-phase case, and for sections 1-3 and 5 for the two-phase case, not having to switch between the laminar and turbulent formulae.

By use of the HEM model, the friction factors are calculated in the same way as in the single-phase case using the Colebrook correlation as in Equation (4.33) and referred to as the 'liquid only' friction factors. Since the two-phase case was solved graphically, as will be discussed later, it was required to calculate the friction factors for all possible flow rates, some of which were naturally below the turbulent threshold of about 1500-2000 for the Reynolds number [6]. There is a considerable disagreement between the predictions of the laminar and turbulent models, especially

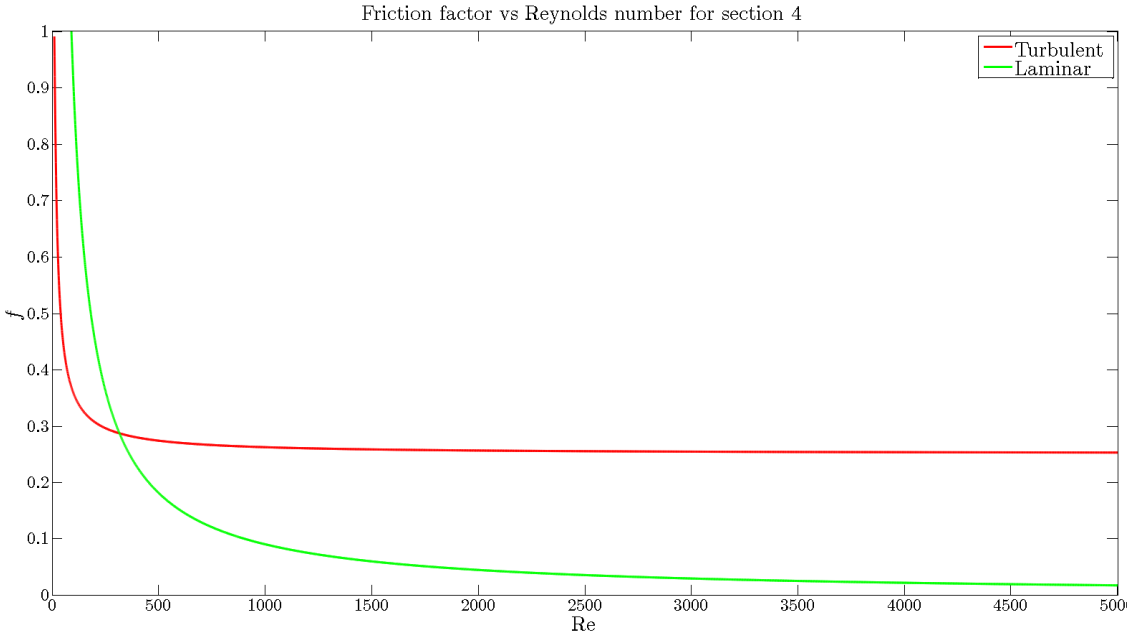

Figure 5.1: Friction factor vs. Reynolds number for section 4 in the range relevant for the cases studied.

in the transition region[3] as seen for example in Figure 5.1.

In order to try and correct for the issue of transitioning from the laminar friction factor to the turbulent one, an attempt was made to use the Churchill friction factor [49]. The Churchill suggested factor is supposed to be valid for the entire range, encompassing both laminar and turbulent regimes:

$$f = 8\left[\left(\frac{8}{\mathrm{Re}}\right)^{12} + \frac{1}{(a+b)^{3/2}}\right]^{1/12}, \tag{5.14}$$

where

$$a = \left[2.457 \ln \frac{1}{\left(\frac{7}{\mathrm{Re}}\right)^{0.9} + \frac{0.27\epsilon}{D_\mathrm{e}}}\right]^{16}$$

$$b = \left(\frac{37,530}{\mathrm{Re}}\right)^{16}.$$

As can be seen in Figure 5.2, the friction factor behaves, as expected, similarly to

[3]The transition region is for Reynolds numbers at the upper edge of the laminar region and lower range of the turbulent region.

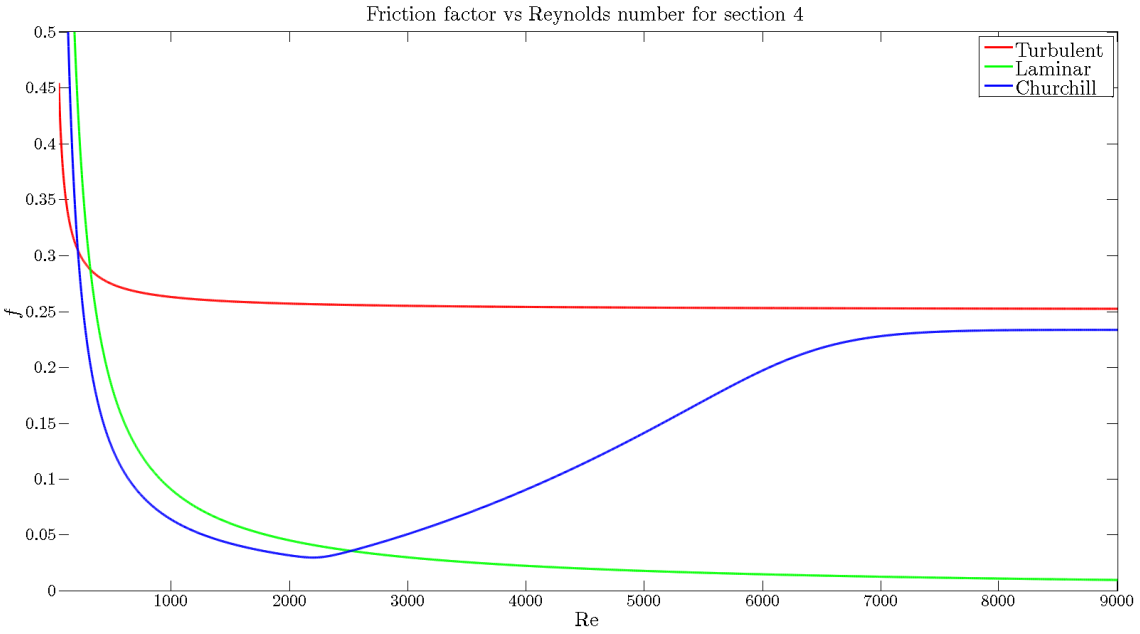

Figure 5.2: Churchill friction factor compared to laminar and turbulent factors for section 4 in the range relevant for the cases studied.

the laminar factor for the laminar range, and similarly to Colebrook in the turbulent range, where the transition range is tailored to connect both. However, as noted above, the transition to turbulent flow is expected to be at lower Reynolds numbers for natural convection. Additionally, it can be seen that the Churchill friction factor is slightly lower than that of both the laminar formula for the laminar range and the turbulent formula for the turbulent range. This contributes to higher flow rates and lower enthalpies, and thus, being less conservative, the Churchill correlation was discarded.

It was subsequently decided to use the conservative among the linear and Colebrook predictions at each flow rate (or correspondingly at each Reynolds number). It can be seen in the example in Figure 5.1 that for section 4, the intersection between both is at about $\mathrm{Re} = 350$. The effective friction factor used is therefore the laminar up to $\mathrm{Re} = 350$ and the turbulent for higher Reynolds numbers. In a similar way, this was incorporated for the friction factor calculation for all sections for the two-phase case. As will be seen, this mostly did not affect the results since for most powers, most of the flow-rate spectrum is in the turbulent region. The switch to laminar friction factors was applicable for very low powers where if boiling is achieved, very low flow rates were observed. The uncovered core treatment uses the same scheme as the two-phase

treatment since in it there is always a two-phase mixture present in the channel. It is in this scenario where the lowest Reynolds numbers were observed and where the flow tends to be laminar throughout all assembly sections.

5.4 Heat Transfer Coefficients Treatment

The single-phase heat-transfer coefficient used in the models is either the laminar resulting from Equation (4.39) or the one resulting from the Dittus-Boelter correlation given in Equation (4.40). It is also used in the two-phase model, since Kandlikar's correlation uses the single-phase coefficient as well (see Equation (4.77)). As addressed by Garland [3], the Dittus-Boelter formula is acceptable for turbulent flow, but not for laminar, as is predominant in the single-phase case. The turbulent range is expected to start at roughly Re=1500, as noted by Zvirin, where the turbulent formula becomes acceptable.

A comparison between the Dittus-Boelter (henceforth - the turbulent) correlation and laminar formulae, is presented in Figure 5.3. The flow rates through the channels corresponding to the span of Reynolds numbers from 0-5000 were used to asses the turbulent against the laminar heat transfer coefficients as in Equation (4.41) along the given span. The fluid properties have been taken for saturated conditions where the intersections between the laminar and turbulent formulae were found to be at the highest Reynolds numbers. Different draining figures almost didn't affect this phenomena. The motivation for seeking the further intersection was to find the extreme case for the transitioning between the two formulae. For a fixed pressure and temperature it can be seen that for most of the laminar region, firmly in the low Reynolds numbers, the turbulent formula underpredicts the heat transfer compared with the laminar formulae. The intersection with a laminar coefficient suitable for a MNR assembly is expected to be somewhere between the two laminar coefficient intersections presented in Figure 5.3, and definitely below Re=1500. Assuming for the moment that the intersection is at the later point corresponding with the parallel plates formula[4], its corresponding Reynolds number is roughly 1300. For flows corresponding with Reynolds number below 1300 the laminar formula is appropriate and in the range $1300 < \mathrm{Re} < 1500$, it is conservative to the turbulent one. Therefore, for Re<1500 the laminar formula for a MNR channel dimensions corresponding ratio would be

[4]For which Nu=8.23, see Equation (4.39).

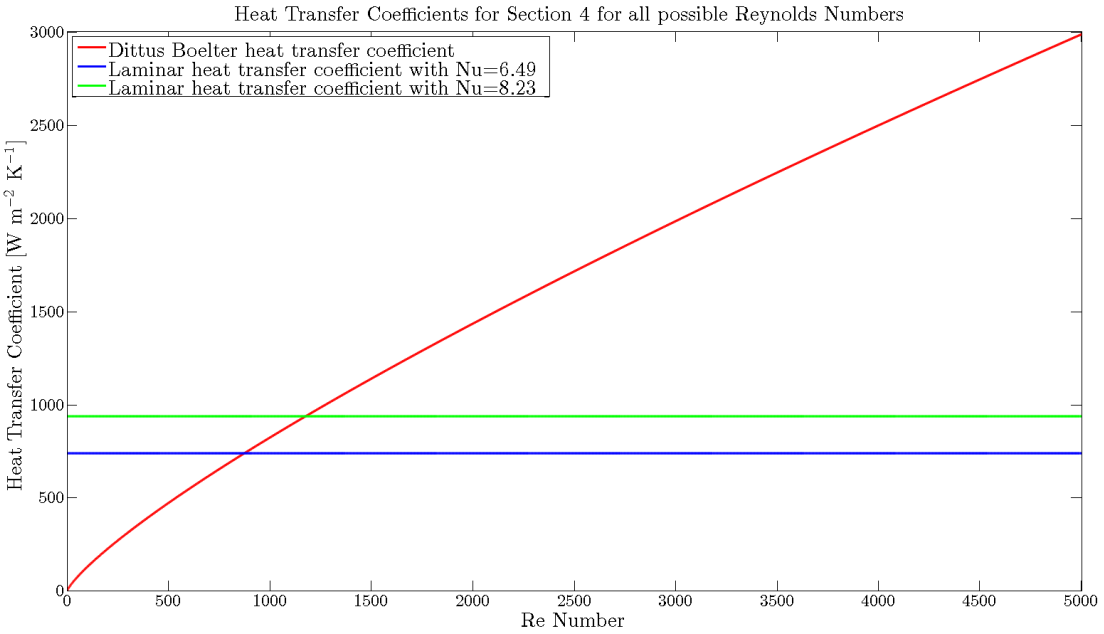

Figure 5.3: Laminar and turbulent heat transfer coefficients as a function of Reynolds number in section 4. Fluid properties are taken for draining to just above core level and saturated pool conditions.

preferable, and in absence of a correlation for the MNR channel ratio, the conservative ratio-of-8[5] formula was chosen. It was found that for the single-phase case, the highest Reynolds number (in section 4 where heat transfer is of interest) for all scenarios was around Re=740, where there is no dilemma regarding the use of the laminar formula. The model therefore uses the laminar ratio-of-8 formula for Re<1500 and the turbulent Dittus-Boelter correlation for Re>1500.

Since for the single-phase case, only Reynolds numbers below 740 were observed, choice between the laminar and turbulent coefficients remains only relevant for some scenarios in the two-phase case. With that being said, it is important to mention that where the choice between the laminar and turbulent single-phase heat transfer coefficients may be relevant, it is of lesser significance. This is because the single-phase heat transfer coefficient only plays a small role in the two-phase formula, in which it is multiplied by terms arising from two-phase considerations (see Equation (4.77)) which add to it a few orders of magnitude. The changes in the two-phase heat transfer coefficient resulting from alternating between the laminar or turbulent single-phase heat transfer coefficient are less noticeable, and the order of magnitude for both the

[5]For which Nu=6.49, see Equation (4.39).

laminar and turbulent cases is around $10^4\,\mathrm{W\,m^{-2}\,K^{-1}}$, which constitutes a very high heat transfer rate for low powers such as in the MNR (see Figure 5.3 for comparison to typical values of the single-phase heat transfer coefficients). The Reynolds numbers in section 4, required for the heat transfer coefficient estimation, are calculated as in the earlier section when used for the friction factor evaluation.

5.5 Power figures for the MNR

Initial full-power figures are required in order to find the decay heat at different times. The full core power is taken as suggested in the MNR and used in its accident analysis chapter, namely the reference core power[6] plus a 17% uncertainty; 5.75 MW. It is the addition of the maximum allowed power by license with the uncertainty margin. Also from the reference core, average plate power is 9.96 kW and maximum plate power is 26.5 kW. The plate power figures are derived from a 5 MW core, and therefore with making the adjustment of adding the uncertainty margin, the resulting plate powers are 11.65 kW for average power and $\dot{q}_0 = 31\,\mathrm{kW}$ for maximum power. The corresponding heat flux from a maximum power plate is calculated to be $415\,\mathrm{kW\,m^{-2}}$.

The average plate power is used to calculate the flow rate through the assembly with $\dot{Q}_0 = 16 \times 11.65\,\mathrm{kW}$ in all related calculations. Conservatively, the maximum plate power is chosen to estimate the temperature rise in the hottest channel using the appropriate fraction of the full assembly flow (adding on top of the conservative choice of taking this fraction as 1/17 of the assembly flow rate, as will be discussed later in the chapter). Note the notations $\dot{q}$ and $\dot{Q}$ which will be henceforth used for the powers of a single plate/channel and a full assembly respectively.

As mentioned in Section 4.5, the most conservative decay profile is that for the infinite run time as given in Equation (4.110). A comparison between some finite run decay power figures and the infinite run decay power is shown in Figure 5.4 where the conservative nature of the infinite-run-time correlation is noticeable.

[6]The reference core is a set of suggested parameters and core configuration for the MNR, deemed as realistically conservative, for use in safety assessments and calculations. The reference core power is 5 MW.

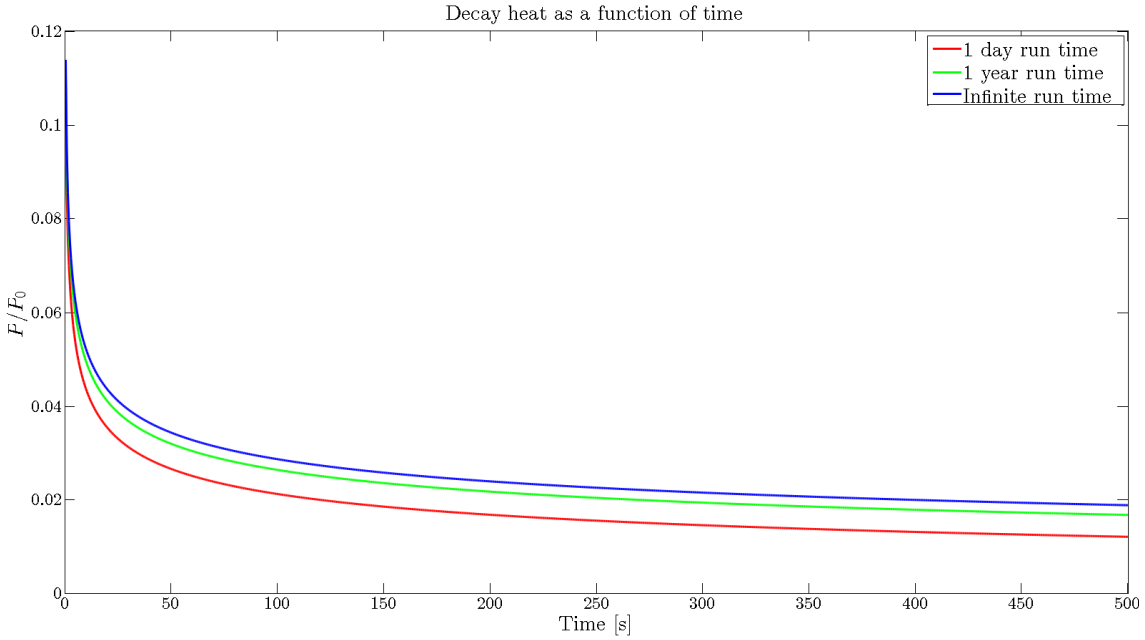

Figure 5.4: A comparison between finite run decay power profiles and an infinite run time decay heat power. Power is normalized to full power P_0.

5.6 Water Properties

All the water properties are calculated using the thermodynamic properties package XSteam, which uses the IAPWS IF-97 standard. Comparisons for values that are not directly obtainable from the package were carried against the miniREFPROR software which relies on the NIST standard reference database 23, v.9.

The primary fluid properties used for the two-phase model are the density and viscosity, mainly for estimations of the liquid-only friction factors. As in the single-phase case these fluid properties are calculated for the average hydrostatic pressure in the core and average temperature in the core, apart from a number of parameters, as will be addressed later in the section.

5.6.1 Pool Related Properties

The starting point of the analysis is, as discussed earlier, at some forced reactor shutdown. When in operation, the pool temperature is usually at around 30 °C. The highest pool temperature allowed before reactor trip is 35 °C.

As mentioned earlier, in draining scenarios the mass in Equation (4.113) is taken

as the final mass after draining for simplicity. A quick estimate of the simplification shows that for a serious draining scenario to just before uncovering the core (taking some 3.5 hours as mentioned earlier), the temperature rise in the pool is around 3 °C. The temperature after heatup is therefore still below the trip threshold of 35 °C. The pool temperature rise for the draining scenarios is therefore calculated starting from final pool inventory at 35 °C as mentioned earlier, being a conservative initial condition. This initial condition is used for all scenarios.

In calculating the mass of the pool for full inventory and for different draining levels a few pieces of data were taken into consideration. Reviewing some of MNR's technical drawings, the total height of water in the pool from the floor to the surface can be asserted to be[7] $H_{\text{full}} = 9.32\,\text{m}$ [50, 51]. Also from the technical drawings, it can be seen that the core centreline resides above the pool floor at 5 feet and 6 inches [50]. It is unclear from the drawing if the centreline represents the centre of the entire assembly or the centre of the fuel region (section 4). It is therefore assumed that the centreline is at the assembly centre, with the resulting core depth being less than assuming otherwise, leaving less pool to drain in an accident scenario and being less suppressing of boiling, both of which are conservative. The height of the core bottom above the pool floor is therefore $H_{\text{core}} = 1.24\,\text{m}$. Denote H as the height of pool water above the top of the core, the total pool height can now be written as:

$$H_{\text{tot}} = H_{\text{core}} + L_{\text{AD}} + H \ , \tag{5.15}$$

where L_{AD} is the length of the assembly as in Figure 4.1, considered to be the vertical length of the core. Therefore, for full inventory, the derived height of the pool surface above the core[8] is slightly less than 7.21 m (for $H_{\text{tot}} = H_{\text{full}}$). See Figure 3.3 for the height figures of the pool and core.

The MNR safety report states the nominal volume of the pool as $V_{\text{nom}} = 378.2\,\text{m}^3$ and the pool's surface area as $A_{\text{pool}} = 43.9\,\text{m}^2$. For a constant surface area throughout

[7] The pool wall is 32 feet and 3 inches above the floor [50] and the gutter which limits the pool surface height is located 20 inches below the wall [51].

[8] Ha [28] presented a drawing where the total pool height was 9.35 m which is close to the one found here, but where the core depth was 7.37 m. It is unclear where the figures in the mentioned drawing were taken from since no reference was mentioned. Blahnik [26] used a figure of 8.11 m for the pool surface height above the grid plate, giving a resulting height above the core top of 7.24 m. The figures used in this work are slightly conservative both to those used by Ha and Blahnik.

the pool structure, multiplying the pool height by the surface area gives:

$$V_{\text{tot}} = A_{\text{pool}} \times H_{\text{full}} = 409.23\,\text{m}^3 \ . \tag{5.16}$$

This figure is larger than the reported nominal volume V_{nom}, probably because of 'shelves' located at about a 3 m depth at the north section of the pool[9], which effectively change the surface area from that point downward. Since the calculations for pool heatup and vaporization that use the aforementioned parameters as input are themselves simplistic, some simplifications are made in order to asses the pool's mass and vaporization at different heights without accounting for geometry changes at those heights.

In order to correct for the reported nominal volume in the calculation of pool mass at different heights, the pool volume is calculated as the total volume from Equation (5.16) minus the assumed volume of the shelves and other possible core and instrumentation components. This again keeps the correct pool volume at full inventory as the reported nominal volume. The resulting volume of the shelves and other components is therefore assumed to be:

$$V_{\text{core}} = V_{\text{tot}} - V_{\text{nom}} = 31.03\,\text{m}^3 \ . \tag{5.17}$$

Observing the MNR technical drawings, it appears that the effective surface area change for the total pool, including the north and south sections, is not significant. Thus, for simplicity, the surface area of the pool at full inventory is taken as constant for all draining heights. Combining the last with the correction for the shelves volume accounts for a realistic representation of the pool mass at different heights.

The mass of the pool inventory for a given core depth H is therefore:

$$M_\infty = \rho_\infty \left(A_{\text{pool}} H_{\text{tot}} - V_{\text{core}}\right) = \rho_\infty \left(A_{\text{pool}} \left(H_{\text{core}} + L_{\text{AD}} + H\right) - V_{\text{core}}\right) \ , \tag{5.18}$$

where Equation (5.15) was used in the last transition. The mass of the pool in normal operation would be the product of the nominal volume and the density of water at 30 °C. The difference between the density for 30 °C and 35 °C produces an estimate of the pool mass being 0.16% lower for 35 °C, making the use of the latter slightly conservative. Since the temperature is mostly unchanged during the draining as was

[9]The section hosting the core.

shown earlier, the initial mass of the pool for all inventories after draining is calculated by using the density of water at 35 °C. For scenarios of further draining to revealing the core assemblies (H turning negative) the pool mass calculation was unnecessary and is therefore not treated here.

With regards to the uncovered core treatment, as noted before, the critical height figure (as defined in Section 4.3) is dependent both on the assembly power and on the inlet temperature which is the pool temperature. The parameter used for the pool level for uncovered core scenarios is the height above the heated section H_{pool} (see Figure 4.3). Define δ as the fraction of pool level to heated section, i.e. the ratio between the pool height above the heated section's bottom and the length of the heated section:

$$\delta \equiv \frac{H_{\text{pool}}}{L_4} \,, \tag{5.19}$$

where again L_4 is the length of the fuel plates (see Figure 4.1). At $\delta = 100\%$ the pool height is at the level of the top of the heated section, and at $\delta = 0\%$ the pool is at the level of the bottom of the heated section[10]. Core uncovery starts at $\delta = 108.12\%$ being the level of the top of the assemblies corresponding with $H = 0$. The height of the pool in terms of δ at the critical height will be subsequently denoted as δ_{crit}. Values for the critical height in terms of δ for a few combinations of assembly power and pool temperature are summarized in Table 5.1.

Table 5.1: Critical height, in terms of δ (percentage of pool height to assembly length), at different powers and pool temperatures.

Percentage of full assembly power / **Pool temperature** [°C]	**100%**	**50%**	**20%**	**10%**	**1%**	**0.1%**	**0.01%**
35	85.36%	38.56%	22.14%	16.67%	11.74%	11.25%	11.20%
45	87.89%	38.14%	21.10%	15.42%	10.31%	9.80%	9.75%
85	101.31%	36.77%	16.72%	10.04%	4.03%	3.43%	3.37%
100	107.99%	36.38%	14.96%	7.82%	1.40%	0.75%	0.69%

It can be seen from Table 5.1 that for high assembly powers as in the 100% power column, the reaching of critical height is sooner for lower subcoolings at inlet[11], while

[10]Not to be confused with the swell height H_{swell} which is the height of the two-phase mixture covering the plates themselves, and is higher than H_{pool}.

[11]The critical height is higher and therefore is reached sooner and with less draining.

for lower powers typical to those found a few hours after shutdown, the reaching of critical height is sooner for higher subcoolings. As mentioned before, in a beam tube break scenario, the time to drain to core level would be around 3.5 hours. In this time, the pool heatup model predicts the pool temperature to rise from 35 °C to 38 °C. However, since the pool heatup calculation is conservative, expecting a lower temperature rise than calculated, and since the uncovered model for lower powers is more conservative for lower pool temperatures (see Table 5.1), the pool temperature chosen for the safety evaluation for a quick draining is 35 °C as for the earlier scenarios.

5.6.2 Fluid Properties at Core Depth

As the pool gradually heats up, two phenomena occur simultaneously. First, the density of the water slightly diminishes with the rise in temperature. In parallel, assuming the mass of the pool stays constant for raising the temperature, the height of the pool rises by the same factor as the drop in density, as can be seen from Equation (4.116):

$$\frac{\rho_{\text{hot}}}{\rho_{\text{cold}}} = \frac{H_{\text{tot}}^{(\text{cold})}}{H_{\text{tot}}^{(\text{hot})}} < 1 \ , \tag{5.20}$$

where H_{tot} is the total height of the pool as earlier. The relation between the total height of the water in the pool H_{tot} to the height of column above the core H is as in Equation (5.15), and by grouping L_{AD} and H_{core} for convenience can be rewritten as:

$$H + \tilde{H} = H_{\text{tot}} \ , \tag{5.21}$$

where L_{AD} again represents the vertical length of the core (see Figure 4.1), $\tilde{H} \equiv H_{\text{core}} + L_{\text{AD}}$ and Equation (5.21) is true for both the 'hot' subscript after heatup and the 'cold' subscript for initial pool temperature.

Examining the pool after heating, the pressure at core depth is given by:

$$p_{\text{hot}} = p_{\text{atm}} + \rho_{\text{hot}} g H^{(\text{hot})} = p_{\text{atm}} + \rho_{\text{hot}} g (H_{\text{tot}}^{(\text{hot})} - \tilde{H}) \ , \tag{5.22}$$

where p_{atm} is atmospheric pressure, $H^{(\text{hot})}$ is the height of pool surface above the core, and where Equation (5.21) was used in the last transition. The equation for the cold

case before the pool heats up is the same with its corresponding densities and heights:

$$p_{\text{cold}} = p_{\text{atm}} + \rho_{\text{cold}} g (H_{\text{tot}}^{(\text{cold})} - \tilde{H}) \ . \tag{5.23}$$

Using Equation (5.20), Equation (5.22) can be rewritten as:

$$p_{\text{hot}} = p_{\text{atm}} + \rho_{\text{cold}} \frac{H_{\text{tot}}^{(\text{cold})}}{H_{\text{tot}}^{(\text{hot})}} g (H_{\text{tot}}^{(\text{hot})} - \tilde{H}) \ . \tag{5.24}$$

Subtracting Equation (5.23) from Equation (5.24) and rearranging results in:

$$\begin{aligned} p_{\text{hot}} - p_{\text{cold}} = \rho_{\text{cold}} g \left[\frac{H_{\text{tot}}^{(\text{cold})}}{H_{\text{tot}}^{(\text{hot})}} (H_{\text{tot}}^{(\text{hot})} - \tilde{H}) - (H_{\text{tot}}^{(\text{cold})} - \tilde{H}) \right] = \dots \\ = \rho_{\text{cold}} g \tilde{H} \left(1 - \frac{H_{\text{tot}}^{(\text{cold})}}{H_{\text{tot}}^{(\text{hot})}} \right) \ . \end{aligned} \tag{5.25}$$

The right-hand side consists entirely of constants. As seen from Equation (5.20) the term in brackets is positive and therefore the hydrostatic pressure of the column of water above the core is larger for warmer liquid. Thus, the combined effect of increasing the pool temperature on the static head above the core is to slightly increase it (at least as long as it remains liquid). As seen from Equation (5.25) it is true for any pool height or column height above core respectively as long as the pool constant mass assumption holds.

The saturation temperature at core depth is dependent on the hydrostatic pressure from the column of water above it, which itself is dependent on the density of water in the pool. As the pressure rises so does the saturation temperature. Therefore when seeking for the saturation temperature at core depth, a conservative simplification is not to calculate the saturation temperature at the core top for every given pool temperature and adjusted height, but to rather take it as the lowest limit for the saturation temperature at 35 °C for any pool height (for different draining events). In a similar manner, since in all scenarios the process is one way, namely, pool heating, the above phenomena can be used to set a conservative limit for any fluid property at the core that monotonically changes with the rise in pressure.

In order to obtain the flow rates in Equations (4.36) and (4.71), knowledge of the fluid properties in the core is required. Apart from the densities, which govern the

flow and are strictly defined in the models, there is some freedom in evaluating the other properties required, such as the thermal expansivity and the viscosity. In the attempt to best represent these properties, they are taken at the average hydrostatic core pressure and with some averaging over temperature. Since the pressure rises linearly with height (in the open pool) the average pressure is simply:

$$\bar{p} = \frac{p_{\text{core}}^{\text{top}} + p_{\text{core}}^{\text{bottom}}}{2} \ . \tag{5.26}$$

The static head at top and bottom is calculated using the density at 35 °C corresponding to the aforementioned effects of pool heating. In any case this pressure change along the entire core is quite small such that fluid properties are nearly unchanged in this pressure range.

Averaging properties over temperature on the other hand is a bit more complicated. Water properties change with temperature is not linear and therefore a property taken at an average temperature isn't necessarily equal to the temperature averaged value of the same property. It however has been found, as will be shown in the results chapter, that the temperature rise along the channel for decay heat powers is in most cases rather modest; between 10 °C to 20 °C. In such a range most fluid properties don't change drastically. From that and since the temperature rise along the channel is linear in the model, it was decided that taking the fluid properties at the average temperature is a reasonable simplification. This requires some iteration, since the temperature rise along the channel is not known at start. After finding the temperature rise along the channel the mean temperature is also given by a simple average:

$$\bar{T} = \frac{T_{\infty} + T_{\text{exit}}}{2} \ . \tag{5.27}$$

The Reynolds number for section 4 is calculated for the single-phase case at average pressure and temperature fluid properties (viscosity) as just discussed, and for the two-phase case with fluid properties at saturation, as suggested by Gambill and Bundy [5]. For sections 1-3 the Reynolds number for producing the friction factor is calculated at average pressure and pool temperature. Section 5's fluid properties are calculated at average pressure like the rest, at exit temperature for single-phase and at saturation temperature for the two-phase case. The same considerations hold for the properties used for the heat transfer coefficient calculation, being the average fluid properties for

the single-phase case and the saturation properties for the two-phase case.

The thermal expansion coefficient β is not given by the XSteam package. It is found from its definition in Equation (4.11). The derivative in the expression is turned to a finite difference over a temperature difference of $10^{-3}\,^{\circ}\mathrm{C}$. This produced a relative error of less than 1% between calculated β values and miniREFPROP values for the required range for the calculations, and even less than 0.1% for temperatures higher than $46\,^{\circ}\mathrm{C}$. XSteam's value for the specific volume is undefined for saturation conditions and therefore was fixed to a hundredth of a degree back if β is to be calculated for such temperature and pressure.

5.7 Hottest Channel Flow Rate Treatment

As mentioned earlier, the flow through the assembly is divided into 17 channels between the 18 fuel plates in section 4 (of the assembly sections). The outer two plates are dummy plates which contain no fuel. The flow is therefore not evenly distributed between all channels and must be at least somewhat different in the two peripheral channels. For the following treatment, the power distribution in the assembly between the different plates is ignored and all the plates are assumed to have the same average power. The earlier statement regarding flow in the outer channels, however, remains true. Identifying the inner channels with the subscript 'in' and the two outer with the subscript 'out', from the conservation of mass it can be noticed that the entire assembly flow rate must be equal to the sum of the individual channel flow rates:

$$\dot{M} = 15\dot{m}_{\mathrm{in}} + 2\dot{m}_{\mathrm{out}} \ , \tag{5.28}$$

where $\dot{m}$ denotes the flow rate in a channel as opposed to the total flow rate in the assembly $\dot{M}$. Also, since the outer channels have only one plate heating them they receive half the heat rate compared to the inner channels:

$$\dot{q}_{\mathrm{in}} = 2\dot{q}_{\mathrm{out}} \ , \tag{5.29}$$

where $\dot{q}$ is the power of a single channel[12].

[12]Each channel accepts heat flux from two plates. Neglecting heat losses from the top and bottom edges (by noting that the plates are very thin), each fuel plate radiates half of its power generation into the two channels it's in contact with. Each inner channel receives two halves of the plate's power,

The flow rate in natural convection is a product of the density gradient along the channel, and therefore is itself proportional to the channel power as shown in Equation (4.36), and can be put as:

$$\dot{m} \propto \sqrt[3]{\dot{q}} \, . \tag{5.30}$$

Therefore the proportion of flow in the inner channels to outer channels is going to roughly behave as follows:

$$\frac{\dot{m}_{\text{in}}}{\dot{m}_{\text{out}}} \propto \frac{\sqrt[3]{\dot{q}_{\text{in}}}}{\sqrt[3]{\dot{q}_{\text{out}}}} \, , \tag{5.31}$$

and by using Equation (5.29):

$$\frac{\dot{m}_{\text{in}}}{\dot{m}_{\text{out}}} \propto \sqrt[3]{\frac{2\dot{q}_{\text{out}}}{\dot{q}_{\text{out}}}}$$

$$\dot{m}_{\text{in}} \propto \sqrt[3]{2}\dot{m}_{\text{out}} \, . \tag{5.32}$$

The above is done under the assumption that the rest of the constants and water properties appearing in Equation (4.36) are fairly insensitive to the change in power such that the power is the dominant figure driving the flow and the other parameters almost cancel out. It is thus argued here that even with the simplification of taking the power of all plates as an equal average power, the flow in the outer channels is still expected to be at the very least lower than the flow in the 15 inner channels, such that taking the inner channel flow rate as 1/17 of the assembly flow rate would be considered conservative (at least for the hottest channel)[13].

In reality, small changes in plate power due to power distributions will lead to subsequent small deviations between any two channels. The power distribution within the assembly is such that the power steadily diminishes towards the middle, making the outer plates the hottest [1]. This model as shown in Equation (4.36) ignores these small deviations by analysing the entire assembly, and taking the combined power of the assembly as the driving term in the equivalent channel for all individual flow paths between the plates combined. To zoom on a single channel in a conservative treatment, the hottest channel should be examined. Since such a channel produces more

thus receiving the equivalent of the power of one plate. Outer channels receive one half of the plate's power since their outer plates contains no fuel and don't generate heat.

[13] If all 17 channels had the same flow, each channel would contribute 1/17 of the assembly's flow. By Equation (5.28), if the outer channels' flow is lower then the inner channels' flow must be higher, and somewhat larger than 1/17 of the assembly flow.

power, it will have a higher flow in accordance with the discussion above, regardless of the expectation for the outer channels to take up less of the flow (per channel) compared to the 15 inner channels[14]. Considering both phenomena, it is asserted that a conservative calculation for a temperature or enthalpy rise along the hottest channel can be performed by use of 1/17 of the assembly's flow rate against the hottest channel's power.

5.8 Numerical Solutions

As shown in Chapter 4, some of the calculations are non analytical and require some form of a numerical treatment in order to be solved. The main computational tool used for both analytical and non-analytical calculations is the programming language MATLAB. Most of the non-analytical calculations entail short scripts, performing mostly iterations of the governing equations to converge on the sought variable in the precision needed. The precision chosen for all such calculations was of the order of 10^{-5} being a high precision considering the uncertainties in the used correlations but still low in terms of computational power and hardware demands.

For the single-phase model, Equation (4.36) is solved by first guessing a set of friction factors, and then iterating until the flow rate converges to within a 10^{-5} relative error from its former value. A reasonable first guess for all friction factors is the value 0.5 from which iteration starts. A flow rate is calculated with these values and then a set of new friction factors is computed which correspond to the given flow rate. For the turbulent friction factor there is an inner iteration, since the value itself is given by an iterative recipe (see Equation (4.33)). It usually converges very quickly, within less than 5 steps. The 'snapshots' of the pool and core states for the single-phase calculations are taken at 5000 equally spaced time values until saturation. For calculations that continue beyond reaching of pool saturation the resolution is kept the same as the one used before reaching saturation. These are sufficient to plot the time evolution and behaviour of the pool core and fuel. For the different conditions of draining within the range examined, the time lapse between each snapshot is between roughly one minute and half an hour. The transient is very slow, and no spikes in

[14]Provided the reasonable assumption that the power of the outer plate is less than twice the power of the middle plates, and thus the power in the outer channels is still somewhat lower than the power in even the lowest power inner channels.

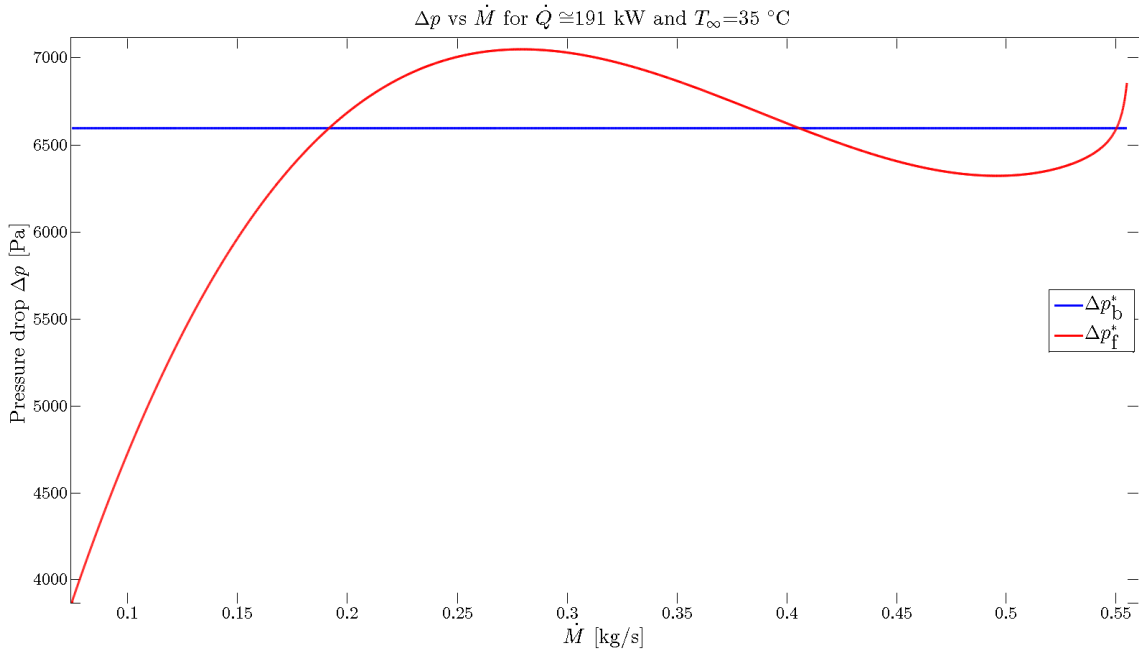

Figure 5.5: Pressure drop as a function of flow rate for the two-phase model. Using Equation (5.33), plotting left against right hand side of the equation.

the pool temperature should occur between the snapshots since the pool heatup is governed by a known analytical equation.

As mentioned earlier, the approach to numerically solve the two-phase case flow rate is to graphically solve Equation (4.71). Following the approach described in Section 4.2.3, separating both sides of the above equation produces:

$$\rho_\infty(L_4+L_5)g = \left(\bar{\rho}_\mathrm{l}L_{1\phi} + \rho_\mathrm{f}\frac{\ln(1+\gamma)}{\gamma}L_{2\phi} + \rho_\mathrm{f}\frac{1}{1+\gamma}L_5\right)g + \left(\sum_i \frac{f_i L_i}{2\rho_i D^i_\mathrm{e} A_i^2} + \sum_j \frac{K_j}{2\rho_j A_j^2}\right)\dot{M}^2 \,. \quad (5.33)$$

Denote the left hand side as the effective driving term Δp^*_b and the right hand side as the effective friction term Δp^*_f. An example to such a procedure, with an assembly power of 20% above full power for illustration, is given in Figure 5.5. The intersections of the right-hand-side curve with the left-hand-side constant term are the solutions for the possible flow rates.

As can be seen from Figure 5.5, there can be up to three solutions for the flow rate at any given power. The middle solution is unstable since it is at a point where an increase

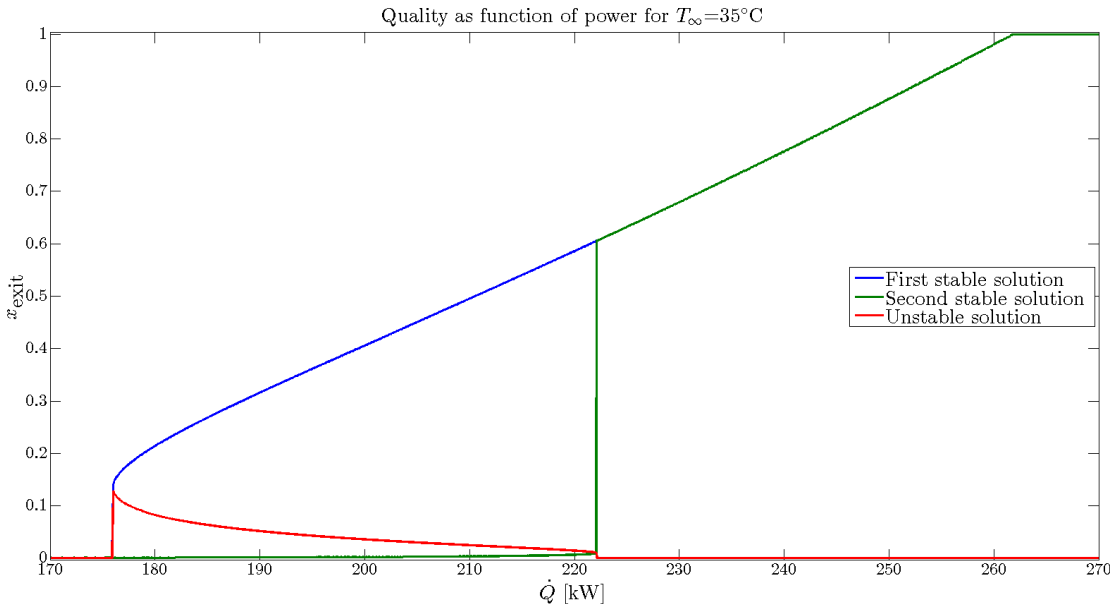

Figure 5.6: Vapour quality as a function of assembly power for pool at 35 °C temperature and full inventory. Using Equation (5.33), inputting a span of assembly powers.

in the flow rate decreases the pressure drop, further contributing to increasing the flow rate, and so forth. The two stable solutions are thus the smallest and the largest flow rates at the intersections of the two curves. These intersections are numerically found by subtracting the constant solution from the variable one, and then observing when the values of the pressure drop change sign from negative to positive or contrariwise. The intersections are taken as the midpoint between every two such opposing-signs points, such that the precision is that of the resolution chosen for the plotting of the curve. The flow rate range is at most between $0\,\mathrm{kg\,s^{-1}}$ to $1\,\mathrm{kg\,s^{-1}}$, and the resolution chosen was that of 5000 points. This means that the last digit precision in the flow rate calculation is on the order of 10^{-4}. After the flow rate is found the exit quality is calculated by use of Equation (4.75).

The latter is also used to determine the limiting conditions for which the vapour quality in the hottest channel begins approaching 100%. This is done by performing the earlier calculation for a fixed pool height and temperature over a span of powers until observing the quality reaching beyond 99%. An example of this is presented in Figure 5.6 where the span of qualities as a function of assembly power is given for the pool at full inventory and nominal temperature. Besides the three distinct solutions for the quality that can be spotted on the plot, it can be seen that for the

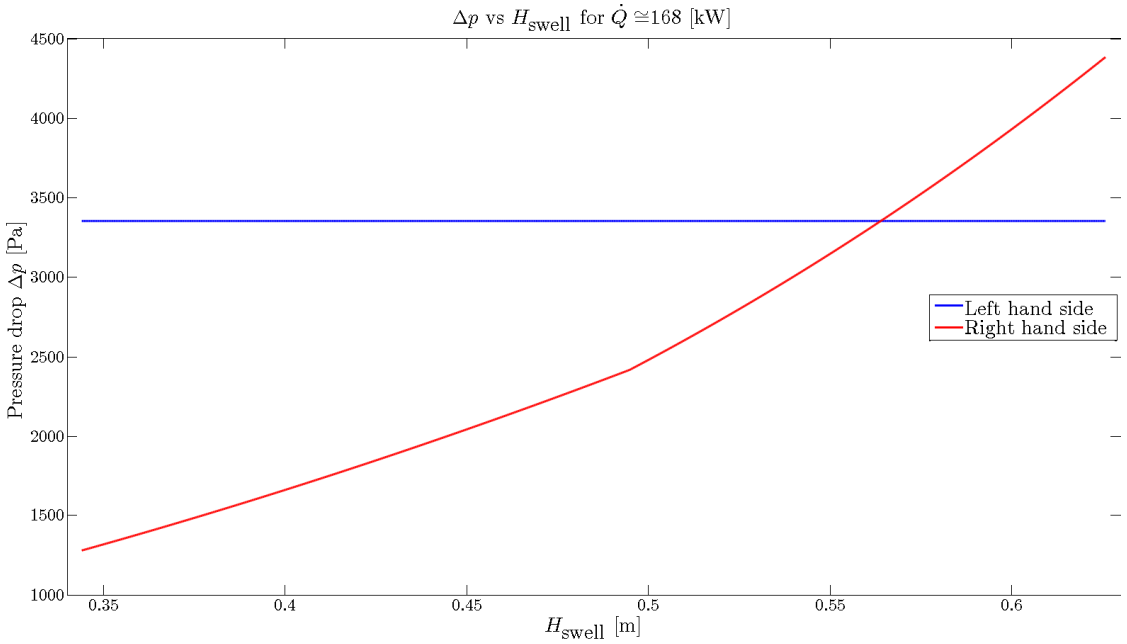

Figure 5.7: Pressure drop as a function of swell height for the below-critical uncovered core model. Using Equation (4.95) after leaving the constant term on the left hand side, plotting both sides of the equation.

given parameters, the onset of boiling is easily spotted at the point where the quality rises very sharply from zero. The two-phase model is not valid for qualities below zero or above one, and can be seen to flatten out again after reaching values very close to it at around 99% quality. The point where this asymptote is reached was therefore considered as the point of first superheating.

The uncovered core numerical solution is performed using the same method described above. For the case of pool heights above the critical height the equations are almost the same (compare Equations (4.71) and (4.87), apart from the the left hand side which changes to $\rho_\infty g H_{\text{pool}}$). For the case of pool heights below critical, the left hand term is the same as the above-critical case, but the right hand side is solved for H_{swell} (see Equation (4.95)). An example for the numerical solution for this case can bee seen in Figure 5.7. In this example the pool is at 55% height of the heated section and the resulting swell height is covering 90% of the fuel.

Chapter 6

Results and Discussion

As discussed earlier, the postulated events examined deal with abnormal core cooling after a forced shutdown due to draining. The first set of events deals with draining scenarios that have been mitigated before core uncovery. These branch into the first stage, at which single-phase natural convection is sustained through the core, and the second stage, when the core reaches saturation and two-phase natural convection commences. Either of the two can be sustained as long as the pool height remains above the critical height[1]. At this point a third mechanism of natural convection, namely uncovered core steaming, governs the flow through the assemblies. If draining is caused by a break in a beam tube, the third stage may be reached rather quickly, mostly skipping the first two. Theoretically, this may also be caused without core uncovery for very high powers, but as will be shown here, will only happen in an MNR assembly for powers much higher than those characteristic of normal MNR operating power.

6.1 First Stage of Draining

Following Chapter 5 the assessment starts with the conservative parameters of the reference core and the highest pool temperature corresponding to the pool temperature trip. These are as mentioned before, $5\,\mathrm{MW} + 17\%$ for core power and $35\,^{\circ}\mathrm{C}$ for the pool temperature. Following the rational of progression from the first set of events onto

[1] Reminding, the pool height at a given power for which the coolant turns to superheated steam at the edge of the heated channel.

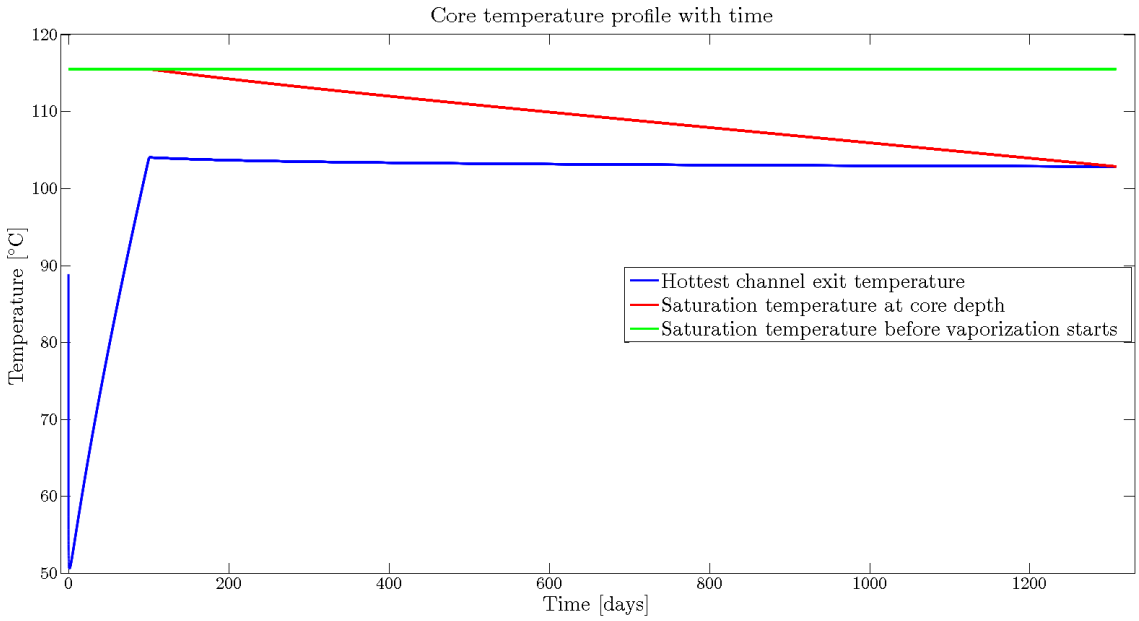

Figure 6.1: Hottest channel exit temperature and core saturation condition vs. time for full pool inventory.

the second and third, the spectrum of pool heights from full inventory to just before core uncovery is examined first. Starting with these parameters, the evolution of the pool temperature, using the simplistic pool heatup model as described in Section 4.6, and the corresponding temperatures at the exit of the hottest channel, using the single-phase convection model as described in Section 4.1, are calculated until the onset of boiling. For drains that resolve before (and above) a certain height is reached, the predicted exit temperature from the hottest channel is still below saturation, even if the pool has reached saturation as predicted by the pool heatup model (since saturation temperature at core depth is higher). In this case, the pool heatup calculation switches to the pool vaporization calculation as given in Equation (4.116) and the calculation continues. The process is presented for full pool inventory in Figure 6.1 where pool vaporization is reached and modelled.

A few phenomena can be spotted along the exit temperature curve of Figure 6.1. Initially, in the first hours, while power is dropping quite quickly and the pool temperature has yet to increase substantially, the exit temperature is dropping quite rapidly in accordance with the power while the inlet temperature is rising much slower. This can be spotted at the lower left corner of the figure. At a certain point, the trend reverses when the power drops to a near asymptote profile. In this region where the power

is almost constant, the difference between the channel exit and inlet temperatures according to Equation (4.13) is almost constant as well. The exit temperature in this region is thus governed mostly by the slowly rising pool temperature which is also the inlet temperature to the core. The point where the model predicts pool saturation is therefore easily spotted, as the point where the exit temperature ceases to rise. From this point on, the exit temperature very slowly reduces in accordance with the slow reduction in decay power, since the inlet temperature has reached a maximum. It can be seen that at the point of pool saturation the assembly power isn't high enough to bring the assembly exit temperature to the saturation temperature. From this point on, any additional heat coming from the core is directed towards vaporizing the pool water. As the model switches to the pool vaporization mechanism, the pool level starts dropping, along with the static head above the core, and with it the saturation parameters at core depth. This is seen in the branching off of the red curve from the green curve representing the initial saturation temperature at core depth. This process of diminishing core saturation temperature is competing to catch up with the channel exit temperature, which at this point, as shown, is also dropping. Eventually, this resolves when the pool level has dropped (again due to vaporization) enough such that the pressure at core depth is now low enough that its corresponding saturation temperature equals the channel exit temperature. This is the point predicting the onset of boiling.

Alternatively, examining the other extreme, for the scenario of draining the pool to right above core top, the core's hottest channel exit temperature reaches saturation before the pool is at saturation. Figure 6.2 presents the exit temperature profile for this second case. It is apparent that there exists a draining to a certain height between the two extremes, below which the core reaches boiling conditions before the pool does and above which it doesn't. Performing the calculation for different draining heights, this 'saturation' height is found to be below 1.91 m above the core. For water heights above the critical height the model shows an additional delay before saturation is reached in the channels, because of the additional amount of time it takes to vaporize a unit height of pool water to bring the channels to saturation, while having the exit temperature also drop in that time.

At this point the heat transfer is by liquid single-phase convection and its evaluation is as in Section 4.1.4. The clad temperatures are subsequently calculated as in Section 4.4 and their profiles for the two above discussed extremes are presented in

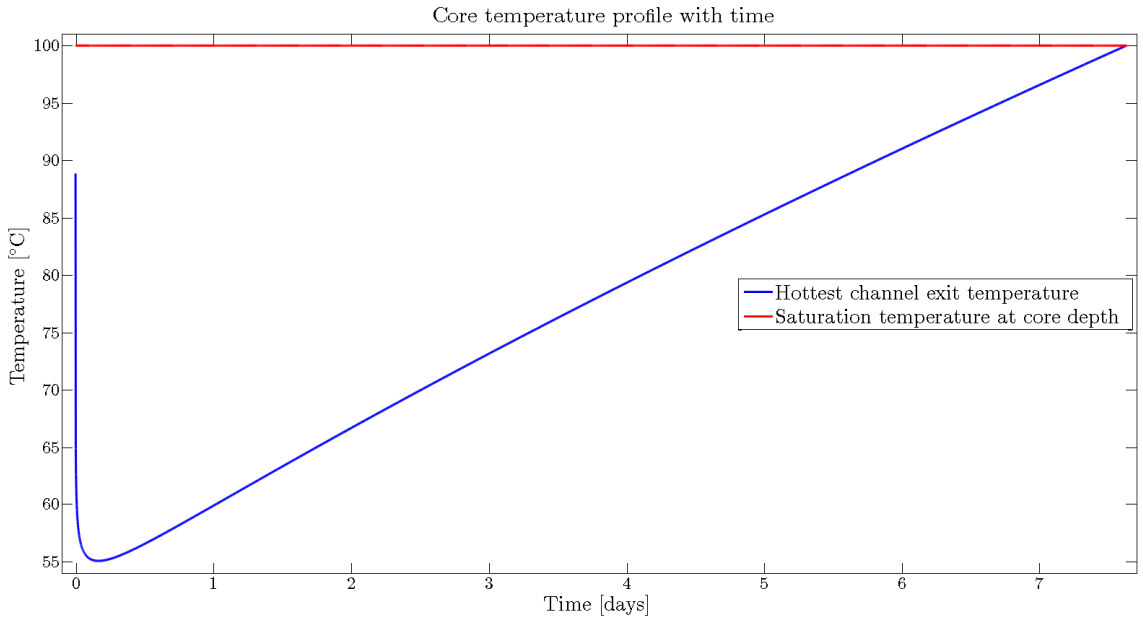

Figure 6.2: Hottest channel exit temperature and core saturation condition vs. time for draining to just before core uncovery level.

Figures 6.3 and 6.4. The fuel temperatures for all scenarios (again as in Section 4.4) were found to be very close to the clad temperatures, usually higher than the clad by no more than 1 °C. This is reasonable given how thin the fuel plates are and the relatively highly conducting materials they are built from. It is found that for all times in the two extremes presented, the clad is well below blistering temperature limits (450 °C). From this it can be concluded that clad temperatures remain within safe values when cooled by the liquid single-phase natural convection mechanism.

A figure of interest is the amount of time it takes to reach saturation and onset of boiling in the hottest channel. Such a summary of times to saturation for different pool draining levels without core uncovery is presented in Table 6.1. The time figures for scenarios of relatively little draining are exceptionally large, predicting some three months to reaching pool saturation and some three and a half years to vaporizing the pool down to a level where boiling starts for the full inventory. With the combination of low powers as are expected in the MNR after shutdown, and the very large body of water in the pool, it is reasonable to expect that a more accurate model, including heat losses to the air and concrete in the containment, would predict the pool heats up even less. Additionally incorporating a model for evaporation for temperatures below saturation, may lead to the result of reaching some steady state pool temperature

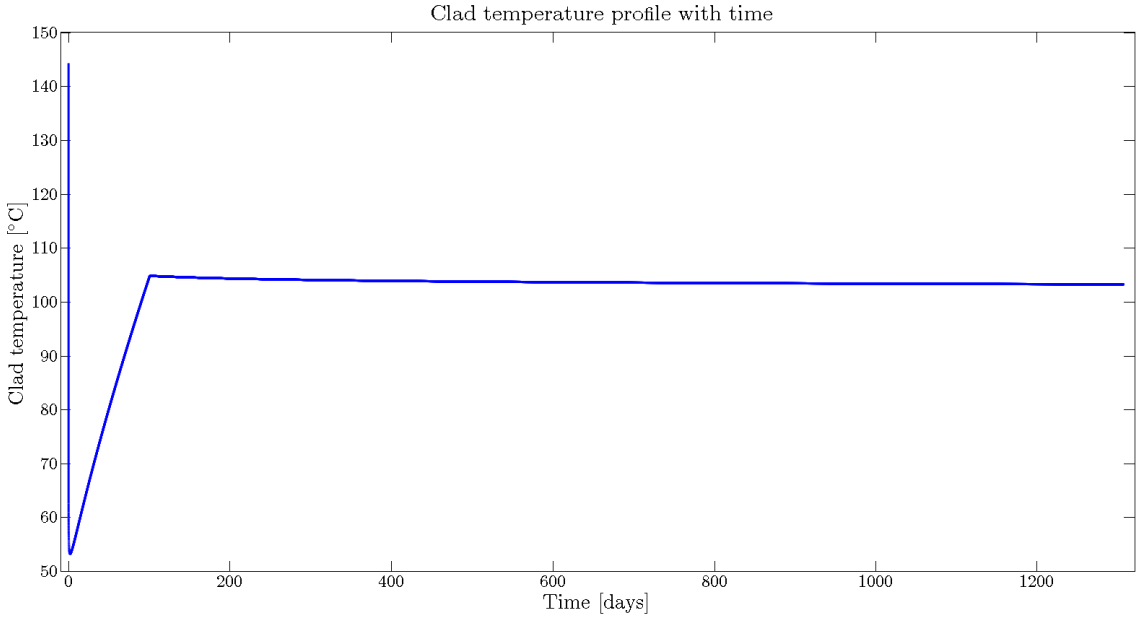

Figure 6.3: The temperature of the clad with time for full pool inventory.

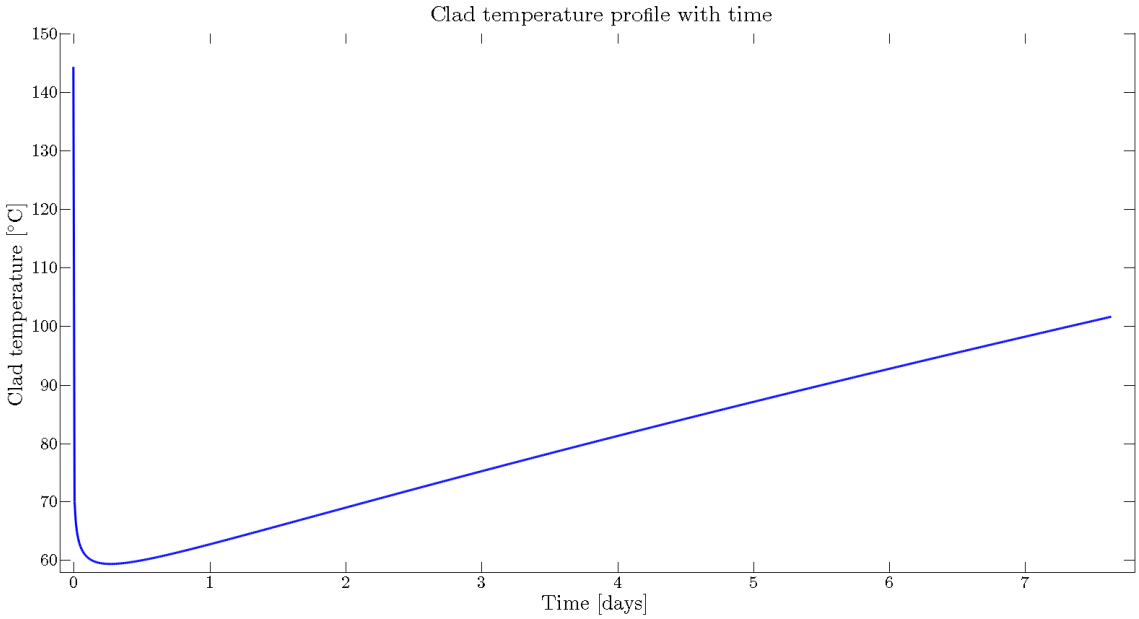

Figure 6.4: The temperature of the clad with time for draining to core level.

below saturation, where evaporation is in steady state with the heat balance on the pool [23]. If left untouched, a pool containing the same amount of water would lose, by evaporation alone, enough inventory to uncover the core after about a year an a half[2]. Since such large times are being output by the simplistic model used, it's hard to assess the pool behaviour without adding the aforementioned additional mechanisms. It is reasonable however to expect, whether heat losses and evaporation lead to quicker or slower reaching of boiling in the core than presented in Table 6.1, that the pool heatup would be on the same order of magnitude in time. It is unreasonable to expect no intervention and 'abandoning' of the facility for such long periods, insuring that there will be some recovery of pool inventory before this happens. Draining events for which the model expects boiling to develop after more than a few weeks can be therefore discarded as non relevant. As a rule of thumb, the saturation height at draining to 1.91 m above the core is chosen as the cutoff, such that draining events that have been resolved above this height cannot plausibly lead to any fuel damage. For draining to just before core uncovery level, boiling is not predicted to start until about a week after shutdown, allowing for sufficient time for intervention in that case as well.

Table 6.1: Time to saturation in the hottest channel for draining mitigated at different heights.

Height above core [m]	**7.21**[3]	**7**	**6**	**5**	**4**	**3**	**2**	**1.91**[4]	**1.8**
Time to saturation [days]	1305	1247	973	716	477	259	58	27	26.3
Height above core [m]	**1.7**	**1.6**	**1.5**	**1.4**	**1.3**	**1.2**	**1.1**	**1**	**0.9**
Time to saturation [days]	25	23.8	22.6	21.4	20.3	19.1	18	17	15.9
Height above core [m]	**0.8**	**0.7**	**0.6**	**0.5**	**0.4**	**0.3**	**0.2**	**0.1**	**0**
Time to saturation [days]	14.9	13.9	12.9	11.9	11	10.1	9.3	8.4	7.5

6.2 Second Stage of Draining

In the next stage after the onset of boiling, two-phase natural convection assumes in the core channels. The parameters associated with the onset of boiling at the times presented in Table 6.1, the important of which being power, pool height and

[2]The MNR safety report mentions evaporation losses of about 500 L a day, which amounts to 633 days required to evaporate the column of water above the core.

[3]Height above core for full pool inventory.

[4]Height below which saturation is reached in the hottest channel before the pool reaches saturation.

pool temperature, were inserted into the two-phase model as given in Section 4.2 in order to find the corresponding flow rates and exit qualities starting from the onset of boiling and onward. The estimated flow rate and corresponding exit quality are input parameters for obtaining the two-phase flow boiling heat transfer, as given in Section 4.2.4. Using the appropriate heat transfer coefficient, the clad and fuel temperatures are calculated as before. It was found that for the second stage starting conditions corresponding with the times presented in Table 6.1, the two-phase model predicted that the liquid is still subcooled at the exit of the hottest channel. In general the two-phase model predicted the onset of boiling at higher powers than those predicted by the single-phase model for most conditions, apart from very low subcooling and low pool heights. Therefore, higher powers than those anticipated by the decay-heat profile at second stage initial conditions, the lowest at which the two-phase model predicted boiling, were used to calculate the flow rates and qualities. The resulting temperatures at these points are presented in Table 6.2. The heights presented in the table are, as earlier, those at which draining was stopped. The actual heights of the pool above the core at the points where boiling started, for the span of draining heights above the saturation height, were between 1.1 m to 1.91 m, since for those scenarios further vaporization was predicted by the model before boiling was reached.

Table 6.2: Clad temperatures at hottest channel's exit for the conditions for onset of boiling from Table 6.1. All temperatures are rounded up to first decimal.

Height above core [m]	**7.21**	**7**	**6**	**5**	**4**	**3**	**2**	**1.91**	**1.8**
Clad temperature [°C]	105.6	105.5	105.7	106	106.2	106.7	108	108.8	108.6
Height above core [m]	**1.7**	**1.6**	**1.5**	**1.4**	**1.3**	**1.2**	**1.1**	**1**	**0.9**
Clad temperature [°C]	108.3	108.1	108	107.8	107.5	107.3	107.2	107	106.8
Height above core [m]	**0.8**	**0.7**	**0.6**	**0.5**	**0.4**	**0.3**	**0.2**	**0.1**	**0**
Clad temperature [°C]	106.6	106.3	106.2	106	105.7	105.6	105.4	105.1	105

As can be seen, using the predictions of the two-phase heat transfer coefficient, the resulting clad temperatures are again far below blistering temperature and are very close to the coolant temperature which is at saturation. From here onward, it is possible to continue the pool level and temperature calculation as has been done up to this point (for example in Figure 6.1) and obtain the corresponding local hottest channel temperature or enthalpy rise in later times. As the boiling continues the conditions in the core may worsen in the sense that higher vapour qualities will be

generated and the heat transfer will deteriorate, although it is also possible that the boiling will die out before that happens if the decay power decrease is faster than the pool vaporization. A limiting condition, both in reality and for the two-phase model, is when the vapour quality at the hottest channel's exit reaches 100%. This is the point before the conditions transfer to the third stage which is core uncovery[5]. Table 6.3 presents the combination of conditions, for the span of possible pool heights and temperatures before uncovery, for which the hottest channel's exit quality approaches 100%.

Table 6.3: Assembly powers [kW] for which the hottest channel's exit quality approaches 100%, given pool (assembly inlet) temperature and pool height above the core.

Height above core [m] / **Pool temperature** [°C]	**7.21**	**7**	**6**	**5**	**4**	**3**	**2**	**1**	**0**
35	261.8	260.2	252.8	245.1	237.1	228.9	220.3	211.4	202
45	256.7	255.3	248	240.4	232.6	224.6	216.2	207.4	198.3
55	251.6	250.2	243	235.7	228.1	220.1	211.9	203.4	194.4
65	246.4	245	238	230.8	223.4	215.6	207.6	199.2	190.5
75	241.1	239.6	232.9	225.8	218.5	211	203.2	195	186.6
85	235.7	234.3	227.6	220.8	213.7	206.3	198.7	190.7	182.4
95	230.1	228.7	222.2	215.5	208.6	201.4	193.9	185.9	177.5
100	227.2	225.9	219.4	212.8	205.8	198.6	190.9	182.3	169.3

It can be seen from Table 6.3 that the two-phase mixture approaches superheating at the exit from the channels for relatively high powers, most of which are above the licensed operating permit for the MNR[6]. The only assembly powers associated with core powers below the maximum nominal licensed one, appear for parameter combinations of pool temperature at 75 °C and above and pool height at 1 m and below. In the time it would take to bring the pool to those conditions the average assembly decay heat power would drop to well below the powers presented in the table. It is therefore concluded that there cannot be steam superheating in the core for scenarios not involving core uncovery in the MNR.

[5]Core uncovery here is meant in the sense of generating superheated steam covering a certain fraction of the heated channels. Under conditions of high enough power this may occur even if the pool is completely covering the core.

[6]For the reference core power plus 17% uncertainty, the resulting average assembly power is 186.5 kW.

To verify that the temperatures of the fuel plates do not exceed safety limits, they are calculated for the conditions of approaching superheating, as given in Table 6.3. The results are given in Table 6.4. This shows, assuming validity of the usage of Kandlikar's two-phase heat transfer coefficient as in Section 4.2.4, that as long as the two-phase mixture hasn't reached superheating conditions, acceptable clad temperatures are maintained in the core. Despite the quite high powers associated with the approach to core uncovery, fuel centerline temperature remains not more than 4 °C hotter than the clad's surface.

Table 6.4: Hottest channel clad temperatures at the exit in °C for conditions where exit quality approaches 100% according to Table 6.3. All temperatures are rounded up to first decimal.

Height above core [m] / **Pool temperature** [°C]	**7.21**	**7**	**6**	**5**	**4**	**3**	**2**	**1**	**0**
35	171.3	170.3	165.5	160.7	155.7	150.6	145.3	139.9	134.3
45	169.6	168.6	163.9	159.2	154.3	149.3	144.1	138.8	133.2
55	167.8	166.9	162.3	157.6	152.8	147.8	142.8	137.5	132.1
65	165.9	165	160.5	155.9	151.2	146.3	141.4	136.2	130.9
75	163.9	162.9	158.5	154	149.4	144.7	139.8	134.7	129.5
85	161.6	160.7	156.4	151.9	147.4	142.7	137.9	132.9	127.7
95	158.9	158	153.7	149.3	144.8	140.1	135.3	130.2	124.8
100	157.3	156.4	152.1	147.7	143.1	138.3	133.2	127.6	120.2

It becomes clear that it is unnecessary to continue the pool evolution calculation after the onset of boiling to find the exact flow rates and exit qualities, since it is apparent that they will be well below the point of superheating. More so, since the decay heat power keeps on dropping, the boiling will eventually die out as long as the core is submerged. There is therefore, no combination of parameters for a covered (submerged below pool level) MNR core that can lead to achieving of unsafe clad temperatures. The only plausible mechanism to bring the core to uncovery is by dropping the pool height to the point of exposing the core.

6.3 Third Stage of Draining

Theoretically, pool level dropping below the level of the core top could occur either by a quick draining or by a very long pool vaporization. Continuing with the earlier

justifications, the latter is dropped for being highly implausible. As addressed before, a fast draining and core uncovery will be associated with a break in one of the beam tubes. As covered in Section 4.3 the exposing of the core by draining will not immediately lead to fuel plate uncovery but rather still produce a two-phase mixture flow out of the assemblies. Such two-phase steady-state flow or intermittent geysering out of the assemblies will occur as long as the pool level is above the critical height[7]. As long as the vapour quality in the mixture is below 100%, which is the case above the critical height, the heat removal mechanism is of two-phase heat transfer and the clad temperatures are expected to remain within safe limits as shown in the earlier section.

Following the reasoning in Section 5.6.1, the parameters chosen for the core uncovery are the assembly power at 3.5 hours after shutdown, and the upper bound of the allowed pool temperature. The critical height for which the fuel begins to be uncovered is calculated as explained in Section 4.3 by setting the swell height at the top of the heated section in Equation (4.95). Under the above conditions the resulting critical height is $H_{\text{crit}} = 7.28\,\text{cm}$ or in terms of fraction of the heated channel, $\delta_{\text{crit}} = 11.64\%$. This again means that when the pool level drops to 7.28 cm above the bottom of the heated section, or in other words to 11.64% of the heated section length, the swell height inside the hottest channel begins to drop below the top of the heated channel height, exposing the top of the fuel plates to steaming. This is the point where the model predicts the two-phase overflow to turn into single phase steaming. To make sure that the clad temperatures indeed remain within the safety limits while in the two-phase overflow mode, they are calculated for pool levels in the span of heights from assembly exposure ($H = 0$, $H_{\text{pool}} = 67.63\,\text{cm}$)[8] to reaching critical height ($H_{\text{pool}} = 7.28\,\text{cm}$). The resulting clad temperatures are presented in Figure 6.5.

For the first 5 cm of draining below $H = 0$, the two-phase model predicts that the given power is not high enough for boiling (no solutions for the flow rate) and therefore coolant and clad temperatures could not be calculated. In this range however the plates are completely covered with liquid or a two phase mixture, which from the earlier sections is sufficient to keep them sufficiently cooled. If, as the two-phase model predicts, the power isn't sufficient to cause volume expanding in the hottest channel

[7] As defined in Section 4.3, the pool height for a given power and inlet temperature below which the coolant within the hottest channel starts exposing the fuel plate to steam. This level is always found between the edges of the heated channels section.

[8] See treatment in Section 4.3 and Figure 4.3, and discussion in Section 5.6.1: H_{pool} is measured from the bottom of section 4 and H is the height of the pool above the top edge of the assembly when the core is submerged.

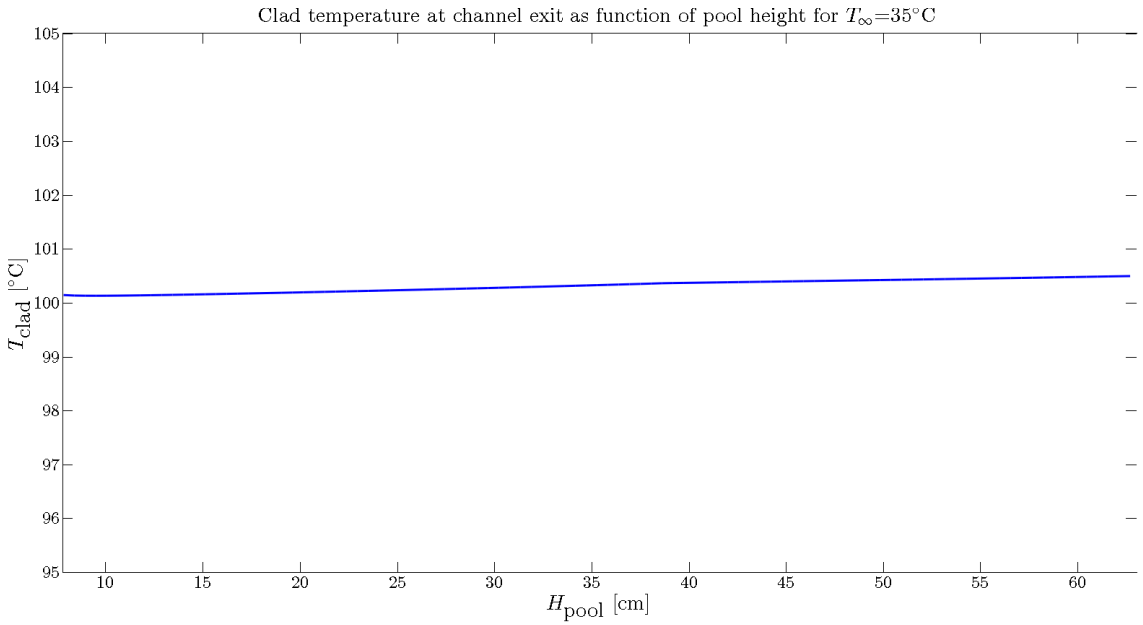

Figure 6.5: Clad temperatures for pool levels uncovering the assembly but above critical height. Calculated for assembly power at 3.5 hours after shutdown.

to overflow from the assembly, the liquid in the channels will heat up to saturation by the pool boiling mechanism, which will then eventually expand the mixture volume to geyser out intermittently as illustrated in Section 4.3. This is not a steady state and therefore is not found as a solution to the steady-state two-phase model. Again, the fuel plates in any case will remain submerged at these conditions, and the temperatures are expected to be similar to those corresponding to low pool heights in Table 6.1. In the rest of the range, as seen from Figure 6.5 the predicted clad temperatures at the top of the channel are sufficiently low and very close to the coolant saturation temperature. Therefore, as assumed, for pool heights above the critical height the clad remains sufficiently cooled.

Next is the stage where the pool height drops below the critical height. The swell height as a function of pool height is presented in Figure 6.6. The swell height is in terms of its ratio with the length of the heated section ϵ and the pool height is in terms of its ratio with the length of the heated section δ. On the one extreme, the swell covers the entire plate section for pool heights above 11.64% of the heated section which is the critical height. On the other extreme, when the pool height drops to the bottom of the fuel plates no swell height could be sustained any longer since all the liquid is below the heated section, and at this point the core is fully exposed.

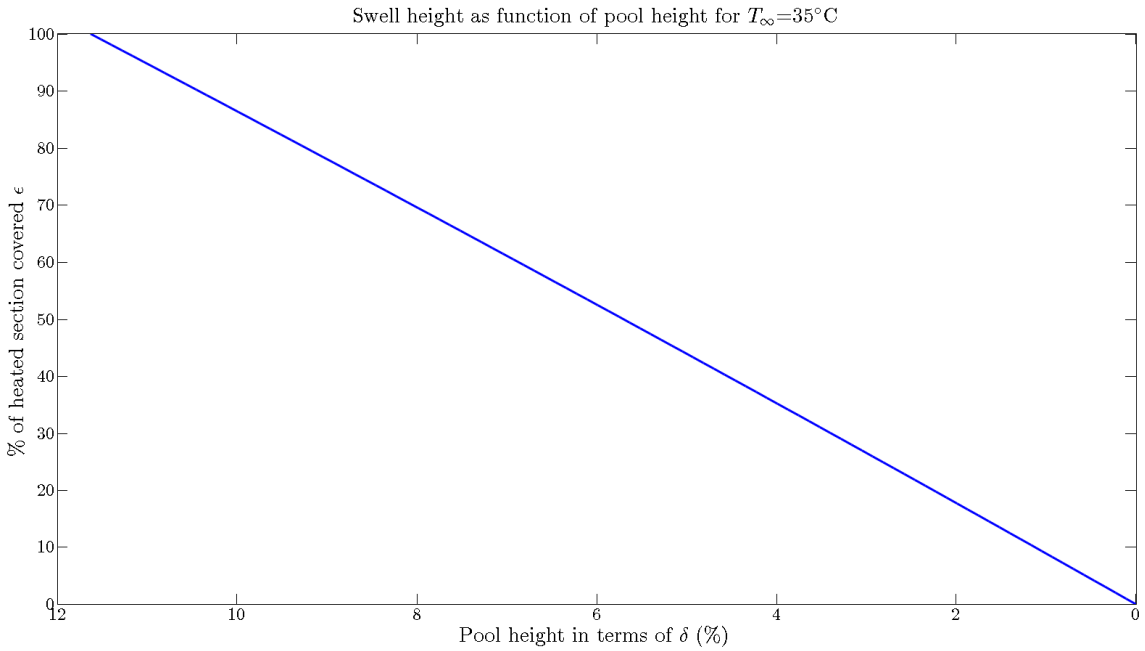

Figure 6.6: Percentage of fuel plate covered as a function of pool height for pool heights below the critical height.

The enthalpy of the exiting steam is used to obtain the required water properties in order to calculate the resulting heat transfer coefficient and clad temperature. The heat transfer coefficient is again the single-phase Dittus-Boelter as given in Equation (4.41) and the clad temperature is calculated as in the earlier cases, illustrated in Section 4.4. The result is given in Figure 6.7. Points of interest are the reaching of clad blistering temperature and clad melting temperature. Blistering occurs at pool height of 5.87 cm above the bottom of the heated section which is at $\delta = 9.4\%$ of the heated channel height. The corresponding swell height is 50.8 cm which covers $\epsilon = 81.2\%$ of the heated channel. Melting occurs at height of 5.05 cm above the bottom of the heated section which is at $\delta = 8.1\%$ of the heated channel height with corresponding swell height of 43.8 cm covering $\epsilon = 70.1\%$ of the heated channel.

In Figure 6.7 the clad temperature calculation is cut off at about 800 °C at pool level $\delta \cong 7.4\%$ above the bottom of the plates, since it is superfluous to keep calculating it further where obvious melting is predicted. It can be concluded that for pool levels covering 9.4% of the core (meaning the heated section or active fuel length) the clad is predicted to be below blistering temperature and above pool levels covering 8.1% of the core the clad is predicted to remain below melting temperature.

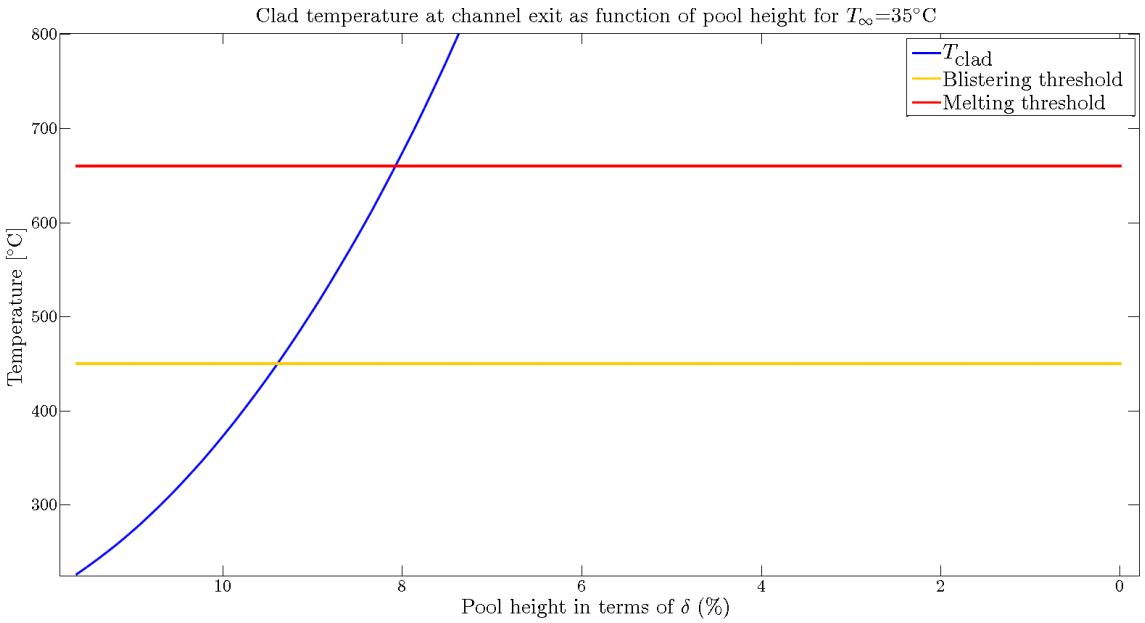

Figure 6.7: Clad temperature at the top of the plate as a function of pool height in terms of δ. Blistering threshold is at 450 °C and melting threshold is at 660 °C.

The MNR safety report states that a break in the lowest located beam tube will leave $\delta = 16\%$ of the fuel submerged. From the calculation above, this figure is still 4.14 cm above the blistering level and 4.96 cm above melting level. The safety report determines that a more plausible break is at a different beam tube, for which the pool would drain to a level of 28% of fuel submerged. In this case the pool level is 11.64 cm above the blistering threshold and 12.46 cm above melting threshold. For both cases the anticipated swell height ϵ covers 100% of the fuel by a two-phase mixture which would keep the clad at much lower temperatures. If left unmitigated, steaming down to the blistering and melting levels would take additional 34.5 and 43.1 hours respectively, calculated by the use of Equations (4.112) and (4.116). It can be summarized that in the scenario of a beam tube break, with a corresponding 3.5 hour draining and decay heat power loss, no core damage is expected to occur as long as the pool level after draining is successfully compensated for steaming to remain at the level of the beam tube bottom where the draining stops.

Chapter 7

Conclusions

A safety analysis has been conducted for postulated accident scenarios in the MNR. Three natural convection models have been developed from first principles in order to address the different scenarios in the scope of the analysis. In order to address the related pool temperature evolution, a simplistic lump capacitance model, using principle energy balance between core power and pool mass was used.

It was shown that, given the assumptions and limitations of the models used, all cases of abnormal cooling for a submerged core do not lead to reaching of safety limits and danger to fuel plate and clad integrity. Initiation of boiling in the hottest channel in the core when draining to just before uncovery occurs only after about 180 hours, just over a week. For a scenario of a break in a beam tube, it was shown that no plate damage is expected for draining down to the lowest beam tube bottom level. From this point, additional drop in pool level can only occur through the steaming of water in the covered parts of the heated sections. Therefore, compensation of pool water is required only for steaming, which is inherently slower than draining. Keeping the pool level covering 5.05 cm of the plates will ensure no clad melting, and keeping it above 7.28 cm will ensure that the plates are entirely covered and no fraction of them is exposed to superheated steam. The time available for intervention to restore pool level before damage occurs is at least 34 hours.

The models developed calculate the steady state natural convection flow rate through an MNR assembly. Since, as mentioned in the literature, the heat transfer and friction correlations have been developed for forced flow conditions, it is required to quantify the uncertainties associated with using those in the natural convection

models developed. Additionally, taking into account the axial power distribution as discussed in Appendix A will improve the accuracy of the models. The main input parameters required for the models are assembly power and liquid inlet temperature. The models are therefore independent of the methods used to obtain these parameters. The decay heat correlation used for calculating the time dependent assembly power was validated and is widely used, but improvements can be made to the pool temperature calculations used in the analysis (from which the inlet temperature is produced). It is recommended to add the heat losses from the pool which were neglected in this treatment. These address the complications arising in long term pool parameters predictions. The important mechanisms of dissipating energy away from the pool are the heat transfer to concrete and air, and steady state pool evaporation at below-saturation temperatures. Studies have shown that this combination leads under certain conditions to reaching a steady state temperature in the pool below that of saturation, with a steady evaporation rate. This would be an improvement over the model used here which neglects evaporation for temperatures belows saturation, and doesn't dissipate heat such that saturation temperature is always eventually reached in the pool.

With adjustments to geometry and pool heatup calculations, the developed natural convection models may be used for other research reactors and possibly spent fuel pool. A combination of the natural convection model to test local fuel temperatures, with a tailored energy balance treatment of a pool, can be useful for modelling cases of spent fuel pools which are inaccessible for long periods of time, as happened for example at unit 4 in the Fukushima Daiichi accident.

Bibliography

[1] *McMaster Nuclear Reactor Safety Analysis Report, Revision 1.* Tech. rep. McMaster Nuclear Reactor, 2012-06 (cit. on pp. 1, 5, 10, 11, 13, 15, 16, 19, 31, 44, 58, 75).

[2] *Natural Circulation in Water Cooled Nuclear Power Plants Phenomena, Models and Methodology for System Reliability Assessments.* Tech. rep. TECDOC-1474. International Atomic Energy Agency, 2005 (cit. on pp. 3, 8).

[3] W. J. Garland. *Thermalhydraulic Modelling of the McMaster Nuclear Reactor.* Tech. rep. TR-97-04. McMaster Nuclear Reactor, 1997 (cit. on pp. 5, 17, 28, 64).

[4] *Safety Analysis for Research Reactors.* Tech. rep. Safety Reports Series No. 55. International Atomic Energy Agency, 2008 (cit. on pp. 5, 9).

[5] W.R. Gambill and R.D. Bundy. "Heat-Transfer Studies of Water Flow in Thin Rectangular Channels. Part II. Boiling Burnout Heat Flux for Low-Pressure Water in Natural Circulation". In: *Nuclear Science and Engineering (US)* 18 (1964) (cit. on pp. 5, 40, 73).

[6] Y. Zvirin. "A Review of Natural Circulation Loops in Pressurized Water Reactors and Other Systems". In: *Nuclear Engineering and Design* 67.2 (1982), pp. 203–225 (cit. on pp. 6, 17, 61).

[7] R. Greif. "Natural Circulation Loops". In: *Journal of Heat Transfer* 110.4b (1988), pp. 1243–1258 (cit. on p. 6).

[8] S. Chatzidakis and A. Ikonomopoulos. "Phenomenological Investigation of Loss of Coolant Accident in a Research Reactor Facility". In: *Nuclear Engineering and Design* 256 (2013), pp. 341–349 (cit. on pp. 7, 8).

[9] A. Bousbia-Salah, B. Meftah, T. Hamidouche, and E. K. Si-Ahmed. "A Model for the Analysis of Loss of Decay Heat Removal During Loss of Coolant Accident in MTR Pool Type Research Reactors". In: *Annals of Nuclear Energy* 33.5 (2006), pp. 405–414 (cit. on p. 7).

[10] T. Hamidouche, A. Bousbia-Salah, and E.K. Si-Ahmed. "Analysis of Loss of Coolant Accident in MTR Pool Type Research Reactor". In: *Progress in nuclear energy* 53.3 (2011), pp. 285–289 (cit. on pp. 7, 8).

[11] T. Hamidouche, A. Bousbia-Salah, and F. D'Auria. "Overview of Accident Analysis in Nuclear Research Reactors". In: *Progress In Nuclear Energy* 50.1 (2008), pp. 7–14 (cit. on pp. 7, 9).

[12] F. D'Auria, A. Bousbia-Salah, A. Petruzzi, and A. Del Nevo. "State of the Art in Using Best Estimate Calculation Tools In Nuclear Technology". In: *Nuclear Engineering and Technology* 38.1 (2006), p. 11 (cit. on p. 7).

[13] J. Dreier and H. Winkler. "Calculations of Partial LOCA in a Swimming-Pool-Reactor with MTR-Elements and Planned Mock-Up Experiment". In: (1984) (cit. on p. 7).

[14] J. Dreier and H. Winkler. "Results of the Mock-Up Experiment on Partial LOCA". In: (1985) (cit. on p. 7).

[15] J. Aharon and I. Hochbaum. "Experimental Investigation Of Open Loop Two Phase Thermosyphon In Narrow Vertical Channel". In: *International Heat Transfer Conference 13*. Begel House Inc. 2006 (cit. on p. 8).

[16] D. Saphier and M.Y. Bettan. "Investigating a Partial LOCA in the IAEA Generic Research Reactor". In: The 23rd conference of the Nuclear Societies in Israel. 2006 (cit. on p. 8).

[17] M. Lee, K.S. Liang, and K.Y. Lin. "Loss Of Cooling Accident Simulation Of Nuclear Power Station Spent Fuel Pool". In: The 19th Pacific Basin Nuclear Conference (PBNC 2014). 2014-08 (cit. on p. 8).

[18] B.Y. Chen, C.L. Yeh, W.C. Wei, and Y.S. Chen. "Thermal Analyses for the Spend Fuel Pool of Taiwan BWR Plants during the Loss of Cooling Accident". In: The 19th Pacific Basin Nuclear Conference (PBNC 2014). 2014-08 (cit. on p. 8).

[19] H. Abdou, D. Delbianco, J. Gonzalez, and V. Garea. "Deterministic Analysis of a Beyond Design Basis Accident in a Low Power, Pin-Type Fuel Research Reactor". In: Joint IGORR 2013 & IAEA Technical Meeting. 2013 (cit. on p. 8).

[20] H. V. Soares, A. L. Costa, C. P. B. Lima, M. A. F. Veloso, I. D. Aronne, and Y. H. de Almeida. "Loss of Coolant Accident Analyses on OSIRIS Research Reactor using the RELAP5 Code". In: *International Conference on Mathematics and Computational Methods Applied to Nuclear Science and Engineering (M&C 2011), Rio de Janeiro, RJ, Brazil*. 2011 (cit. on p. 8).

[21] A. Kaliatka, V. Ognerubov, and V. Vileiniskis. "Analysis of the Processes in Spent Fuel Pools of Ignalina NPP in Case of Loss of Heat Removal". In: *Nuclear Engineering and Design* 240.5 (2010), pp. 1073–1082 (cit. on p. 8).

[22] T. E. Collins and G. Hubbard. *Technical Study of Spent Fuel Pool Accident Risk at Decommissioning Nuclear Power Plants*. Tech. rep. NUREG-1738. US Nuclear Regulatory Commission (USNRC), 2001 (cit. on p. 8).

[23] D. Wang, I. C. Gauld, G. L. Yoder, L. J. Ott, G. F. Flanagan, M. W. Francis, E. L. Popov, J. J. Carbajo, P. K. Jain, J. C. Wagner, et al. "Study of Fukushima Daiichi Nuclear Power Station Unit 4 Spent-Fuel Pool". In: *Nuclear Technology* 180.2 (2012), pp. 205–215 (cit. on pp. 8, 85).

[24] W. J. Garland and C. Heysel. "McMaster Nuclear Reactor Safety Analysis Methodology Overview". In: IAEA Technical Meeting on Safety Analysis for Research Reactors. International Atomic Energy Agency. Vienna, Austria, 2002-06 (cit. on p. 9).

[25] C. Blahnik. *Assessment of MNR Core Flow Distribution Tests*. Tech. rep. McMaster Nuclear Reactor, 2001 (cit. on p. 9).

[26] C. Blahnik. *Hydraulic Properties of MNR Core Components*. Tech. rep. McMaster Nuclear Reactor, 2001 (cit. on pp. 9, 58–60, 68).

[27] W. J. Garland. *Single Phase Friction Factors for MNR Thermalhydraulic Modelling*. Tech. rep. TR-98-02. McMaster Nuclear Reactor, 1998 (cit. on pp. 9, 26, 58).

[28] T. S. Ha. "Hydraulic Studies of the 18-Plate Assembly in the McMaster Nuclear Reactor". MA thesis. McMaster University, 2002 (cit. on pp. 9, 10, 13, 14, 57, 59, 68).

[29] S.I. Osamusali, J.S. Chang, and P. Ernst. "Heat Transfer and Flow Studies of McMaster Nuclear Reactor Fuel Element". In: *Proceedings of the 12th Simulation Symposium on Reactor Dynamics and Plant Control (CNS)* 2A-5 (1986). Canadian Nuclear Society (cit. on pp. 9, 60).

[30] R. Yu. "The Numerical Investigation of Turbulent Flow and Heat Transfer in MNR 18 Plate Nuclear Fuel Assembly". MA thesis. McMaster University, 2002 (cit. on p. 9).

[31] T. Ha and W. J. Garland. "Hydraulic Study of Turbulent Flow in MTR-Type Nuclear Fuel Assembly". In: *Nuclear Engineering and Design* 236.9 (2006), pp. 975–984 (cit. on pp. 9, 59, 60).

[32] N. E. Todreas and M. S. Kazimi. *Nuclear systems II: Elements of Thermal Hydraulic Design*. Vol. 2. Taylor & Francis, 1990 (cit. on pp. 16, 20, 25, 36, 39, 100).

[33] Y. Zvirin, A. Shitzer, and G. Grossman. "The Natural Circulation Solar Heater-Models with Linear and Nonlinear Temperature Distributions". In: *International Journal of Heat and Mass Transfer* 20.9 (1977), pp. 997–999 (cit. on pp. 20, 100).

[34] F. P. Incropera, D. P. Dewitt, T. L. Bergman, and A. S. Lavine. *Fundamentals of Heat and Mass Transfer*. seventh. John Wiley & Sons, 2011 (cit. on pp. 22, 29, 40, 41, 50, 52).

[35] B. R. Munson, D. F. Young, and T. H. Okiishi. *Fundamentals of fluid mechanics*. New York, 1990 (cit. on pp. 26, 59).

[36] *Roughness & Surface Coefficients of Ventilation Ducts*. 2015. URL: `http://www.engineeringtoolbox.com/surface-roughness-ventilation-ducts-d_209.html` (cit. on pp. 27, 61).

[37] F. P. Incropera, D. P. Dewitt, T. L. Bergman, and A. S. Lavine. *Introduction to Heat Transfer*. John Wiley & Sons, 2011 (cit. on p. 28).

[38] W. M. Kays, M. E. Crawford, and B. Weigand. *Convective Heat and Mass Transfer*. Tata McGraw-Hill Education, 2012 (cit. on p. 28).

[39] N. E. Todreas and M. S. Kazimi. *Nuclear Systems I: Elements of Thermal Hydraulic Design*. Vol. 1. Taylor & Francis, 1990 (cit. on pp. 33, 39).

[40] S. G. Kandlikar. "A general Correlation for Saturated Two-Phase Flow Boiling Heat Transfer Inside Horizontal and Vertical Tubes". In: *Journal of Heat Transfer* 112.1 (1990), pp. 219–228 (cit. on pp. 40, 41).

[41] S. G. Kandlikar. "Flow Boiling Maps for Water, R-22 and R-134a in the Saturated Region". In: *9th International Heat Transfer Conference, Jerusalem, Aug.* 1990 (cit. on p. 41).

[42] J. C. Luxat. *EP 4NE3 Advanced Nuclear Engineering Course Notes, Chapter 4*. McMaster University. 2012 (cit. on pp. 50, 52).

[43] M. M. El-Wakil. *Nuclear Heat Transport*. American Nuclear Society, 1978 (cit. on p. 53).

[44] American Nuclear Society and American National Standards Institute. *American National Standard Decay Heat Power in Light Water Reactors*. ANSI/ANS. American Nuclear Society, 2005 (cit. on p. 53).

[45] *Severe Accident Management Guidance Technical Basis Report, vol. 2: The Physics of Accident Progression*. Tech. rep. TR-101869. Hillview Av., Palo Alto, Cal., USA: Electric Power Research Institute, 1992-12 (cit. on p. 53).

[46] I.E. Idelchik. *Handbook of Hydraulic Resistance: Coefficients of Local Resistance and of Friction*. NTIS, 1960 (cit. on pp. 59, 60).

[47] Crane Company. Engineering Division. *Flow of Fluids Through Valves, Fittings, and Pipe*. Technical paper. Crane Canada, 1984 (cit. on pp. 59, 60).

[48] H.W. King. *Handbook of Hydraulics*. MacGraw-Hill, 1954 (cit. on p. 59).

[49] S. W. Churchill. "Friction-Factor Equation Spans All Fluid-Flow Regimes". In: *Chemical Engineering* 84.24 (1977), pp. 91–92 (cit. on p. 62).

[50] *Technical Drawing Number 1800*. McMaster Nuclear Reactor (cit. on p. 68).

[51] *Technical Drawing Number 3501*. McMaster Nuclear Reactor (cit. on p. 68).

Appendix A

Axial Power Profile

The simplification of using a uniform axial heat flux shape in the heated sections deviates from the actual flux shape expected in the MNR channels. This usage of uniform flux in the single-phase and two-phase models was justified by Zvirin [33] and used in the treatment in the book "Nuclear Systems" [32]. An important difference in the uncovered case, for swell heights exposing the fuel plates, is that only a fraction of the total plate power is then absorbed in the two-phase mixture. This directly affects the steaming rate, as can be seen from its definition in Equation (4.92). The steaming rate is used back in determining the swell height itself in the transcendental Equation (4.95). Therefore, as the author is unaware of a precedent as Zvirin's justification for the earlier case, usage of this simplification for the uncovered core treatment should be more carefully examined.

For a uniform heat flux, the fraction of power going into the two-phase mixture is equal to the ratio of the swell height to the heated section's length ϵ as in Equation (4.97). This power deposited into the coolant is a linear function of the height z resulting from integration of the axial power density. When looking at a pure cosine shape axial power distribution, the fraction of power emitted to a given swell height is not equal to the fraction of the swell to channel heights anymore, apart from at exactly 50% uncovery arising from symmetry. The profile of total power along z this time resembles an S shape with only the total power throughout and the total power up to the middle of the channel being the same as in the uniform case.

In the MNR and other reactors, neutron reflections back to the core exist such that the axial power does not completely drop to zero at the edges. This shape looks

as, and is accordingly called, a truncated cosine. When examining a truncated cosine axial power distribution an interesting phenomenon can be spotted with regards to the total power profile. For greater truncation, the power at the edges is higher and the axial distribution shape becomes closer to that of a uniform distribution. This contributes to the total power profile along the channel also becoming closer to that of the linear function in the uniform case. This means that the larger the reflections at the edges, the more appropriate the uniform axial power profile approximation becomes.

As seen in Chapter 6, swell heights of below 70% of the heated channel height are expected to lead to fuel damage. Since, as seen from Equation (4.100), once the swell height has been established, the enthalpy rise above it is independent of power, the discussion and analysis for the uniform case is for swell heights above 70%. By incorporating the use of a truncated cosine, this temperature may be reached somewhat lower along the top half of the channel. Given the above, it is still safe to assume that the swell height must be at least above the 50% point before damage occurs, limiting the discussion to the upper half of the active fuel length. As mentioned earlier, the total power deposited into the two-phase mixture up to the midpoint as calculated by the uniform power assumption is equal to the midpoint power calculated by the cosine assumption from symmetry, both being equal to half of the full plate power. For the same reason any truncated cosine shape which total power is the full plate power is also going to produce an equal result at the midpoint. The net effect for swells above the midpoint is therefore that the uniform approximation underpredicts the amount of heat deposited into the two-phase mixture and overpredicts the amount of heat deposited into the superheated steam[1]. This contributes to lower steaming rates and higher steam exit temperatures than in reality, which is conservative. This effect is going to be less pronounced for greater truncations as these differences between the S and the linear shapes diminish.

[1]Above the midpoint, the integrated cosine S curve is above the linear line for all points except for the endpoint.

Appendix B

MATLAB Scripts

Ahead are the MATLAB scripts used for the calculations. The code has been written and executed on version R2014a of the software. The main scripts running the scenarios are `Texit_profiles`, `flow_rate_2ph` and `swell_height` for the three stages as discussed in Chapter 6.

B.1 Fuel Properties

The script `fuel_props` creates all the variables for the physical parameters associated with the assembly and fuel plate:

```
% Fuel assembly properties
global Lth epsi Vf kf Lf Lc kc L1 L2 L3 L4 L5 D1 D2 Dh3 Dh4 Dh5 A1 A2...
    A3 A4 A5 Pw3 Pw4 Pw5 K01 K12 K23 K34 K45 K50 klam4 ktur4 ktur35 Lbc
cp_f=0.1706e3; %+-1.04e-4T[K] [J/kg-K] Fuel meat specific heat [MNR
% Safety report p. 16.3-1]
kf=73; %+-6(%) [W/m-K] Fuel meat conductivity [MNR Safety report p.
% 16.3-1] in temperature range to clad melting
Vf=19.064e-6; %[m^3] Fuel meat volume [MNR Safety report p. 16.3-19]
Lf=0.51*1e-3; %[m] Fuel meat thickness [MNR safety report p. 5-7]
rho_f=5.728e3; %[kg/m^3] Fuel meat density [MNR Safety report p. 16.3-19]
cp_c=0.76635e3; %+-4.6e-4*T[K] [J/kg-K] clad specific heat [MNR Safety
% report p. 16.3-1]
kc=123; %+-6(%) [W/m-K] Clad conductivity [MNR Safety report p. 16.3-1]
```

```
Vc=(28.409+9.2465)*1e-6; %[m^3] Clad volume (clad covering meat + clad
% beyond fuel meat) [MNR Safety report p. 16.3-19]
rho_c=2.7e3; %[kg/m^3] Clad density [MNR Safety report p. 16.3-19]
Lc=0.381*1e-3; %[m] clad thickness [MNR safety report p. 5-7 (a typo in
% that page saying 0.038mm)]
% Geometry - Divide the assembly to 5 main parts:
% Compartment 1 = snout entrance, Compartment 2 = after snouts expansion,
% Compartment 3 = inlet of fuel assembly
% Compartment 4 = fuel assembly with plates, Compartment 5 = outlet of
% fuel assembly
epsi=0.002; %[m] Surface roughness for aluminium -
% http://www.engineeringtoolbox.com/major-loss-ducts-tubes-d_459.html
D1=50.8e-3; %[m] Snout's inner diameter
D2=62.7e-3; %[m] Snout diameter after expansion
theta=2*20; %[deg] angle of snout's expansion
gap=3.1557e-3; %[m] gap between fuel plates at centre of channel
% [MNR p. 16.3-23] 3mm according to [p. 5-7]
wp=1.2643e-3; %[m] Fuel plate width(thickness) (x-y plane)
L=66.32e-3; %[m] Main assembly (rectangular part) inner length (x-y
% plane)
W=gap*17+wp*16; %[m] Main assembly (rectangular part) width (x-y plane)
Np=18; %[non dimensional] # of plates (including dummies)
%z plane:
Lbc=600e-3; %[m] Fuel meat height (within the plate)
Ltot=873e-3; %[m] Fuel assembly total height - if you add the #s on
% page 16.3-24 you get 88.3cm (the discrepancy
% lies probably in that the two sources have different values for L1.
% 13.6-24 has 13.7cm whereas 5.4 says 12.7
% Also, still haven't found a source which tells exactly where the fuel
% meat sits within the plates.
L1=12.7e-2+1.905e-2; %[m] Snout's entrance height (chapter 5.4 is
% correct, snout narrow side is 12.7cm)
L2=2.54e-2; %[m] Snout's expansion height (between end of expansion and
% entrance to the rectangular duct)
```

```
L3=2.54e-2; %[m] Rect duct entrance height (before start of fuel plates)
L4=62.55e-2; %[m] Fuel plate height (a bit larger than the fuel meat
% height Lbc which isn't along the whole plate)
L5=5.08e-2; %[m] Exit rect duct between fuel plates and pool
Lth=Lbc/2+L5; %[m] Effective length over which the heating takes place.
% should be Lcd instead of L5 (a bit bigger)
phi=27.4622; %[deg] arc length of fuel plates (when taking curvature
% into account)

A1=pi*D1^2/4; %[m^2] area 1
A2=pi*D2^2/4; %[m^2] area 2
A3=4899e-6; %curved rectangle area of assembly from safety report
A4=208.485e-6;%[m^2] cross section area of single channel
A4=(Np-1)*A4; %[m^2] total cross section area of compartment 4
A5=A3;
Pw3=282e-3; %[m] perimeter of area 3
Pw4=140.144e-3;%2*gap+l1+l2; %[m] perimeter of a single area between
% plates
Pw4=(Np-1)*Pw4; %[m] total wetted perimeter of area 4
Pw5=Pw3;

Dh3=4*A3/Pw3; %[m] Hydraulic diameter of rectangular duct (area 3)
Dh4=4*A4/Pw4; %[m] Hydraulic diameter of the fuel plate
% assembly (of area 4)
Dh5=Dh3;

%Minor losses vary in literature. The ones taken were the conservative
% among different sources
K01=0.5; %[Non dimensional] Snout entrance minor loss coefficient
% [Crane P. A-29] [Idelchik P.122]
%Assembly mounted to grid plate, which presumably acts as a wall. For
% a free standing pipe K=1 (arguably not the case)
K12=0.3404;%[Non dimensional] Snout expansion minor loss coefficient
% (gradual expansion) - polynomial extrapolation
```

```
%between D2/D1=1.2 to D2/D1=1.4 (since D2/D1=1.24) [Handbook of
% Hydraulics H. W. King P.6.37]
% K12=2.6*sin(theta/2)*(1-(D1/D2)^2)^2 - [Crane P. A-26]
K23=(1-A2/A3)^2; %[Non dimensional] Snout connection to assembly minor
% loss coefficient (sudden expansion) [Idelchik P.160]
%and [Munson,Yound,Okiishi Fundamentals of fluid mechanics 3rd. ed.
% P.501]
K34=0.66;% 0.5*(1-(Dh4/Dh3)^2)^2 %[Non dimensional] Fuel plates entry
% (approx {conservative} as sudden contraction) [Crane P. A-26]
K45=1;% (1-(Dh4/Dh5)^2)^2 %[Non dimensional] Fuel plates exit (approx
% {conservative} sudden expansion)
%Approximating is as expansion from a total cross section area of the
% flow channels in compt 4 to compt 5
%and uniform velocity distribution [Crane P.2-11]
K50=1; %[Non dimensional] Assembly exit (free discharge) [Idelchik
% P.509]

gap_eff=Pw4/(Np-1)/4-sqrt((Pw4/(Np-1))^2/16-A4/(Np-1)); %effective
% width for rectangular approximation
leff=A4/(Np-1)/gap_eff; %effective length for rect approx. keeping
% wetted perimeter, flow area and hyd diameter the same
ratio4=gap_eff/leff; %[Non dimensional] ratio between width (smaller)
% and length (average between inner and outer sides of the plate) (bigger)
% of the rectangular channel
% this way it is consistent with the wetted perimeter
klam4=1.503-1.894*ratio4+2.034*ratio4^2-0.755*ratio4^3; %[Non
% dimensional] laminar friction correction for rectangular channels
ktur4=1.097-0.177*ratio4+0.083*ratio4^2; %[Non dimensional] turbulent
% friction correction for rectangular channels reference [Single phase
% friction factors - W. J. Garland]
Weff=Pw3/4-sqrt((Pw3)^2/16-A3);
Leff=A3/Weff;
ratio35=Weff/Leff; % ratio of width and length of sections 3 and 5
klam35=1.503-1.894*ratio35+2.034*ratio35^2-0.755*ratio35^3;
```

```
ktur35=1.097-0.177*ratio35+0.083*ratio35^2;
```

B.2 Water Properties

The function `fluid_props` returns all the water properties at a given temperature and pressure. The package XSteam for MATLAB is required for this function.

```
function [rho,beTa,my,nu,k,alpha,cp,h,hf_p,hfg_p,rhof,rhog,hg_p] =...
    fluid_props(P,T)
%Water properties at temperature T[C] and pressure P[bar]
%If only pressure is specified, fluid properties are taken for saturated
%liquid

if nargin==1 % If only pressure is specified, properties are taken for
% liquid at saturation (except for explicit vapor properties rhog & hg)
T=XSteam('Tsat_p',P);
end

rho=XSteam('rho_pt',P,T); %[kg/m^3] Water density
if isnan(rho)==1
rho=XSteam('rhoL_p',P);
end

beTa=XSteam('v_pt',P,T)^-1*(XSteam('v_pt',P,T+1e-3)-...
    XSteam('v_pt',P,T))/1e-3; %[1/K] Thermal/Volumetric expansion
% coefficient
% beta is calculated from approximation to the derivative that defines
% it. It's with very good agreement with miniREFPROP, slightly above its
% values (by 0.03% at most)
if isnan(beTa)==1 %fix problem with XSteam specific volume being NaN
% close to saturation temperatures
    Tbelow_sat=XSteam('Tsat_p',P)-0.01;
    beTa=XSteam('v_pt',P,Tbelow_sat)^-1*(...
        XSteam('v_pt',P,Tbelow_sat+1e-3)-XSteam('v_pt',P,Tbelow_sat...
        ))/1e-3; %beTa at saturation for atm pressure less than 1%
```

```
% difference for pressures between 1 and 45 atmospheres
end

k=XSteam('tc_pT',P,T); %[W/m-K] Thermal conductivity
if isnan(k)==1
k=XSteam('tcL_p',P);
end

my=XSteam('my_pT',P,T); %[Pa-s]=[kg/(s*m)] Viscosity
if isnan(my)==1
my=XSteam('my_pT',P,Tbelow_sat);
end

nu=my/rho; %[m^2/s] Kinematic viscosity

cp=XSteam('Cp_pT',P,T)*1e3; %[J/(kg-K)] Water specific heat capacity
if isnan(cp)==1
cp=XSteam('CpL_p',P)*1e3;
end

alpha=k/(rho*cp); %[m^2/s] Thermal diffusivity

h=XSteam('h_pT',P,T)*1e3; %[J/kg] Specific enthalpy
if isnan(h)==1
h=XSteam('hL_p',P)*1e3;
end

hf_p=XSteam('hL_p',P)*1e3; %[J/kg] Liquid saturation enthalpy
% vaporization @ a given pressure
hg_p=XSteam('hV_p',P)*1e3; %[J/kg] Saturated steam enthalpy
hfg_p=hg_p-hf_p; %[J/kg] Latent heat of vaporization @ a given pressure
rhof=XSteam('rhoL_p',P); %[kg/m^3] Saturated liquid density
rhog=XSteam('rhoV_p',P); %[kg/m^3] Saturated vapour density
end
```

B.3 Pool and Core Properties

The script `pool_core_props` creats all the variables for the physical parameters associated with the reactor pool and core:

```
% Pool and core properties - requires z (height of water above core) and
% Tinf in order to calculate properties at core depth
global g
q0=26.5e3*1.17; %[W] hottest channel
%q - Power of a single plate. The plate gives half power to it's right
% flow channel and half to it's left. Every inner flow channel (apart
% from the outer two) gets two halves q/2 of power, thus q of a single
% plate.
Qass0=16*9.96e3*1.17; %[W] avg channel power times 16 to total power in
% assembly
P0=5e6*1.17; %[W] full core power

Apool=43.9; %[m^2] pool surface area
Vnom=378.2; %[m^3] nominal pool volume at normal operation (~30[C])

Znom=9.3218; %[m] pool total height above floor
zbottom=1.2399; %[m] height of core above pool floor
zcore=0.87315; %[m] core dimensions
Vcore=Apool*Znom-Vnom; %[m^3] assumed volume of core and instrumentation
% inside the pool

g=9.8; %[m/s^2]
Patm=1.01325; %[bar] atmospheric pressure
Tsat=XSteam('Tsat_p',Patm); %[C] pool saturation temperature at
% atmospheric pressure

% Properties at core depth
rho=fluid_props(Patm,Tinf);
Z=zbottom+zcore+z; %[m] total height of water above floor for height
% above core 'z' for pool inventory calculations
```

```
M=rho*(Apool*Z-Vcore); %[kg] mass of water in the pool
Pcore_top=(Patm*1e5+rho*g*z)/1e5; %[bar] Pressure at the top of the core,
% rho*g*h are in [Pa], change to [bar] for XSteam
Pcore_bot=(Patm*1e5+rho*g*(z+zcore))/1e5; %[bar] hydrostatic pressure at
% pool floor regarded as core bottom
Pcore_avg=(Pcore_top+Pcore_bot)/2;
Tcore_sat=XSteam('Tsat_p',Pcore_top);
Tcore_avg=(Tcore_sat+Tinf)/2;

[~,~,~,~,~,~,~,~,~,hfg_pool]=fluid_props(Patm); %[J/kg] water latent
% heat of vaporization @ 1atm
[~,~,~,~,~,~,~,~,hf_pool]=fluid_props(Patm,Tinf); %[J/kg] saturated
% liquid enthalpy
[~,~,~,~,~,~,~,hpool]=fluid_props(Patm,Tinf); %[J/kg] enthalpy at given
% temp and pressure
cp_avg=(hf_pool-hpool)/(Tsat-Tinf); %pool cp avg over 35-100 [C]
```

B.4 Single Phase Flow Rate

The function `flow_rate` calculates the single-phase natural-convection flow rate in steady state for a given assembly power:

```
function M_end=flow_rate(rho,beTa,cp,my4,Qass,my0,my5)
%Qass - Power of a single fuel assembly (16 plates) Q_dot [W]
global Lth epsi L1 L2 L3 L4 L5 D1 D2 Dh3 Dh4 Dh5 A1 A2 A3 A4 A5 K01...
    K12 K23 K34 K45 K50 g klam4
tol=1e-6; conv=1;
conv_f1=1;conv_f2=1;conv_f3=1;conv_f4=1;
%initial guess for friction factor (contains a guess for initial flow
% rate M_dot)
f1=0.5; %[Non dimensional] Major loss friction factor (initial guess)
f2=f1; f3=f1; f4=f1; f5=f1;
Mdot(1) = (2*beTa*rho^2*g*Lth*Qass/cp*(f1(1)*L1/(D1*A1^2)+f2(1)*L2/...
    (D2*A2^2)+f3(1)*L3/(Dh3*A3^2)+f4(1)*L4/(Dh4*A4^2)+f5(1)*L5/...
```

```
    (Dh5*A5^2)+K01/A1^2+K12/A1^2+K23/A2^2+K34/A4^2+K45/A4^2+K50/...
    A5^2)^(-1))^(1/3);

%K01 associated with velocity in sect1
%K12 associated with velocity in sect1
%K23 associated with velocity in sect2
%K34 associated with velocity in sect4
%K45 associated with velocity in sect4
%K50 associated with velocity in sect5

counter=0;
while conv>tol
counter=counter+1;
Re1=D1*Mdot(1)/(A1*my0);
Re2=D2*Mdot(1)/(A2*my0);
Re3=Dh3*Mdot(1)/(A3*my0);
Re4=Dh4*Mdot(1)/(A4*my4);
Re5=Dh5*Mdot(1)/(A5*my5);

conv_f1=1;
while conv_f1>tol
f1(2)=(-2*log10(epsi/(D1*3.7)+2.51/(Re1*sqrt(f1(1)))))^(-2);
conv_f1=abs((f1(2)-f1(1))/f1(1));
f1(1)=f1(2);
end
conv_f2=1;
while conv_f2>tol
f2(2)=(-2*log10(epsi/(D2*3.7)+2.51/(Re2*sqrt(f2(1)))))^(-2);
conv_f2=abs((f2(2)-f2(1))/f2(1));
f2(1)=f2(2);
end
conv_f3=1;
while conv_f3>tol
f3(2)=(-2*log10(epsi/(Dh3*3.7)+2.51/(Re3*sqrt(f3(1)))))^(-2);
```

```
conv_f3=abs((f3(2)-f3(1))/f3(1));
f3(1)=f3(2);
end
f4=klam4*64/Re4;
conv_f5=1;
while conv_f5>tol
f5(2)=(-2*log10(epsi/(Dh5*3.7)+2.51/(Re5*sqrt(f5(1)))))^(-2);
conv_f5=abs((f5(2)-f5(1))/f5(1));
f5(1)=f5(2);
end

Mdot(2) = (2*beTa*rho^2*g*Lth*Qass/cp*(f1(1)*L1/(D1*A1^2)+f2(1)*L2/...
    (D2*A2^2)+f3(1)*L3/(Dh3*A3^2)+f4(1)*L4/(Dh4*A4^2)+f5(1)*L5/...
    (Dh5*A5^2)+K01/A1^2+K12/A1^2+K23/A2^2+K34/A4^2+K45/A4^2+K50/A5^2)...
    ^(-1))^(1/3);

conv=abs((Mdot(2)-Mdot(1))/Mdot(1));
Mdot(1)=Mdot(2);

if counter>50
    break
end

end
M_end=Mdot(1);

end
```

B.5 Time to Emit a Given Energy

The function `time_to_heat` calculates the time it takes to emit a given amount of energy, in accordance with the used decay heat profile as in Equation (4.112):

```
function [t]=time_to_heat(Qtot,Qdot0)
%Qdot0 [W]
```

```
%Qtot [J]
t=(148*Qtot/(19*Qdot0))^(50/37); %[s] time to accumulation of Qtot
% Joules emitted from fuel
end
```

B.6 Time to Pool Saturation

The function `pool_sat_time` calculates the time to raise the pool temperature from nominal to saturation:

```
function t=pool_sat_time(Tinf,Mpool,cp_avg,P,P0)
% calculates time to pool (mass Mpool[kg]) saturation from
% temperature Tinf[C]
Qpool=Mpool*cp_avg*(XSteam('Tsat_p',P)-Tinf); %heat energy that needs to
% be transferred to heat the pool to saturation
t=time_to_heat(Qpool,P0);
end
```

B.7 Decay Heat

The function `decay_heat` calculates the decay heat power and total energy released after time t from shutdown for a given starting power:

```
function [Q_dot,Q]=decay_heat(t,Qdot0) %t in [s]
% calculates the heat rate and total heat emitted by time t[s] according
% to El-Wakil's correlation
Q_dot=0.095*Qdot0*t.^(-0.26); %[W] decay heat
Q=(19/148)*Qdot0*t.^(37/50); %[J] heat energy added
end
```

B.8 Single Phase Heat Transfer

The function `heatranscoef` calculates the heat transfer of single-phase convection:

```
function [h]=heatranscoef(mdot,cp,my,k)
% calculates the single phase heat transfer coefficient
% Strictly between two plates (the function uses A4/17)
global Dh4 A4
h=k./Dh4.*0.023.*(Dh4.*mdot./(my.*(A4/17))).^0.8.*(cp.*my./k).^0.4;
%[W/m^2] heat transfer coef.
Re4=mdot.*Dh4./my/(A4/17);
if max(Re4<1500)==1 % skip the loop if Re isn't smaller than 1500
    % anywhere
    for i=1:max(size(mdot))
        if Re4(i)<1500 % Use Nu=6.49 for laminar range
            if isscalar(k)==1
                h(i)=6.49*k/Dh4;
            else
                h(i)=6.49*k(i)/Dh4;
            end
        end
    end
end
end
```

B.9 Fuel and Clad Temperatures

The function `fuelclad` calculates the fuel and clad temperatures given the coolant temperature, the heat transfer coefficient and the plate power:

```
function [Tc,Tm]=fuelclad(qdot,Tf,h)
% calculates fuel and clad temperatures given plate power and coolant
% temperature. Strictly between two plates (the function uses A4/17)
global Vf kf Lf Lc kc
q_dens=qdot/Vf;
Tc=Tf+q_dens.*Lf/2./h; %[C] temperature of clad
Tm=Tf+q_dens.*(Lf^2/8/kf+Lf*Lc/2/kc+Lf/2./h); %[C] temperature of fuel
% Tm=Tc+q_dens.*(Lf^2/8/kf+Lf*Lc/2/kc);
end
```

B.10 Times to Reach Saturation in the Core

The function `Texit_profiles` calculates the time to reaching saturation in the hottest channel in the core using the earlier functions and scripts for all scenarios from full inventory to before uncovery. It also calculates the temperatures at the exit from the hottest channel using the function to calculate heat transfer `heatranscoef`, and the function to calculate clad temperatures `fuelclad`:

```
% Calculate the time until saturation in channel exit for different pool
% drain heights
clear;
tn=5000; %number of samples in the timespan
tol=1e-5;
%%%%%%%%%%%%%%%%%%%%%%%%%%%%%%%%%%%%%%%%%%%%%%%%%%% Tinf and z as input:
Tinf=35; %[C] pool temperature (starting point for analysis at max
% operationally allowed 35[C])
z=1.0; %[m] height above the core to which water is drained. Critical
% height=1.903 [m]

fuel_props;
pool_core_props;

t=pool_sat_time(Tinf,M,cp_avg,Patm,P0); %[s] time to heat the pool to
% saturation
t_pool_sat=t;
t=linspace(1,t,tn);
dt=t(2)-t(1);
Tcore_sat0=Tcore_sat; %saturation temperature at core depth before
% boiling off
[Qcore_dot,Qcore]=decay_heat(t,P0); %[W] and [J] full core power
[Qdot,Q]=decay_heat(t,Qass0); %[W] and [J], the heat rate and total heat
% of an assembly as functions of t
[qdot,q]=decay_heat(t,q0); %[W] and [J], the heat rate and total heat of
% a single channel
Tpool=Tinf+Qcore./(M*cp_avg); %[C] pool temperature as function of time
```

```
% to saturation
z0=z;

%Texit Profile until saturation
Tcore_avg=(Tcore_sat+Tinf)/2;
for i=1:max(size(t))
mdot(i)=0.5;
conv=0.1;
Texit(i)=Tcore_avg; % Temporary value for calculation of my5
while conv>tol
    [rho_core(i),beTa_core(i),my_core(i),~,kl(i),~,cp_core_avg(i)]= ...
        fluid_props(Pcore_avg,Tcore_avg);
    [~,~,my0]=fluid_props(Pcore_avg,Tpool(i)); % Pool temperature for
    % sections 1-3
    [~,~,my5]=fluid_props(Pcore_avg,Texit(i)); % Section 5 temperature
    % (Texit)

    mtemp=flow_rate(rho_core(i),beTa_core(i),cp_core_avg(i),...
        my_core(i),Qdot(i),my0,my5)/17; %[kg/s] flow in inner channel,
    % in steady state is 1/16 of the assembly flow
    conv=abs((mdot(i)-mtemp)/mdot(i));
    mdot(i)=mtemp;
    Texit(i)=qdot(i)/(mdot(i)*cp_core_avg(i))+Tpool(i);
    Tcore_avg=(Texit(i)+Tpool(i))/2;
end
if Texit(i)>Tcore_sat
    break
end
end

if (Texit(end)-Tcore_sat)>0
conv=find((Texit-Tcore_sat)<0); %Index of reaching of saturation
t_sat=t(conv(end));
Tcore_sat=Tcore_sat*ones(1,i);
```

```
    disp('Below critical height');
else
    Tcore_sat=Tcore_sat*ones(size(t));
%Texit profile after saturation (if it didn't reach channel saturation
% before)
[~,~,~,~,~,~,~,~,~,~,rho_sat]=fluid_props(Patm);
while Texit(end)<Tcore_sat(end)
        i=i+1;
t(i)=t(i-1)+dt;
[Qcore_dot(i),Qcore(i)]=decay_heat(t(i),P0);
[Qdot(i),Q(i)]=decay_heat(t(i),Qass0);
[qdot(i),q(i)]=decay_heat(t(i),q0);

dZ=(Qcore(i)-Qcore(i-1))/(hfg_pool*rho_sat*Apool);
Z=Z-dZ;
z=z-dZ;
Pcore_top=(Patm*1e5+rho*g*z)/1e5; % rho at 35[C] justified by
        % the discussion "Saturation temperature at core depth"
Tcore_sat(i)=XSteam('Tsat_p',Pcore_top);
Pcore_bot=(Patm*1e5+rho*g*(z+zcore))/1e5; % same, changed to
        % rho_sat % March 9th - fix to z+zcore
Pcore_avg=(Pcore_top+Pcore_bot)/2;

        mdot(i)=1;
        conv=0.1;
        Texit(i)=Tcore_avg; % Temporary value for calculation of my5
        while conv>tol
            [rho_core(i),beTa_core(i),my_core(i),~,kl(i),~,...
                cp_core_avg(i)]=fluid_props(Pcore_avg,Tcore_avg);
            [~,~,my0]=fluid_props(Pcore_avg,Tsat); % Pool temperature
            % for sections 1-3
            [~,~,my5]=fluid_props(Pcore_avg,Texit(i)); % Section 5
            % temperature (Texit)
```

```
            mtemp=flow_rate(rho_core(i),beTa_core(i),cp_core_avg(i),...
                my_core(i),Qdot(i),my0,my5)/17; %[kg/s] flow in inner
            % channel, in steady state is 1/16 of the assembly flow
            conv=abs((mdot(i)-mtemp)/mdot(i));
            mdot(i)=mtemp;
            Texit(i)=qdot(i)/(mdot(i)*cp_core_avg(i))+Tsat;
            Tcore_avg=(Texit(i)+Tsat)/2;
        end
end
t_sat=t(end); %[seconds], time to saturation
    disp('Above critical height')
end
% i=Index of reaching of saturation
Re4=17*mdot.*Dh4./A4./my_core;
Tcore_sat0=Tcore_sat0*ones(size(t));
t_days=t(1:i)./(3600*24); %[days], time to saturation
t_weeks=t_days./7;

str=num2str(t_sat/(3600*24),'%-.1f');
combinedStr=strcat('Time to saturation in the core =',str,' days');
disp(combinedStr);
```

B.11 Two Phase Heat Transfer

The function `heatranscoef2ph` calculates the heat transfer of two-phase convection:

```
function [h2ph]=heatranscoef2ph(mdot,x,cp,my,k,hfg,rhof,rhog,qdot)
% Strictly between two plates (the function uses A4/17)
% Use saturated liquid water properties
global Vf Lf A4
G=mdot/(A4/17); %mass flux
q_flux=qdot/Vf*Lf/2;
h=heatranscoef(mdot,cp,my,k); % the (1-x)^0.8 probably comes from here.
% Usage of Re_l=rho*v*D*(1-x)/my
htemp=1.136.*x.^0.72.*(1-x).^(-0.72).*(rhof./rhog).^0.45+667.2.*...
```

```
    (q_flux./hfg./G).^0.7;
h2ph=0.6683.*x.^0.16.*(1-x).^(-0.16).*(rhof./rhog).^0.1+1058.*...
    (q_flux./hfg./G).^0.7;
h2ph=max(htemp,h2ph)*(1-x)^0.8.*h; % Kandlikar correlation
% [Kandlikar - A General Correlation for Saturated Two-Phase Flow 1990]
end
```

B.12 Two Phase Flow Rate

The script `flow_rate_2ph` calculates the natural convection two-phase flow rate in steady state for a given assembly power and inlet temperature, for all heights above critical. It also calculates the temperatures at the exit from the hottest channel using the two-phase heat transfer coefficient calculated by `heatranscoef2ph`:

```
% flow rate at two-phase conditions
clear
Tinf=35;
z=3;
fuel_props;
Heff=L4+L5;

% For core uncovering after quick draining, use Tinf=35 above and
% uncomment here and method c. for power calculation:
t=3.5*3600; % Input time of uncovering
Heff=L4+L5-0.1; % Input height above start of section 4,
% for t=3.5h Hcrit=0.0728
delta=Heff/L4;
z=0;

pool_core_props;

% % Plate power, either choose a. manual input or b. fraction of full
% % plate power or or c. input time after shutdown
% % (Comment out whichever two are not used)
```

```
% %a:
% Qdot=177.48e3;
% qdot=q0*Qdot/Qass0;

% % b:
% alph=1.2;
% Qdot=Qass0*alph;
% qdot=q0*alph; % Using the same calculation that was conservative for
% 1ph - hottest channel

%c:
[Qdot,~]=decay_heat(t,Qass0);
[qdot,~]=decay_heat(t,q0);

tol=1e-5; res=5e3;
[~,~,~,~,~,~,~,~,~,hf,hfg,~,~,hg]=fluid_props(Pcore_avg); % Liquid
% saturation specific enthalpy & latent heat
[~,~,~,~,~,~,~,~,~,hin]=fluid_props(Pcore_avg,Tinf); % Inlet specific
% enthalpy, calculated for avg pressure
[~,~,~,~,~,~,~,~,~,~,~,~,~,rhof,rhog]=fluid_props(Pcore_avg,Tinf); % Ignoring
% Tinf for saturated conditions
[~,~,my0]=fluid_props(Pcore_avg,Tinf);
[~,~,my4]=fluid_props(Pcore_avg); % Friction factors need to be based on
% Re based on saturation conditions [HT studies of water flow in thin
% rectangular channels II]
[~,~,my5]=fluid_props(Pcore_avg);
rhol_avg=fluid_props(Pcore_avg,Tcore_avg);
rhol=fluid_props(Pcore_bot,Tinf);

xin=(hin-hf)/hfg;
Mdot(2)=Qdot/(tol-xin*hfg); %[kg/s] flow rate for xout=1e-5 (instead of
% 0 to prevent NaN in Dpf(end))
Mdot(1)=Qdot/(1-xin)/hfg; %[kg/s] flow rate for xout=1
Mdot=linspace(Mdot(1),Mdot(2),res);
```

```
Re1=D1.*Mdot./(A1*my0);
Re2=D2.*Mdot./(A2*my0);
Re3=Dh3.*Mdot./(A3*my0);
Re4=Dh4.*Mdot./(A4*my4);
Re5=Dh5.*Mdot./(A5*my5);

%%%%%% Section 1
f1=0.5*ones(size(Re1));
conv_f=1;
while conv_f>tol
ftemp=(-2.*log10(epsi./(D1.*3.7)+2.51./(Re1.*sqrt(f1)))).^(-2);
conv_f=abs((ftemp-f1)./f1);
f1=ftemp;
end
f1(1:(find(Re1<10,1,'last')))=0;
ftemp=64./Re1;
f1(1:find(abs(f1-ftemp)==min(abs(f1-ftemp))))=...
    64./Re1(1:find(abs(f1-ftemp)==min(abs(f1-ftemp))));
%%%%%% Section 2
f2=0.5*ones(size(Re2));
conv_f=1;
while conv_f>tol
ftemp=(-2.*log10(epsi./(D2.*3.7)+2.51./(Re2.*sqrt(f2)))).^(-2);
conv_f=abs((ftemp-f2)./f2);
f2=ftemp;
end
f2(1:(find(Re2<10,1,'last')))=0;
ftemp=64./Re2;
f2(1:find(abs(f2-ftemp)==min(abs(f2-ftemp))))=...
    64./Re2(1:find(abs(f2-ftemp)==min(abs(f2-ftemp))));
%%%%%% Section 3
f3=0.5*ones(size(Re3));
conv_f=1;
while conv_f>tol
```

```
ftemp=(-2.*log10(epsi./(Dh3.*3.7)+2.51./(Re3.*sqrt(f3)))).^(-2);
conv_f=abs((ftemp-f3)./f3);
f3=ftemp;
end
f3(1:(find(Re3<10,1,'last')))=0;
ftemp=klam35*64./Re3;
f3(1:find(abs(f3-ftemp)==min(abs(f3-ftemp))))=...
    klam35*64./Re3(1:find(abs(f3-ftemp)==min(abs(f3-ftemp))));
%%%%%% Section 4
f4=0.5*ones(size(Re4));
conv_f=1;
while conv_f>tol
ftemp=(-2.*log10(epsi./(Dh4.*3.7)+2.51./(Re4.*sqrt(f4)))).^(-2);
conv_f=abs((ftemp-f4)./f4);
f4=ftemp;
end
f4=f4.*ktur4; %correction for turbulent flow in section 4
f4(1:(find(Re4<10,1,'last')))=0; %fix instabilities for very low turbulent
% f (in all sections)
ftemp=klam4*64./Re4;

f4(1:find(abs(f4-ftemp)==min(abs(f4-ftemp))))=...
    klam4*64./Re4(1:find(abs(f4-ftemp)==min(abs(f4-ftemp))));

%%%%%% Section 5
f5=0.5*ones(size(Re5));
conv_f=1;
while conv_f>tol
ftemp=(-2.*log10(epsi./(Dh5.*3.7)+2.51./(Re5.*sqrt(f5)))).^(-2);
conv_f=abs((ftemp-f5)./f5);
f5=ftemp;
end
f5(1:(find(Re5<10,1,'last')))=0;
ftemp=klam35*64./Re5;
```

```
f5(1:find(abs(f5-ftemp)==min(abs(f5-ftemp))))=...
    klam35*64./Re5(1:find(abs(f5-ftemp)==min(abs(f5-ftemp))));

clear ftemp; clear conv_f

Dpdr=g*Heff*rhol*ones(size(Mdot)); %Effective driving term, a constant

xout=xin+Qdot/hfg./Mdot;
gamm=xout.*rhof/rhog;
L1ph=-xin./(xout-xin)*L4;
L2ph=L4-L1ph;
Dpf=g*(L1ph*rhol_avg+log(1+gamm)./gamm.*L2ph*rhof+L5./(1+gamm)*rhof)+...
    Mdot.^2.*(f1.*L1./(2*rhol*D1*A1^2)+f2.*L2./(2*rhol*D2*A2^2)+...
    f3.*L3./(2*rhol*Dh3*A3^2)+f4.*L1ph./(2*rhol_avg*Dh4*A4^2)+...
    f4.*L2ph./(2*rhof*Dh4*A4^2).*(1+gamm/2)+f5.*L5/(2*rhof*Dh5*...
    A5^2).*(1+gamm)+K01/(2*rhol*A1^2)+K12/(2*rhol*A1^2)+K23/(2*...
    rhol*A2^2)+K34/(2*rhol*A4^2)+K45/(2*rhof*A4^2).*(1+gamm)+K50/...
    (2*rhof*A5^2).*(1+gamm));

temp=find(diff(sign(Dpf-Dpdr))); %find where Dpr-Dpdr changes sign
% (intersections and thus solutions)
if isempty(temp)==1
    disp('No solutions for flow rate')
    break
end
Mdot(end+1)=0;
Mdot=(Mdot(1:end-1)+Mdot(2:end))/2; %calculate average between flow rates
Mdot=Mdot(temp); %Solutions for flow rate (average of flow rate that gives
% negative and positive (Dpf-Dpdr)
xout=xin+Qdot/hfg./Mdot; %Solutions for exit quality

Re4=Dh4.*Mdot./(A4*my4);
mdot=Mdot/17;
[rho,~,my4,~,k,~,cp,~,~,hfg,rhof,rhog,~] = fluid_props(Pcore_avg); % The
```

```
% viscosity here (slightly) changed since the temperature is being
% evaluated at saturated conditions at channel exit as opposed to
% the Re #
h2ph=heatranscoef2ph(min(mdot),max(xout),cp,my4,k,hfg,rhof,rhog,qdot);
[Tc,Tm]=fuelclad(qdot,Tcore_sat,h2ph);
```

B.13 Uncovered Core Steaming

The script `swell_height` calculates the natural steaming rate in steady state, for a given assembly power and inlet temperature and height of core uncovry (for heights below critical). It also calculates the temperatures at the exit from the hottest channel similarly to the former scripts:

```
% Swell height and corresponding clad temperatures for uncovered fuel
clear
tol=1e-5; res=5e3;
Tinf=35;
z=0.0;
fuel_props;
pool_core_props;
delta=0.28; % Critical height at 3.5 hour power figure  and pool temp
% is at delta=0.1164 (11.64% covering plate region)
Hpool=delta*L4; % The pool height above plates for delta=11.64% is
% 7.28cm Plate power, either a. choose fraction of full plate power or
% b. time after shutdown (Comment out either a or b)

% % a:
% alph=1; % Highest temperature at z=7.92 aplh=1.7121 (273kW)
% Qdot=Qass0*alph
% qdot=q0*Qdot/Qass0; % Using the same calculation that was conservative
% for 1ph - hottest channel

%b:
t=3.5*3600;
[~,Qcore]=decay_heat(t,P0);
```

```
[Qdot,~]=decay_heat(t,Qass0);
[qdot,~]=decay_heat(t,q0);

[~,~,~,~,~,~,~,~,hf,hfg,~,~,hg]=fluid_props(Pcore_avg); % Liquid
% saturation specific enthalpy & latent heat
[~,~,~,~,~,~,~,hin]=fluid_props(Pcore_avg,Tinf); % Inlet specific
% enthalpy, calculated for avg pressure
[~,~,~,~,~,~,~,~,~,~,rhof,rhog]=fluid_props(Pcore_avg,Tinf); % Ignoring
% Tinf for saturated conditions
[~,~,my0]=fluid_props(Pcore_avg,Tinf);
[~,~,my4]=fluid_props(Pcore_avg); % Friction factors need to be based
% on Re based on saturation conditions [HT studies of water flow in thin
% rectangular channels II]
[~,~,my5]=fluid_props(Pcore_avg);
rhol_avg=fluid_props(Pcore_avg,Tcore_avg);
rhol=fluid_props(Pcore_bot,Tinf);
gamm=rhof/rhog;
rhom_avg=rhog*log(1+gamm);
xin=(hin-hf)/hfg;

Hswell=linspace(Hpool,L4,res);
theta=-xin/(1-xin);
L1ph=theta.*Hswell;
L2ph=(1-theta).*Hswell;
phi4=1+gamm/2;
Dh=hg-hin;
Mdot=Qdot.*Hswell./Dh./L4;

Re1=D1.*Mdot./(A1*my0);
Re2=D2.*Mdot./(A2*my0);
Re3=Dh3.*Mdot./(A3*my0);
Re4=Dh4.*Mdot./(A4*my4);

if max([max(Re1) max(Re2) max(Re3) max(Re4)])>1500
```

```
%%%%%% Section 1
f1=0.5*ones(size(Re1));
conv_f=1;
while conv_f>tol
ftemp=(-2.*log10(epsi./(D1.*3.7)+2.51./(Re1.*sqrt(f1)))).^(-2);
conv_f=abs((ftemp-f1)./f1);
f1=ftemp;
end
f1(1:(find(Re1<10,1,'last')))=0;
ftemp=64./Re1;
f1(1:find(abs(f1-ftemp)==min(abs(f1-ftemp))))=...
    64./Re1(1:find(abs(f1-ftemp)==min(abs(f1-ftemp))));
%%%%%% Section 2
f2=0.5*ones(size(Re2));
conv_f=1;
while conv_f>tol
ftemp=(-2.*log10(epsi./(D2.*3.7)+2.51./(Re2.*sqrt(f2)))).^(-2);
conv_f=abs((ftemp-f2)./f2);
f2=ftemp;
end
f2(1:(find(Re2<10,1,'last')))=0;
ftemp=64./Re2;
f2(1:find(abs(f2-ftemp)==min(abs(f2-ftemp))))=...
    64./Re2(1:find(abs(f2-ftemp)==min(abs(f2-ftemp))));
%%%%%% Section 3
f3=0.5*ones(size(Re3));
conv_f=1;
while conv_f>tol
ftemp=(-2.*log10(epsi./(Dh3.*3.7)+2.51./(Re3.*sqrt(f3)))).^(-2);
conv_f=abs((ftemp-f3)./f3);
f3=ftemp;
end
f3(1:(find(Re3<10,1,'last')))=0;
ftemp=klam35*64./Re3;
```

```
f3(1:find(abs(f3-ftemp)==min(abs(f3-ftemp))))=...
    klam35*64./Re3(1:find(abs(f3-ftemp)==min(abs(f3-ftemp))));
%%%%% Section 4
f4=0.5*ones(size(Re4));
conv_f=1;
while conv_f>tol
ftemp=(-2.*log10(epsi./(Dh4.*3.7)+2.51./(Re4.*sqrt(f4)))).^(-2);
conv_f=abs((ftemp-f4)./f4);
f4=ftemp;
end
f4=f4.*ktur4;
f4(1:(find(Re4<10,1,'last')))=0; %fix instabilities for very low
% turbulent f (all sections)
ftemp=klam4*64./Re4;
f4(1:find(abs(f4-ftemp)==min(abs(f4-ftemp))))=...
    klam4*64./Re4(1:find(abs(f4-ftemp)==min(abs(f4-ftemp))));
clear ftemp; clear conv_f

else
f1=64./Re1;
f2=64./Re2;
f3=klam35*64./Re3;
f4=klam4*64./Re4;
end

Dpdr=g*Hpool*rhol*ones(size(Mdot)); %Effective driving term, a constant
Dpf=g*(rhol_avg*theta.*Hswell+rhom_avg*(1-theta).*Hswell)+...
    (Qdot.*Hswell./Dh./L4).^2.*(f1.*L1./(2*rhol*D1*A1^2)+f2.*L2./...
    (2*rhol*D2*A2^2)+f3.*L3./(2*rhol*Dh3*A3^2)+f4.*theta.*Hswell./...
    (2*rhol_avg*Dh4*A4^2)+f4.*(1-theta).*Hswell./(2*rhof*Dh4*A4^2).*...
    (1+gamm/2)+K01/(2*rhol*A1^2)+K12/(2*rhol*A1^2)+K23/(2*rhol*A2^2)+...
    K34/(2*rhol*A4^2));

Hcrit=Dpf(end)/rhol/g;
```

```
delta_crit=Hcrit/L4;

temp=find(diff(sign(Dpf-Dpdr))); %find where Dpr-Dpdr changes sign
% (intersections and thus solutions)
if isempty(temp)==1
    disp('No solutions for swell height')
    break
end
Hswell(end+1)=0;
Hswell=(Hswell(1:end-1)+Hswell(2:end))/2; %calculate average between
% Hswell points
Hswell=Hswell(temp); %Solutions for flow rate (average of flow rate that
% gives negative and positive (Dpf-Dpdr)

Mdot=Hswell.*Qdot./L4./Dh; %Solutions for exit quality
mdot=Mdot/17;
eps=Hswell/L4; % Covered portion of swell
hout=hin+Dh/eps; %[J/kg] Exit vapour enthalpy
Tv_exit=XSteam('T_ph',Patm,hout/1e3); %[C] Exit vapour temperature
cp_v=XSteam('cp_ph',Patm,hout/1e3)*1e3; %[J/kg-K] Exit vapour specific
% heat
my_v=XSteam('my_ph',Patm,hout/1e3); %[Pa-s]=[kg/s-m] Exit vapour
% viscosity
kv=XSteam('tc_ph',Patm,hout/1e3); %[W/m-K] Exit vapour conductivity

h=heatranscoef(mdot,cp_v,my_v,kv); %[W/m^2] Exit vapour convective heat
% transfer coefficient
[Tc_exit,Tm_exit]=fuelclad(qdot,Tv_exit,h); %[C] Clad and fuel upper
% edge temperatures
```